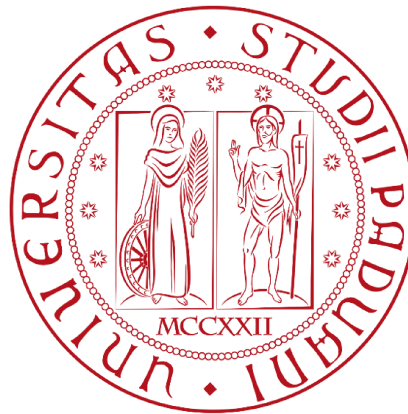# UNIVERSITÀ DEGLI STUDI DI PADOVA

DIPARTIMENTO DI BIOLOGIA

Corso di Laurea in Biologia Molecolare

ELABORATO DI LAUREA

**Tracheal reconstruction strategies:
a comparison between new cryopreserved and decellularized allografts**

Tutor: Prof.ssa Elena Stocco
Dipartimento di Neuroscienze

Co-tutor: Prof.ssa Silvia Barbon
Dipartimento di Neuroscienze

Laurenda: Alice Leandri

INDEX

1. ABSTRACT

In clinical practice, tracheal injuries are primarily handled through resection and tensionless end-to-end anastomosis (TRA). However, this approach is not feasible in case of lesions exceeding the 50% or the 30% of the trachea length, in adults and in children, respectively. Currently, in such conditions, long-term airway stenting is the only established option; however, it may be responsible of some complications boosting research on the identification of valuable tracheal substitutes able to overcome the TRA limitations. In this scenario, the study presented in this thesis work deals with the development and comparison between two promising tracheal substitutes consisting in cryopreserved and decellularized tracheal grafts. Specifically, pig-derived grafts were processed through cryopreservation and decellularization and then analyzed for their DNA and xenoantigen content, extracellular matrix (ECM) features, ultrastructure and mechanical behaviour. Moreover, *in vitro* cytotoxicity and *in vivo* biocompatibility evaluations were performed to verify the grafts' safety effects on cells and to ensure their compatible integration with host tissues. Evidence provided by the experimental data showed that both strategies allow an effective reduction of graft immunogenicity, especially with the decellularization approach. The cryopreserved samples displayed minimal changes in their microscopic structure, include a reduced number of cilia in the respiratory epithelium and less dense mucosa and submucosa; in contrast, decellularization partly altered the tracheal segments by removing cellular elements while leaving behind a disorganized connective tissue. Considering the ECM components, the collagen content was preserved, while the decellularized graft was depleted of glycosaminoglycans (GAGs), consistent with its change in mechanical proprieties. The grafts both guarantee cytotoxicity absence, as also proved by biocompatibility assay *in vivo*. These substitutes are both worthy options, but more *in vivo* studies are required to validate them.

2. STATE OF ART

2.1 Anatomy of trachea

The trachea is a tube-shaped organ that belongs to the respiratory system. It is located between the larynx and the bronchi and extends from the cervical vertebra C6 to the thoracic vertebra T4, measuring 10-13 cm in adults. Most of the trachea lies within the thoracic inlet and the chest.

The trachea comprises 16-20 incomplete rings of hyaline cartilage that run forward and sideways, interconnected by the intercartilaginous membrane. The purpose of these rings is to add stiffness to the tracheal wall and prevent it from collapsing. The trachealis smooth muscle forms the posterior edge and regulates the organ's diameter through the contraction. For this organization, it is characterized by a typical D-shaped cross-section structure.

The luminal side is lined with ciliated pseudostratified columnar cells and goblet cells. The secretory cells produce mucus that contains IgA, lysozymes, lactoferrin and peroxidases, and it is fundamental to trap foreign agents, which are then expelled by the upward movement of the cilia. In addition to mucociliary clearance, trachea protects the respiratory tract by humifying and heating inhaled gas. Below the mucosa lies the submucosa, which is primarily composed of connective tissue. Additionally, it contains neurons, blood vessels, and glands. The glands release mucus which is added to that produced by the goblet cells. The arteries, that supply the trachea, insert laterally into the organ. In the cervical part of the trachea (C6-C7), blood is provided by the branches of the inferior thyroid arteries, while at the thoracic level (T1-T4), vascularization occurs through the branches of the bronchial arteries. At the level of the intercartilaginous membrane, the arteries branch out posteriorly and anteriorly, surrounding the trachea. Additionally, branches occur above and anteriorly to allow anastomosis with the other arteries. [1]

2.2 Long-segment tracheal lesions

Various lesions can develop in the trachea and are divided between those congenital and those acquired. Congenital lesions are often associated with underlying genetic mutations or syndrome such as tracheomalacia, tracheoesophageal fistula, and complete tracheal rings. On the other hand, acquired lesions can affect patients of all ages and are caused by factors like iatrogenic causes, blunt and penetrating trauma, neoplasms (both benign and malignant), inflammatory conditions, and inhalation injuries. Such lesions impair air flow, especially in the pediatric population where the tracheal diameter does not reach 1 cm up to eight years of age. Therefore, early recognition and proper management of injuries are crucial, as many can be life-threatening. In clinical practice, resection and tensionless end-to-end anastomosis (TRA) represent the treatment of choice but it is not a viable option if the damage exceeds 50% of the trachea length in adults or 30% in children. [2 e 3]

2.1.1. Current repair options in surgical practice

Within the severe circumstances described above, the only established option is long-term airway stenting. Airway stents have been adopted to manage tracheobronchial pathologies since the second half of the 20th century. Currently, many different stents are available with specific materials and designs: silicone and metal stents are the most widely used. Silicone stents are affordable and straightforward to manage; the most commonly used ones are the Dumon and Hood stents. Meanwhile, metal stents can be easily inserted through flexible

bronchoscopy with fluoroscopic guidance. Although they can provide timely relief to patients, there are also potential issues that come with this treatment method. Examples of complications include infection, migration of the device, mucous plugging or granulation tissue formation. Currently, researchers are working to enhance biodegradable stents development, up to a progressive customization of the devices also recurring to 3D printing technology. [4]

2.1.2 New perspectives in tracheal substitutes

To date, a significant amount of research is conducted on tracheal replacement by the adoption of airway substitutes. However, meeting all the necessary requirements makes it difficult to create an optimal substitute. In fact, an ideal substitute is expected to show lateral rigidity and longitudinal flexibility while being biocompatible with surrounding tissues. Additionally, it should have an airtight lumen coated with a ciliate epithelium. The development and insertion process should be simple and reproducible without requiring prolonged immunosuppression therapy for the patient. In clinical practice, various techniques have been employed over the years but to date none of them has yet become an established therapy option.

Several synthetic prostheses have been developed, despite a higher risk of granulation, infection and potential harm to nearby organs were possibly associated with them. Briefly, prostheses come in two types: solid and porous; these latter are considered to be more biocompatible compared to their solid counterparts because their structural porosity allows for connective tissue to grow into, while encouraging the migration of the tracheal epithelium.

Complex tubular grafts, also using autologous tissues, have been attempted too. In particular, fasci-cutaneous flaps have been combined with a rigid structure to reproduce the tracheal rings. In clinical practice, such stiff architecture has been produced either synthetically or by strips of cartilage. However, this approach presents challenges in both constructing the substitute and promoting the formation of a ciliated epithelium capable of mucus production.

The use of aortic allograft has been also considered while searching for a tracheal substitute. This graft is biocompatible with surrounding tissues and enables the patient to avoid strong immunosuppressive therapies. However, there is a risk of degeneration over time due to the lack of specific revascularization. It may also lack lateral stiffness, which increases the likelihood of stents being required. The use of stents can pose various complications for the patient.

Trachea transplantation is another viable option that has been attempted for tracheal reconstruction, but this procedure involves numerous and complex surgeries and an extended period of immunosuppressive treatment. Moreover, it presents a complex challenge in restoring blood flow: direct transplantation is not a feasible solution, but the grafts require initial placement in a heterotopic position to encourage revascularization. [5,6]

Within this scenario, cryopreservation and decellularization represent promising strategies for new tracheal graft development.

Cryopreserved tracheal allografts

Cryopreservation is a method that allows for the long-term preservation of biological samples by freezing them at extremely low temperatures. This method guarantees the maintenance of the precise structure of organelles, cells, tissues, or any other biological construct. Recently, the use of cryoprotective agents (CPA) and temperature control equipment has significantly improved the effectiveness of preserving cells and tissues. Storing tissue allografts is often done through cryopreservation and there are four main steps involved. First, the grafts are mixed with CPAs prior to cooling. Then, they are cooled to a low temperature and stored in liquid nitrogen vapour. When needed, the allograft is thawed under controlled conditions and the CPAs are removed from the grafts. Through this approach, it is possible to obtain an allograft that maintains the histological and mechanical characteristics, ideally reducing tracheal allogenicity. This reduction is closely linked to the alteration of the tracheal epithelium and lamina, which are targets of rejection. According to our knowledge, despite cryopreservation is broadly adopted for various tissues including amniotic membrane, bone, menisci, vascular tissue and heart valves, evidences on cryopreserved trachea effectiveness are still scant and more research is required. [7]

Decellularized tracheal allografts

The process of decellularization is a commonly used technique within the field of tissue engineering. This discipline involves the principles of both engineering and biological sciences to develop functional tissues or organs for therapeutic purposes. To accomplish this, a support structure (scaffold) is integrated with the patient's own cells and biologically active molecules. [5]

In the field of tissue engineering for tracheal grafts, scaffolds can be categorized into two types: synthetic and biological(decellularized allografts). Synthetic scaffolds are expected to undergo biodegradation along with new, functional tissue regeneration; they are particularly interesting due to their intrinsic reproducibility, allowing to mimic structural and mechanical features of the targeted organ. However, they may have a lower attitude to support cells' growth. Biological scaffolds include decellularized ECM. Briefly, decellularization strategies involve the use of chemical and/or enzymatic and/or physical treatments to isolate the ECM component from the immunogenic cellular elements which are removed by the procedure. Together with donor cells removal, the efficacy of decellularization is also associated with the preservation of the structural and signaling elements of the extracellular matrix. Such types of scaffolds act as a supporting structure, reproducing the original ECM's biological and mechanical function while well supporting the patient's cells colonization and proliferation. [5]

Currently, there are still many doubts about the procedure-related effects on immunogenicity, tissue organization and ECM features of the grafts. Therefore, preclinical studies are crucial in determining the success of clinical outcomes. In preparation for future clinical use, conducting orthotopic studies using animal disease models is an important step for their validation. Furthermore, the use of large animals that share similar dimensions with humans will also allow facing the technical difficulties of clinical practice. [5]

3. AIM OF THE THESIS

The study presented in this thesis aimed to develop, describe and compare cryopreserved and decellularized pig-derived tracheal grafts for future use in clinical practice. The first method was based on a cryopreservation protocol by "Fondazione Banca dei Tessuti del Veneto"; briefly, after soaking tracheal segments in cryoprotectant, a controlled freezing was performed followed by subsequent preservation within liquid nitrogen vapor. In parallel, the method based on decellularization consisted in a complex physical, chemical and enzymatic protocol recurring to different phases where, each cycle, consisted in lyophilization, followed by the use of the DNAse-I enzyme and the Tergitol^{TM} detergent. The tissue substitutes were compared for their immunogenicity (histology and fluorescence/ DNA quantification/immunohistochemistry), ECM characteristics (histology/ morphometric analyses), ultrastructure (Scanning Electron Microscopy (SEM)), mechanical behaviour, cytotoxicity in vitro (extract test followed by MTT colorimetric assay/direct seeding), and biocompatibility in vivo (histology/ immunohistochemistry/SEM). The findings of this study will contribute to a deeper comprehension of these novel tracheal substitutes, ultimately enhancing their translation to medicine.

4. MATERIALS AND METHODS

4.1 Trachea isolation

Ten adult pigs, from a local butcher, were used to obtain the tracheas used for this study purposes. After excision, two tracheal segments measuring approximately 5 cm were isolated from each pig, thoroughly cleaned of any mucus and submerged in an antibiotic solution composed of BASE medium, gentamicin, vancomycin and meropenem for 48 h. One of the segments of each animal was intended for cryopreservation, while the other for decellularization.

4.2 Trachea cryopreservation

Ten of the tracheal segments underwent to cryopreservation by "Fondazione Banca dei Tessuti del Veneto ONLUS" (FBTV). Preliminarily, the tracheal segments underwent a second cleaning to remove mucus and were decontaminated with the same antibiotic solution as before for 48 h. The segments were then immersed in a sterile saline solution for 5 minutes before being placed into ethylene-vinyl acetate bags designed to withstand low temperatures. The bags contained a solution comprising BASE medium, 10% dimethylsulfoxide (CPA), and 10% human serum albumin. Finally, a programmable cryogenic equipment was employed to gradually cool the segments to a temperature of -140 °C. The segments were then stored in liquid nitrogen vapor.

4.3 Trachea decellularization

Prior to decellularization, the segments underwent decontamination by using a 2% solution of streptomycin and penicillin in sterile deionized water (dH_2O). This process consisted in 3 washes under stirring, each lasting for 30 min. The decellularization process involved 12 cycles; each cycle consisted of 4 phases:

1. Tissue freezing at -20 °C and lyophilization for 12 h. Lyophilization is used to remove ice crystals from a previously frozen tissue through sublimation and desorption, producing a completely dry, stable scaffold. After freeze-drying, the tissue can be immersed in solutions containing detergents and enzymes to remove cells. Because the scaffold is free of water, these solutions can penetrate better inside and act effectively. The formation of intracellular ice crystals during this process can lead to cell membrane disruption, genetic material fragmentation, and ultimately, cell lysis.

2. Treatment with 10,000 kU DNAse-1 in 1 M NaCl at room temperature (RT) for 6 h; washing with dH_2O; soaking in 0.05% trypsin+0.02% EDTA solution in dH_2O at 37 °C for 1 h. Hence, extensive washing in dH_2O occurred. These enzymatic process aims to separate the ECM from the cellular component.

3. Washing with 2% Tergitol™ detergent solution + 0.8% ammonium hydroxide in dH_2O at +4 °C for 3 days under stirring. These chemical treatment enables the solubilization of the cytoplasmic component.

4. Washing with dH_2O at +4 °C for 2 days under stirring to remove chemical residues

4.4 Cryopreserved and decellularized tissues characterization

4.4.1. DNA visualization
To assess the presence and distribution of nuclei within decellularized and cryopreserved samples compared to the native trachea, 5 μm specimens were stained with 4,6-diamidino-2-phenylindole (DAPI) and photomicrographs were captured using a Leica LMD6 connected to a high-resolution digital camera.

4.4.2. DNA extraction and quantification
To examine the DNA content, samples were treated using DNeasyBlood&Tissue kit under the manufacturer's protocol. DNA samples were then quantified using Qubit 4 fluorometer and kit.

4.4.3. Xenoantigen identification
Within the scenario of xenotransplantation, the main contributors to hyperacute rejection are the superficial epitopes Alpha-Gal. Immunohistochemistry was employed to evaluate the treatments' effectiveness in concealing or deactivating these epitopes. Tracheal samples (NativeT, CryoT, DeCellT) were fixed in 10% formalin and embedded in paraffin. Subsequently, 3 μm thick sections were cut from the embedded samples. After dewaxing and rehydration, an immunohistochemical reaction was conducted using the anti-Alpha-Gal primary antibody. Visualization of the reaction was achieved using a labelled polymer and 3,3'-diaminobenzidine. Alpha-Gal immunoreactivity was then quantified using photomicrographs acquired under a Leica DM4500B microscope connected to a high-resolution digital camera.

4.4.4. Histological and morphometric analyses
Specimens from the NativeT, CryoT and DecellT tissues were fixed in a 10% formalin solution in Phosphate Buffered saline (PBS) and embedded in paraffin. Following dewaxing and rehydration, sections measuring 5 μm underwent the stainings described below. Haematoxylin and eosin staining was employed for a broad tissue characterization thus allowing to verify the presence and distribution of cell nuclei and the integrity of the ECM. The preservation of ECM structural proteins was verified by the use of Weigert Van Gieson staining (elastic fibers), Masson's Trichrome and Sirius Red staining (collagen fibers), Alcian-blue staining (GAGs).
Morphometric analysis of ECM elements was conducted using photomicrographs taken with a Leica DM4500B microscope equipped with a high-resolution digital camera. The quantification data were presented as the percentages of green-stained area for collagen, purple-stained area for elastic fibers, and red-orange and green stained areas for type I and III, respectively, relative to the total acquisition field area. GAGs were quantified using the Chondrex Inc. Glycosaminoglycans Assay Kit under the Manufacturer instructions.

4.4.5. Ultrastructural analyses by Scanning Electron Microscopy
The Scanning Electron Microscope (SEM) is an advanced imaging instrument allowing for high-resolution visualization of the surface morphology and topography of materials.[10] Tracheal tissues were analyzed with SEM to assess their ultrastructure, considering both the external and the luminal side. Before SEM imaging, samples underwent fixation with 2.5% glutaraldehyde in 0.2 M PBS to preserve tissue's structure, dehydration using a series

of ethanol solutions, drying (critical point drying), and finally coating with a thin layer of gold (conductive material).

4.4.6. Mechanical behaviour

NativeT, DecellT, and CryoT samples from three donors () were sectioned transversally to form ring-like structures (three-rings/each) The dimensional characteristics of these samples were evaluated by measuring the medio-lateral diameters (d1), proximal-distal diameters (d2), tracheal wall thickness (t), and segment length (L) utilizing the image analysis software Fiji. (Fig. 1A). Subsequently, the Bose ElectroForce Planar Biaxial Test Bench was adopted to perform compression tests. Briefly, two parallel flat plates were arranged with the tracheal samples on the lower plate (Fig. 1B). The upper plate was gradually moved towards the samples at a steady speed of 0.2 mm s−1 until the proximal-distal diameter (d2) was reduced by 50% from its initial measurement. A compression curve was generated to analyze the compression behaviour, representing the force per unit of length of the sample (f) against the tracheal compressive deformation (s) in the proximal-distal direction. The tracheal compressive deformation (s) was calculated as the ratio of the plate displacement (Δu) to the initial diameter (d2) ($s = \Delta u / d2$) (Fig. 1C). The force per unit length of the sample (f) was determined by dividing the force value (F) measured by the load cell by the sample's length (L) ($f = F/L$). To estimate the sample's stiffness, the secant compressive modulus (k) was calculated by measuring the slope of the secant line at 20% and 50% compressive deformation (the range in which there is a homogeneous contact between the upper plate and the sample). The values of the secant compressive modulus k were analyzed through ANOVA ($p < 0.05$).
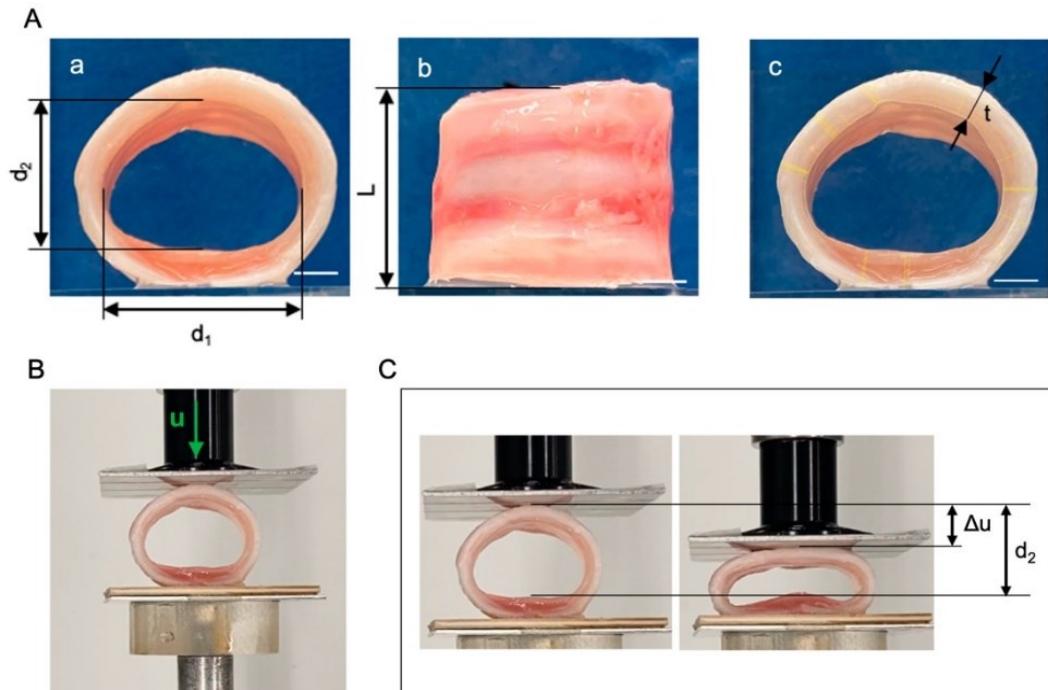

Fig. 1: (A) Tracheal samples and their measurements of the medio-lateral diameters (d1), proximal-distal diameters (d2), tracheal wall thickness (t), and segment length (L). **(B)** Apparatus adopted for the mechanical test. **(C)** Trachea samples in their original and compressed states and the representation of the plate displacement Δu and the initial diameter d2.

4.4.7. *In vitro* Cytotoxicity

Cryopreserved and decellularized matrices cytotoxicity was assessed *in vitro* using the MTT assay. Briefly, this technique involves a yellow dye called 3-(4,5-dimethylthiazol-2-yl)-2,5-diphenyltetrazolium bromide (MTT) which, living cells, with active metabolism, can transform into a purple formazan product. The quantity of formazan generated is directly linked to the number of viable cells present in the sample. The formazan must be solubilized in order to measure its absorbance with a spectrophotometer. The resulting value is then used to determine the relative cell viability under the given experimental conditions. [11]

In this study, human bone marrow-derived stromal cells (HM1-SV40) were adopted to investigate the cytotoxicity of the matrices. The CryoT and the DecellT samples were soaked into HM1-SV40 cell proliferation medium for 72 hours at 37 °C. Simultaneously, HM1-SV40 cells were cultured on a separate 24-well plate. After 24 hours, the original cell culture medium was replaced with the tissue extract medium. In addition, two control groups were included in the experiment: a positive control treated with a cytotoxic substance (dimethyl sulfoxide) and a negative control with no treatment. After 24 hours of treatment, the cell survival rate was evaluated using the MTT assay. For this assessment, the cell culture medium was substituted with 0.5 mg/mL MTT in α-MEM and incubate for 4 hours. The formazan produced was then dissolved in 2-propanol acid and the optical density of the solutions was measured at 570 nm. The results of the cytotoxicity test were expressed as percentages of viable cells compared to the untreated control. To determine the number of cells, an MTT standard curve was employed.

The cytocompatibility was also evaluated by examining scaffold's ability to support cell's attachment and growth. Firstly, HM1-SV40 cells were cultured and expanded in a proliferation medium. Simultaneously, cryopreserved and decellularized tracheal patches (0.5 × 0.5 cm2) were sterilized using an antibiotic/antimycotic solution, followed by washing in PBS and UV light exposure. After overnight incubation of the tracheal scaffolds in the cell proliferation medium, 100,000 HM1-SV40 cells were seeded on the luminal side of the scaffolds and cultured for 3 and 7 days. SEM analysis was conducted to observe and verify cell adhesion and proliferation on the scaffold surface.

4.4.8. *In vivo* Biocompatibility

To assess *in vivo* biocompatibility, DecellT and CryoT specimens in a disc-like shape were implanted in six 12-week-old female Balb/C mice. Before the implantation procedure, mice were anesthetized, shaved and disinfected (with Betadine) at the level of the dorsal skin. A subcutaneous pouch was created using a 10 mm surgical blade, and the scaffolds were placed onto the latissimus dorsi muscle with the epithelial side in direct contact with the muscle tissue. After the surgery, the mice received antibiotic/anti-inflammatory treatment for 5 days. After a 14-day post-implantation period, the scaffolds were retrieved and fixed for further characterization using histological, immunohistologic and SEM analyses.

The scaffolds underwent staining by H&E, Masson's Trichrome, Sirius Red, Alcian-blue, Weigert Van Gieson (for the same purpose as described in Section 4.4.3), and von Kossa (to assess potential calcification of the specimens after implantation).

Moreover, presence of inflammatory cells was also assessed through anti-CD3 and anti-F4/80 antibodies, diluted in PBS to label lymphocytes and monocytes/macrophages, respectively. At first, 3-5 μm sections were treated with 10 mM sodium citrate buffer at 90 °C for 10 minutes. Afterward, a blocking serum was used to remove unspecific binding,

and primary antibodies were applied and incubated at room temperature for an hour. The binding of primary antibodies was identified using anti-rabbit/mouse serum and developed with 3,3′-diaminobenzidine. The sections were finally counterstained with haematoxylin. Negative control sections were incubated without primary antibodies. Immunoreactivity was then quantified using photomicrographs acquired under a Leica DM4500B microscope connected to a high-resolution digital camera.

4.5. Statistical Analysis

The results are shown as the average value with the standard deviation (SD) from at least three separate tests. To find any meaningful distinctions among the different groups, it was used a statistical test called one-way analysis of variance (ANOVA) followed by the Tukey post hoc test for multiple comparisons. When comparing only two groups, it was used an unpaired t-test. If the p-value was equal to or less than 0.05, the differences were considered significant.

5. RSULTS AND DISCUSSION

5.1. Characterization of the grafts' macroscopic appearance

After being cryopreserved for 13 months, the samples displayed an external whitish aspect and an inner pinkish lumen. The overall tubular structure of the samples was effectively preserved. The DecellT samples were subjected to lyophilization to promote decellularization solutions adsorption; 12 decellularization cycles were performed to obtain a patent, whitish sample. (Fig. 2)
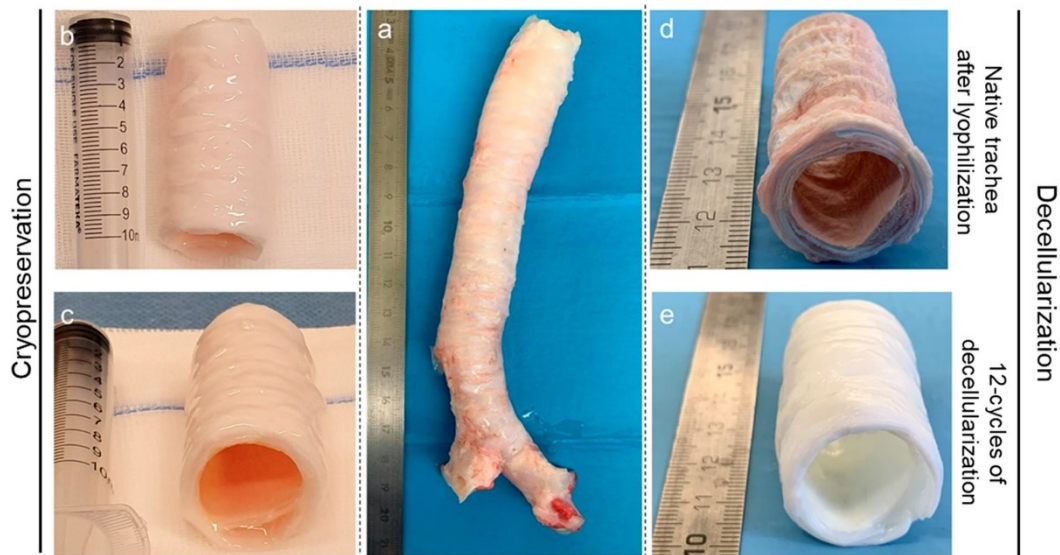

Fig. 2: Fresh trachea gross appearance (a); gross appearance of cryopreserved trachea (b, c); gross appearance of lyophilized trachea before decellularization (d); decellularized trachea (e).

5.2. The protocols reduce the immunogenic potential of the Tracheal Substitutes

The immunogenicity of decellularized and cryopreserved samples represents a prominent area of concern, as it is closely linked to the risk of graft rejection upon implantation. Qualitative verification of cell residues was conducted through DAPI staining, highlighting nuclei presence within the samples(blue dots). As expected, cells were uniformly distributed in the whole NativeT thickness. In contrast, the CryoT had fewer luminescent elements that were nearly not visible in the DecellT samples, mainly localized at the peripheries of the lacunae.

This evidence was confirmed by DNA quantitative analyses, which revealed a substantial DNA content reduction in both the CryoT and DecellT samples when compared to the NativeT reference group. Specifically, the NativeT group exhibited a DNA content of 522.30 ± 157.70 ng/mg, whereas the CryoT and DecellT specimens showed a reduction of 60.4% (206.21 ± 71.26 ng/mg) and 91% (55.84 ± 7.06 ng/mg), respectively. Notably, the decellularization approach exhibited high efficacy in reducing the immunogenic potential of the samples versus cryopreservation ($p < 0.01$) groups. (Fig. 3)
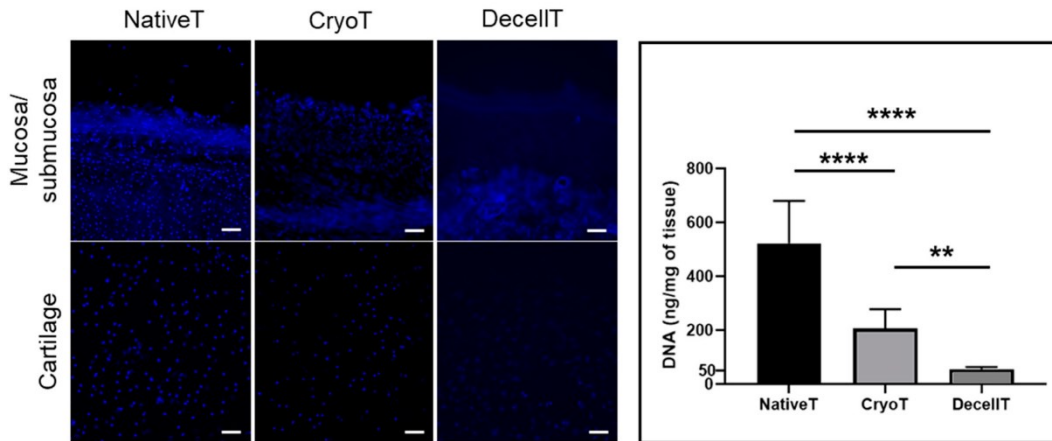
Fig. 3: NativeT, CryoT and DecellT samples after DAPI staining (cells nuclei are visible as blue markers), with the respective quantification of residual DNA (**: $p < 0.01$; ****: $p < 0.0001$).

Given the pig origin of the specimens, Alpha-Gal epitopes immunolocalization was focused. In Native T samples positive immunoreaction was detected within the mucosal and submucosal layers; the xeno-antigens' content was nearly absent within cartilage regions In CryoT specimens, despite a reduction, a certain level of immunopositivity persisted within the mucosal and submucosal regions. In contrast, the DecellT samples did not show Alpha-Gal positive elements in the whole tissue thickness (Fig. 4).

Quantitative analysis showed for the NativeT group an immunoreactivity percentage of $23.56 \pm 1.87\%$ and $10.46 \pm 0.54\%$ at the mucosa/submucosa layer and at the adventitia layer, respectively. These measurements surpassed those of the CryoT group (adventitia: $3.68 \pm 0.33\%$, mucosa/submucosa: $8.76 \pm 0.93\%$), and notably exceeded those of the DecellT group (adventitia: $0.02 \pm 0.031\%$, mucosa/submucosa: $0.20 \pm 0.18\%$), furtherly confirming decellularization protocol efficacy in reducing sample immunogenicity.
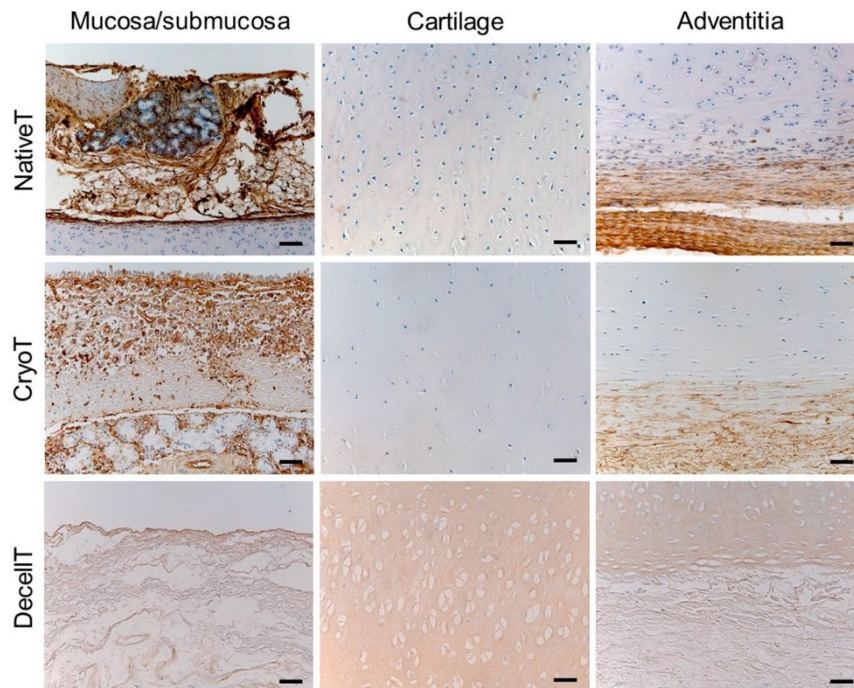

Fig. 4: NativeT, CryoT and DecellT samples evaluated for the Alpha-Gal epitopes immunolocalization (positive reactions appeared in brown).

20

5.3. The protocols efficiency in maintaining ECM composition

Histological analysis was employed to investigate tissue architecture and assess the preservation of ECM characteristics.

H&E staining guaranteed a broad overview over of the tissues appearance, highlighting cells nuclei distribution and tissue organization. The CryoT retained the typical microscopic structure with only slight alterations, consisting in a limited number of cilia at the level of the respiratory epithelium and a relatively less dense mucosa and submucosa compared to the NativeT. As for cartilage, it maintained a compact organization, and the chondrocytes were still clearly identifiable. The adventitia, although recognizable, demonstrated reduced organizational arrangement versus the NativeT samples. Nuclei were decreased but not entirely absent, as seen in section 5.2. On the other hand, the decellularization process partly altered the histological features of tracheal segments by removing cellular components and leaving behind a disorganized connective tissue. The respiratory epithelium was not evident, and the mucosa and submucosa lost their distinct features. The cartilaginous component exhibited void and expanded lacunae, likely due to mechanical stress during lyophilization. The adventitia was also less organized than in the NativeT and CryoT groups. (Fig. 5)
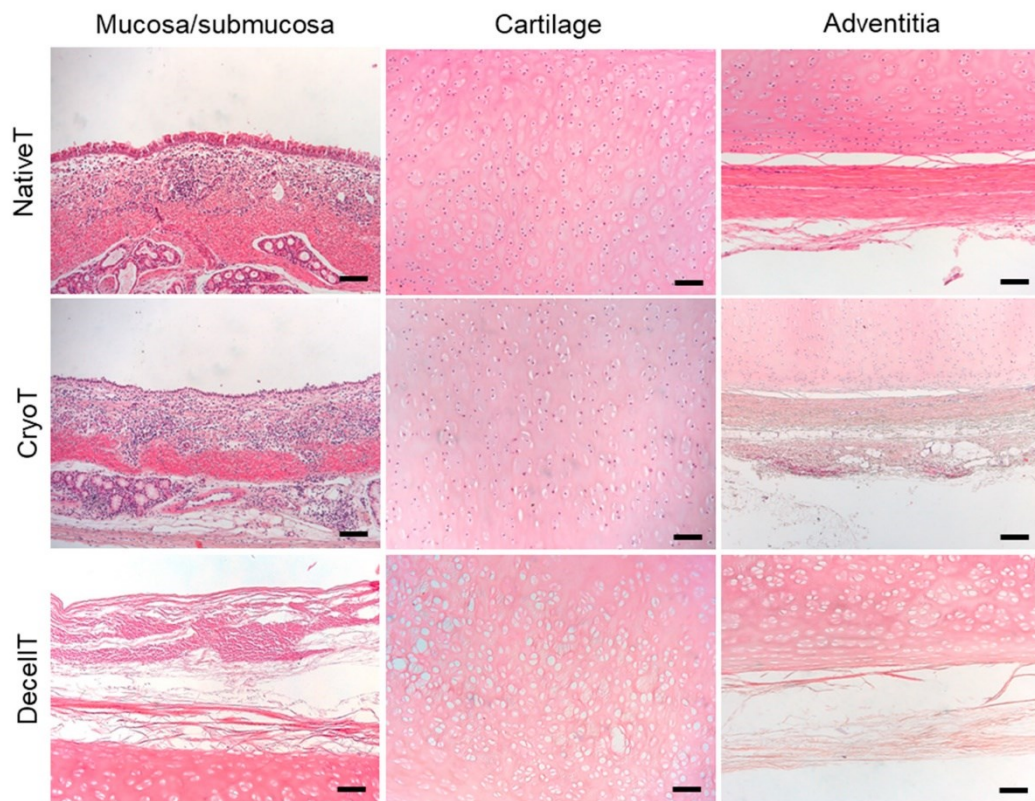

Fig. 5: Histological characterization of NativeT, CryoT and DeCellT sections stained with Hematoxylin and Eosin

Alcian Blue staining was used to investigate the presence of GAGs and cytoplasmatic granules. Comparing the cryopreserved samples with the native tissue, a similar shade of blue was observed. However, the decellularized samples exhibited a less color intensity, suggesting that the decellularization process likely led to a GAG reduction. Indeed, a quantitative analysis assigned a GAG content of 2.79 ± 0.04 µg/mg to the DeCellT group,

in contrast to the values of µg/mg 5.21± 0.90 µg/mg and 4.93 ± 0.60 µg/mg observed in the CryoT and NativeT groups, respectively. (Fig. 6)
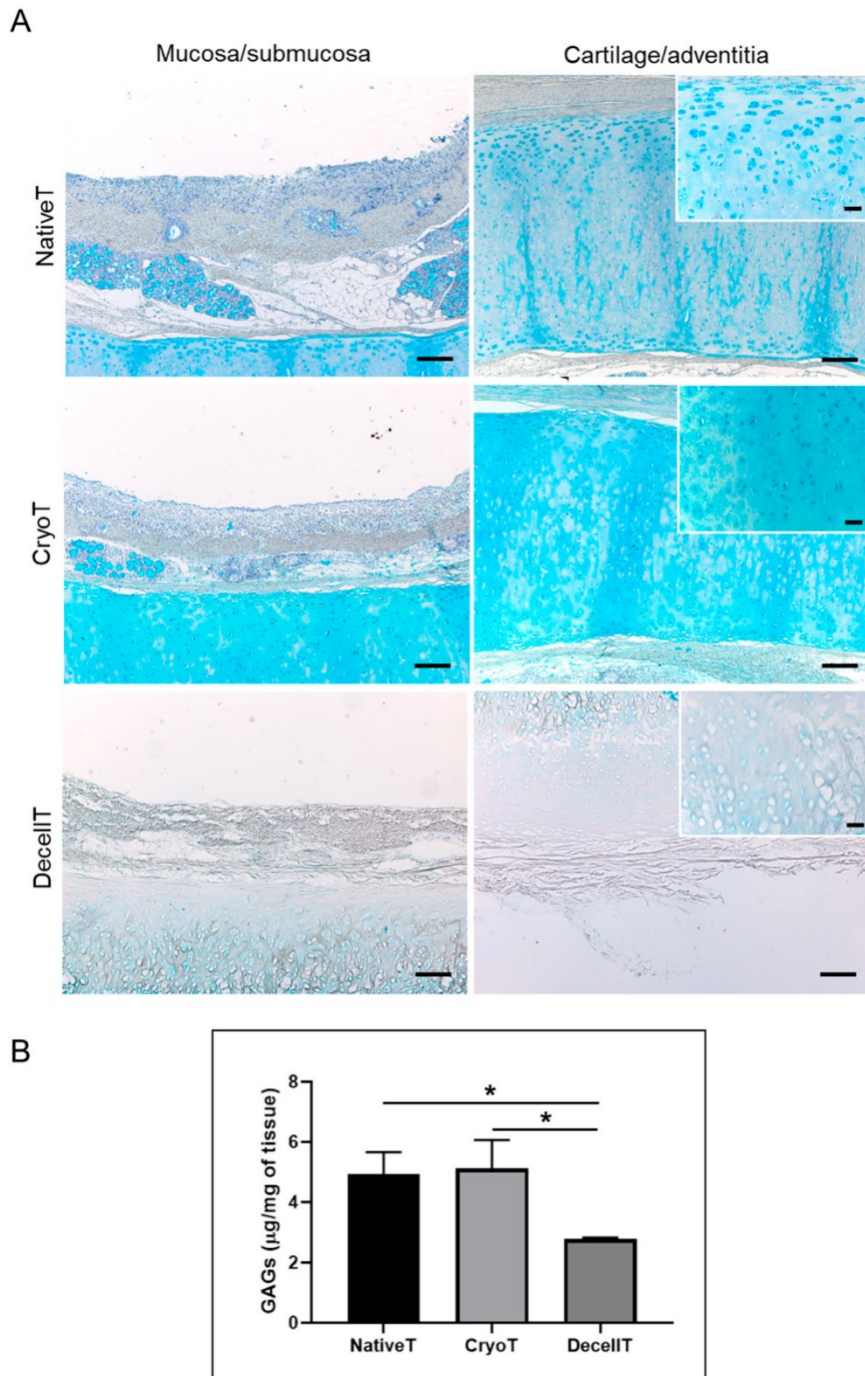

Fig. 6: Histological characterization of NativeT, CryoT and DeCellT sections stained with Alcian Blue staining, with the respective GAGs' quantification (*: p < 0.05).

Collagen distribution was evaluated through Masson's trichrome and Picrosirius Red stainings. The first staining allowed for the visualization of collagen's overall distribution within the tissue. At the hyaline cartilage level, collagen appeared as uniformly rapresented, with no significant differences between the three groups. This observation was further proved by the quantitative analysis (90.71 ± 1.79% for NativeT; 83.27 ± 14.30% for CryoT, and 84.41 ± 7.95% for DeCellT). Conversely, the DecellT group exhibited statistically

higher total collagen values within the mucosa/submucosa region and adventitia in comparison to the other two groups. In terms of the mucosa/submucosa compartment, the values were as follows: DecellT: 37.48 ± 2.99%; NativeT: 14.44 ± 2.59%; CryoT: 13.12 ± 6.61%. As for the adventitia, the percentages were: DecellT: 39.83 ± 3.73%; CryoT: 38.37 ± 4.18%; NativeT: 25.07 ± 5.23% (with a significance of $p < 0.05$). (Fig. 7)
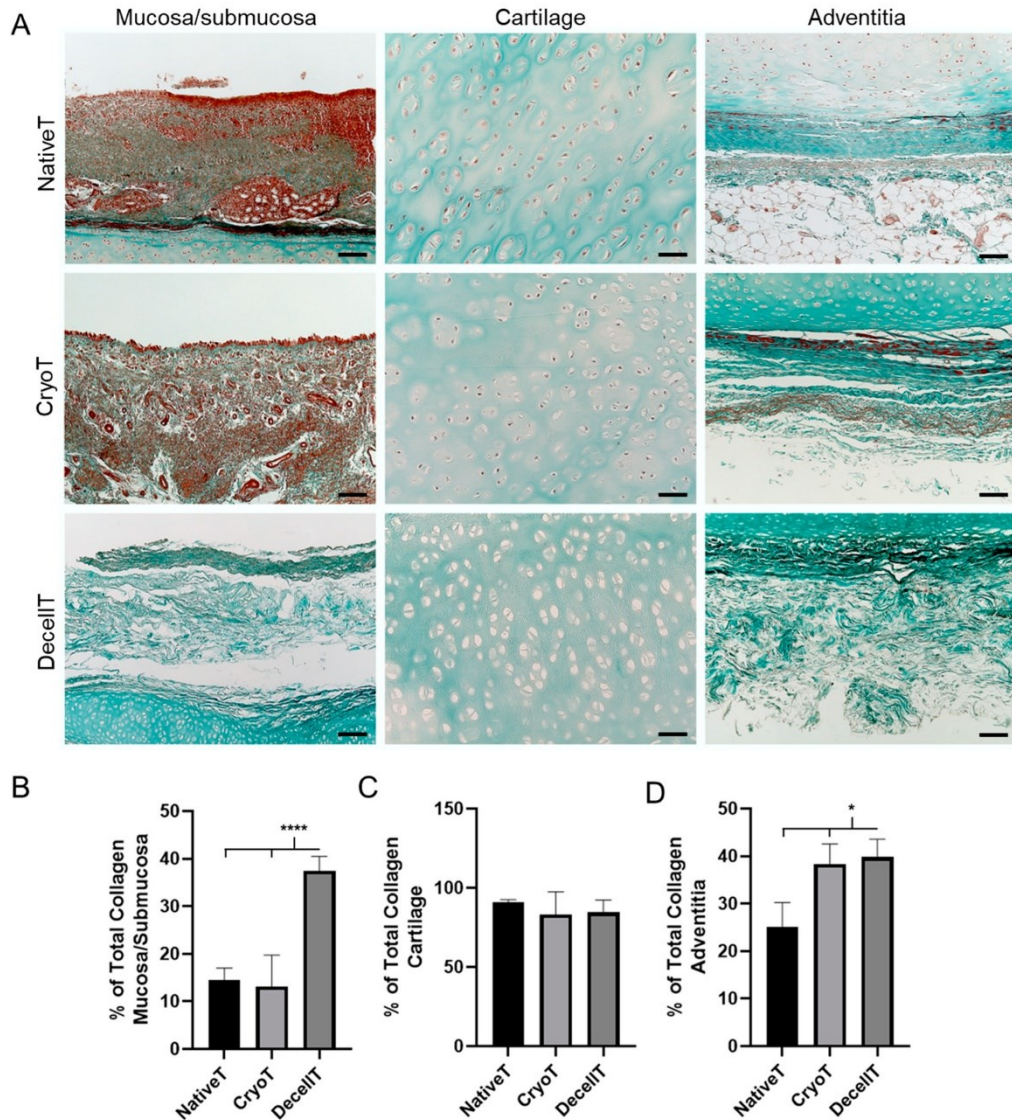

Fig. 7: Histological characterization of NativeT, CryoT and DeCellT sections stained with Masson's Trichome staining; with the respective collagen quantification in the mucosa/submucosa, cartilagineous compartment and adventitia. (*: $p < 0.05$; ****: $p < 0.0001$).

Picrosirius Red staining was employed to specifically recognize collagen type I (orange-red) and type III (green) fibers, utilizing the technique of polarized light microscopy. A prominent presence of collagen type I was detected in the mucosa/submucosa, perichondrium and adventitia across all three groups. Notably, the DecellT specimens exhibited a distribution of collagen type I also within the cartilaginous compartment. On the contrary, collagen type III was less evident here.

Quantitative analysis within the mucosa/submucosa/cartilage compartments highlighted that DecellT samples exhibited a statistically significant lower amount of collagen type I and III in comparison to the CryoT group (type I: $3.85 \pm 1.04\%$ and $8.41 \pm 2.05\%$, respectively; type III: $1.20 \pm 0.68\%$ and $4.15 \pm 1.01\%$, respectively). On the contrary, moving to the adventitia, the DecellT group displayed higher values for both collagen type I and type III compared to the other groups. Although the difference was not statistically significant for collagen type I (NativeT: $11.08 \pm 3.14\%$; CryoT: $13.89 \pm 4.06\%$; DecellT: $17.46 \pm 2.48\%$), it was ($p < 0.01$) when comparing DecellT ($21.22 \pm 2.26\%$) with CryoT ($10.48 \pm 3.08\%$) and NativeT ($8.32 \pm 2.82\%$), respectively. (Fig. 8)
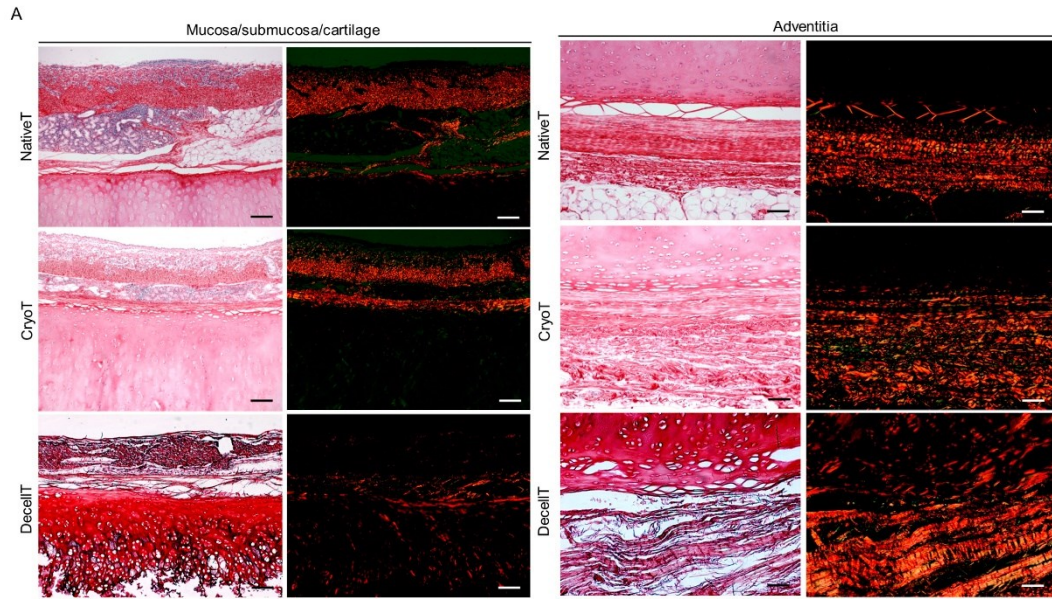

Fig. 8: Histological characterization of NativeT, CryoT and DeCellT sections stained with Picrosirius Red staining (left) and visualized under polarized light microscopy (right)

Weigert Van Gieson staining was used to investigate the elastic fibers content. Generally, they are primarily packed within the lamina elastica, the layer of tissue that separates the mucosa from the submucosa. Additionally, elastic fibers can be situated beneath the epithelial layer, on gland surfaces, and along the cartilaginous ring. Within the CryoT samples, the arrangement of elastic fibers resembled their natural configuration. In contrast, in the DecellT tissues the elastic fibers' content was altered, and the only remnants were observable in the lamina elastica as well as in the deeper and outer layers of the cartilaginous ring. (Fig. 9)

In terms of quantitative analyses, the DecellT samples had the lowest elastic fibers content (mucosa/submucosa: $0.99 \pm 0.41\%$; adventitia: $0.42 \pm 0.19\%$) within the cohort. Conversely, the CryoT samples showed a higher elastic fiber content (mucosa/submucosa: $5.15 \pm 0.94\%$; adventitia: $2.02 \pm 0.25\%$) in comparison to the DecellT samples but lower than the NativeT samples (mucosa/submucosa: $6.67 \pm 0.64\%$; adventitia: $3.72 \pm 0.43\%$).
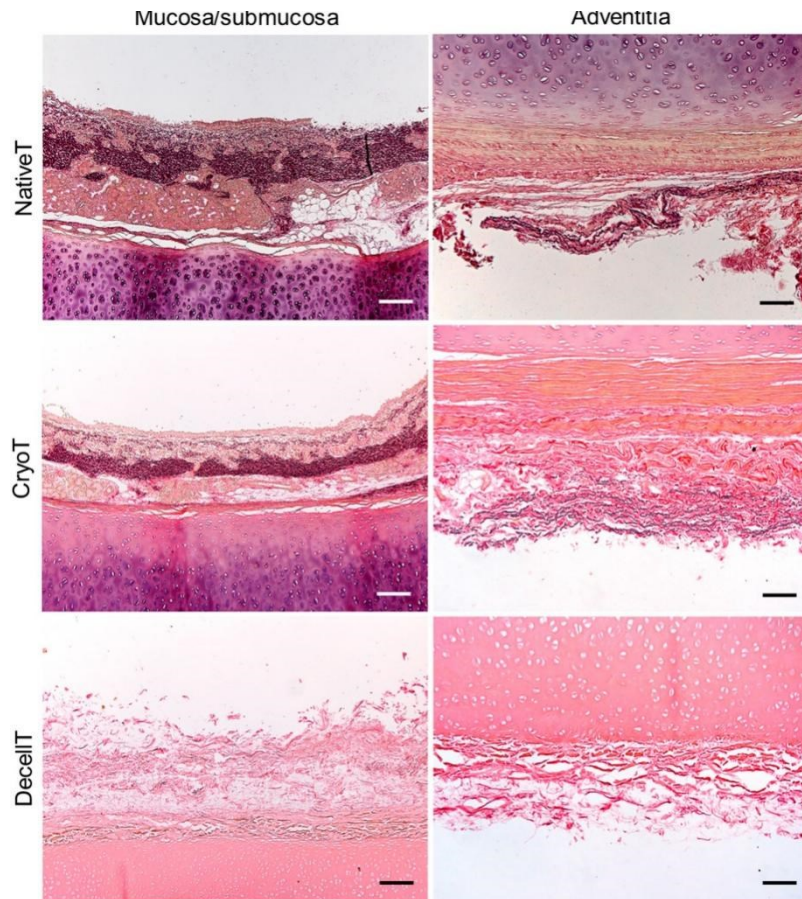
Fig. 9: Histological characterization of NativeT, CryoT and DeCellT sections stained with Weigert Van Gieson staining.

5.4. Characterization of the grafts' ultrastructure

Scanning electron microscopy was employed to examine the ultrastructural composition of both the respiratory epithelium and adventitia in the specimens.

NativeT displayed the distinctive characteristics of a standard respiratory epithelium: complete with intact cilia and microvilli. In contrast, CryoT and DecellT presented altered ultrastructure because of the processes they underwent to. CryoT samples showed a notable level of de-epithelization with significant loss of cilia. In the DecellT the epithelium was completely removed, but a disorganized basal membrane remained identifiable. As for the adventitia, the CryoT samples exhibited no significant differences compared to the native tissues. In contrast, within the DecellT samples, while the collagen fibers remained distinguishable, they presented partial fusion possibly ascribable the treatment they underwent to.

5.5. The two grafts show different mechanical properties

ECM morpho-structural alteration likely impact on the grafts' mechanical properties. To evaluate the retention of tracheal biomechanics, a compression test was conducted. The outcomes were presented through a compression curve, representing the force per unit of length of the sample (f) against the tracheal compressive deformation (s) in the proximal-distal direction (Fig. 10A). The response to compression was quite comparable between the NativeT and CryoT samples. On contrary, the DecellT, showed the tendency to undergo a compression deformation of 50% with a reduced force applied per unit of length, thus

suggesting a notably reduction in stiffness. (Fig 10B) Indeed, when comparing the values of compressive stiffness, a significant distinction was highlighted between the DecellT and NativeT samples ($p < 0.05$) . (Fig 10C)
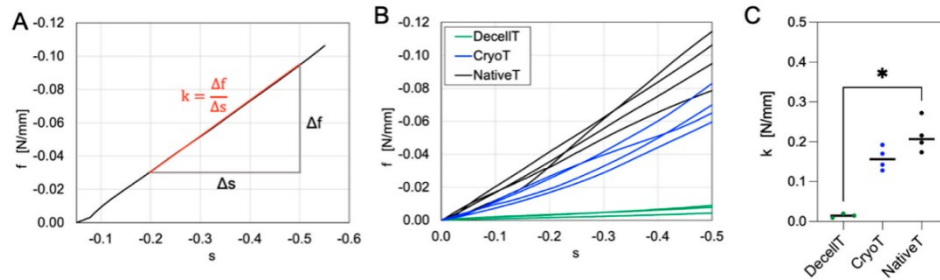

Fig. 10: (A) The general compression curve; stiffness was evaluated using the compressive modulus (k), derived from the slope of the secant line at 20% and 50% compression. **(B)** The compression curve of the three groups. **(C)** Comparison of the values obtained from the three groups

5.6. Cytocompatibility of the grafts

To evaluate the potential cytotoxicity of cryopreserved and decellularized tracheal tissues, HM1-SV40 cells were cultivated for a 24-hour period in a culture medium derived from tissue extracts. Subsequently, these cells were analyzed through microscopic observation and an MTT assay. Under microscopic examination, the cells did not exhibit any modification in morphology, viability, and ability to grow. Furthermore, the MTT assay results highlighted that their total number exceeded the threshold of 70%, suggesting that the cells were exposed to a non-cytotoxic medium (77.3% for the cryopreserved samples and 99.8% for the decellularized samples).The cytocompatibility was furtherly assessed by direct cells seeding over CryoT and DecellT samples followed by SEM analysis. After 3 days of culture, the ability of cells to adhere was already evident; at day 7 a notable increase in the number of attached cells was observed, proving their ability to proliferate over the support. (Fig. 11)
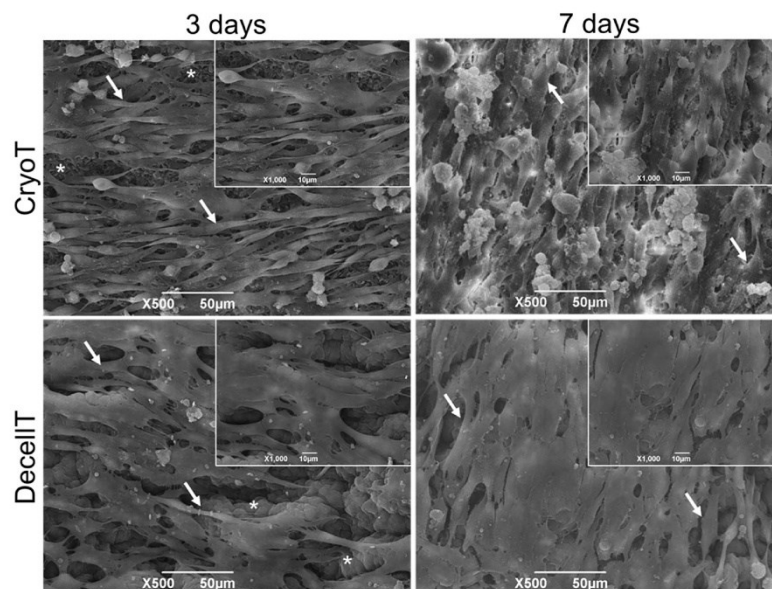

Fig. 11: SEM analysis showing cells adhesion and proliferation on the CryoT and DecellT surface.

5.7. Biocompatibility of the grafts

To assess *in vivo* biocompatibility, DecellT and CryoT specimens were implanted in female Balb/C mice (subcutaneous implant) and evaluated after14 days, by histology, immunohistochemistry and SEM.

As evidenced by H&E and Alcian Blue staining, the cartilaginous compartment remained intact, and it was easily recognizable in all sections with no evident alterations. Regarding the periphery of the implants, there was a mild host response in both groups, which is compatible with the nature of the surgical procedure. The connective tissue layer surrounding the implants (rich in elastic fibers as shown by Weigert Van Gieson staining) exhibited similar properties in both CryoT and DecellT samples, although the sheath was slightly thicker in the CryoT group at the mucosa-latissimus dorsi muscle interface. This difference may indicate a variation in the host's response to the two types of implants in this specific region. Through the use of Von Kossa, it was possible to verify the absence of potential calcification of the specimens after implantation (at both the subcutis-cartilage and the mucosa-latissimus dorsi muscle interface). (Fig. 12)
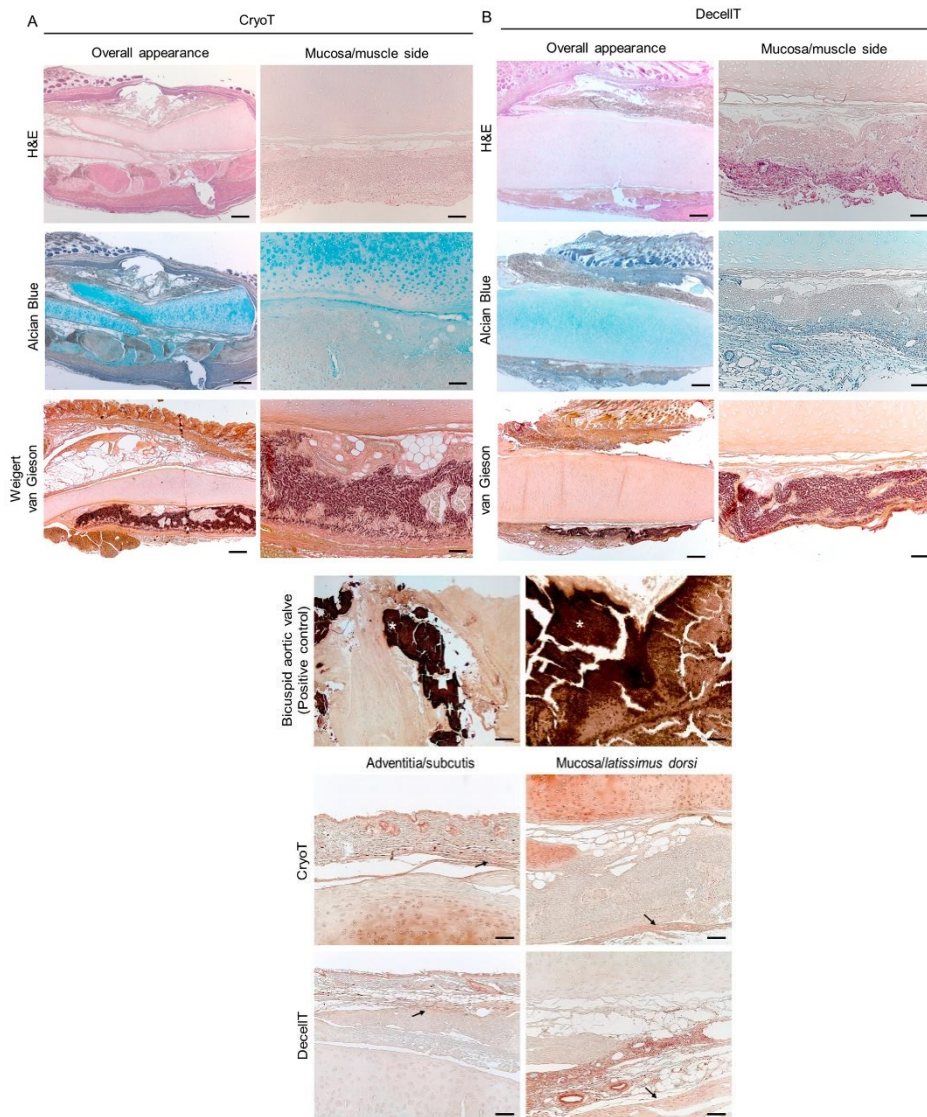

Fig. 12: Histological characterization of CryoT (A) and DeCellT (B) explants stained with Haematoxylin end Eosin, Alcian Blue and Weigert van Gieson. (C) Histological characterization of the subcutis-cartilage and the mucosa-latissimus dorsi muscle interface of the CryoT and DecellT explants by von Kossa staining.

The presence of inflammatory cells (lymphocytes and macrophages) was assessed through the use of anti-CD3 and anti-F4/80 immunostaining. As expected , mild lympho-monocytic infiltration was found at the level of the connective tissue surrounding the implants. Subsequently, the amount of CD3-positive and F4/80-positive components was determined highlighting no significant disparities between the CryoT group (CD3: 2.43 ± 0.42%; F4/80: 2.26 ± 0.85%) and the DecellT group (CD3: 3.11 ± 1.50%; F4/80: 2.58 ± 0.61%). (Fig. 13)
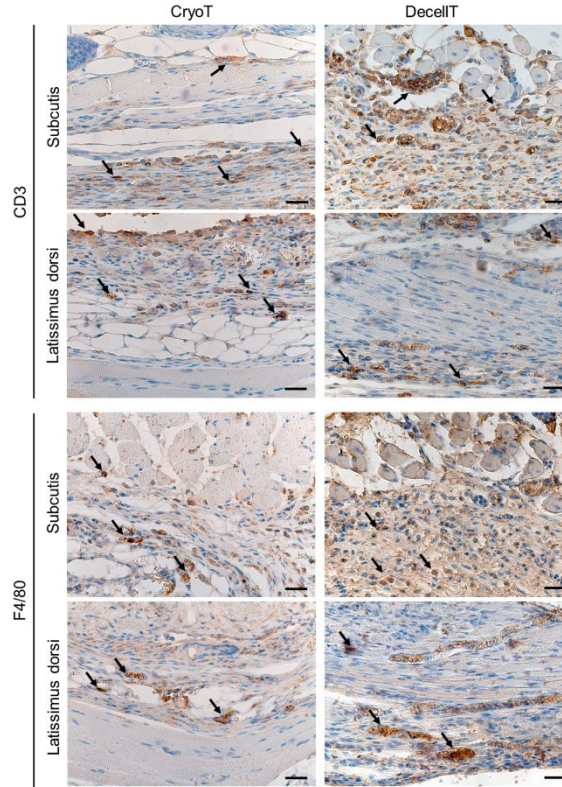
Fig. 13: The detection of CD3+ and F4/80+ cells (identifiable by their brown-stained appearance and indicated by black arrows) is observed at the interfaces connecting the tracheal samples with the surrounding host tissues.

Finally, SEM analysis was conducted to analyse the ultrastructure of the explants. The CryoT samples displayed numerous cellular components along the respiratory epithelium side. These cells were either combined in a single layer or had a rounded appearance. Conversely, on the side facing the adventitia, there were minimal host cells present. In contrast, the DecellT were extensively populated by host cells on both sides of the explants. (Fig. 14)

Fig. 14: SEM analysis of CryoT and DecellT explants

5.8. Discussion

The field of tracheal substitutes has been marked by many challenges in finding suitable solutions that combine structural integrity and immunocompatibility. The study presented in this thesis provide a characterization of two potential approaches for tracheal substitutes: cryopreservation and decellularization.
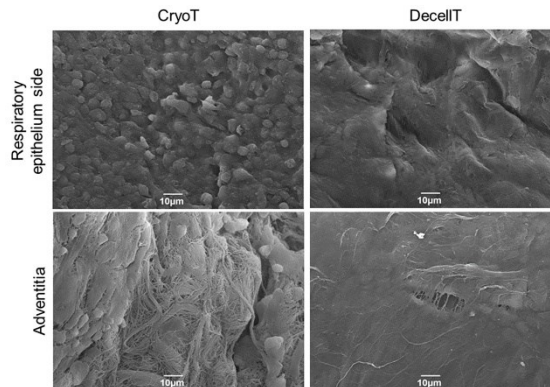
Cryopreservation has been shown to maintain the native tissue characteristics in ECM ultrastructure and composition, with only minor alterations. Moreover, CryoT samples exhibited a surprisingly reduction in genetic material despite the limited tissue manipulation required for the process. This suggests that cryopreservation has the potential to modify the antigenicity of the tissue; therefore, the modulation of freezing and thawing periods might further decrease the tissue's potential to trigger an immune response. Conversely, contrasting evidence has indicated that extended periods of cryopreservation may not impact the viability of chondrocytes and, consequently, the allogenicity of tracheal tissue. So, it remains important to confirm the immunomodulatory effect of cryopreservation on tracheal allografts for their future use in the clinical application of tracheal transplantation.

On the other hand, decellularization has been proven to be efficient in removing cellular components and xeno-antigens. However, it led to alterations in tissue composition, particularly in GAGs' reduction, which are essential for tissue mechanics and signaling. Increasing the number of decellularization cycles or using a more aggressive approach improves the removal of cellular portions but also raises the risk of damaging the ECM. In consideration of this, the possibility of generating a scaffold that is not entirely decellularized but in which the immunogenic cells are removed, and the "immune-privileged" chondrocytes are partly maintained, is under investigation.

The cytocompatibility assessment demonstrated that both CryoT and DecellT supported cell adhesion and colonization. This is promising for the potential of these substitutes to be repopulated by cells prior to be implanted and/or *in situ* after transplantation. The results of the subcutaneous implantation also indicated a comparable immune response by both substitutes, suggesting that neither approach induced excessive inflammation.

In conclusion, the study results confirm that trachea allograft/xenograft may be both worthy options, but further preclinical studies, especially in large animals, are needed to determine their outcomes in the clinical application. Integrating cryopreservation and decellularization techniques may offer a synergistic approach that resolves the limitations of each method and open the way for more effective tracheal reconstruction strategies.

6. REFERENCES

1. Mieczkowski, B., & Seavey, B. F. (2023). Anatomy, Head and Neck, Trachea. In *StatPearls*. StatPearls Publishing.
2. Farley, L. S., & Schlicksup, K. E. (2023). Tracheal Injury. In *StatPearls*. StatPearls Publishing.
3. Walton, S., & Rogers, D. (2022). Tracheal Reconstruction. In *StatPearls*. StatPearls Publishing.
4. Ayub, A., Al-Ayoubi, A. M., & Bhora, F. Y. (2017). Stents for airway strictures: Selection and results. *Journal of Thoracic Disease*, 9(Suppl 2), S116.
5. Stocco, E., *et* al, (2023). Preclinical and clinical orthotopic transplantation of decellularized/engineered tracheal scaffolds: A systematic literature review. *Journal of tissue engineering*, *14*, 20417314231151826.
6. Etienne, H., *et* al, (2018). Tracheal replacement. The *European respiratory journal*, 51(2), 1702211.
7. Jang, T. H., Park, S. C., Yang, J. H., Kim, J. Y., Seok, J. H., Park, U. S., Choi, C. W., Lee, S. R., & Han, J. (2017). Cryopreservation and its clinical applications. *Integrative medicine research*, 6(1), 12–18.
8. Stocco, E., *et* al, (2023). Development and In Vitro/In vivo Comparative Characterization of Cryopreserved and Decellularized Tracheal Grafts. *Cells*, 12(6), 888.
9. Nguyen, J. N. T., & Harbison, A. M. (2017). Scanning Electron Microscopy Sample Preparation and Imaging. *Methods in molecular biology (Clifton, N.J.)*, *1606*, 71–84.
10. Riss, T. L., Moravec, R. A., Niles, A. L., Duellman, S., Benink, H. A., Worzella, T. J., & Minor, L. (2013). Cell Viability Assays. In S. Markossian (Eds.) et. al., *Assay Guidance Manual*. Eli Lilly & Company and the National Center for Advancing Translational Sciences.

Development and In Vitro/In Vivo Comparative Characterization of Cryopreserved and Decellularized Tracheal Grafts

Elena Stocco [1,2,3], Silvia Barbon [1,2,3,*], Marco Mammana [2,4], Diletta Trojan [5], Alice Bianchin [5], Francesca Favaretto [5], Martina Contran [1], Giovanni Zambello [4], Andrea Vogliardi [6], Marta Confalonieri [7], Silvia Todros [7], Piero G. Pavan [7,8], Filippo Romanato [2,6], Maria Teresa Conconi [9], Veronica Macchi [1,2,3], Raffaele De Caro [1,2,3,*], Federico Rea [2,4] and Andrea Porzionato [1,2,3]

1 Section of Human Anatomy, Department of Neuroscience, University of Padova, 35121 Padova, Italy
2 L.i.f.e.L.a.b. Program, Consorzio per la Ricerca Sanitaria (CORIS), Veneto Region, 35128 Padova, Italy
3 Foundation for Biology and Regenerative Medicine, Tissue Engineering and Signaling-TES, Onlus, 35136 Padova, Italy
4 Thoracic Surgery Division, Department of Cardiac, Thoracic, Vascular Sciences and Public Health, Padova University Hospital, Via Giustiniani, 2, 35128 Padova, Italy
5 Tissue Bank, Fondazione Banca dei Tessuti del Veneto ETS, 31100 Treviso, Italy
6 Department of Physics and Astronomy 'G. Galilei', University of Padova, 35131 Padova, Italy
7 Department of Industrial Engineering, University of Padova, 35131 Padova, Italy
8 Fondazione Istituto di Ricerca Pediatrica Città della Speranza, 35127 Padova, Italy
9 Department of Pharmaceutical and Pharmacological Sciences, University of Padova, 35131 Padova, Italy
* Correspondence: silvia.barbon@unipd.it (S.B.); raffaele.decaro@unipd.it (R.D.C.); Tel.: +39-049-827-2325 (S.B.); +39-049-827-2321 (R.D.C.)

Abstract: Tracheal reconstruction represents a challenge when primary anastomosis is not feasible. Within this scenario, the study aim was to develop a new pig-derived decellularized trachea (DecellT) to be compared with the cryopreserved counterpart (CryoT) for a close predictive analysis. Tracheal segments underwent decellularization by a *physical + enzymatic + chemical* method (12 cycles); in parallel, cryopreserved samples were also prepared. Once decellularized (histology/DNA quantification), the two groups were characterized for Alpha-Gal epitopes/structural proteins (immunohistochemistry/histology/biochemical assays/second harmonic generation microscopy)/ultrastructure (Scanning Electron Microscopy (SEM))/mechanical behaviour. Cytotoxicity absence was assessed in vitro (extract-test assay/direct seeding, HM1SV40 cell line) while biocompatibility was verified in BALB/c mice, followed by histological/immunohistochemical analyses and SEM (14 days). Decellularization effectively removed Alpha-Gal epitopes; cartilage histoarchitecture was retained in both groups, showing chondrocytes only in the CryoT. Cryopreservation maintained few respiratory epithelium sparse cilia, not detectable in DecellT. Focusing on ECM, preserved structural/ultrastructural organization and collagen content were observed in the cartilage of both; conversely, the GAGs were significantly reduced in DecellT, as confirmed by mechanical study results. No cytotoxicity was highlighted by CryoT/DecellT in vitro, as they were also corroborated by a biocompatibility assay. Despite some limitations (cells presence/GAGs reduction), CryoT/DecellT are both appealing options, which warrant further investigation in comparative in vivo studies.

Keywords: trachea; decellularization; cryopreservation; tracheal cartilage; respiratory epithelium; immunogenicity; tissue engineering

1. Introduction

Tracheal resection with primary end-to-end anastomosis (TRA) is the treatment of choice for several conditions leading to airway narrowing (e.g., trauma, infections, tumor growth, softening, and congenital tracheal stenosis). However, this therapeutic option is not applicable if the affected length exceeds 50% of the trachea in adults and 30% in children, being associated with high risk of suture tension and anastomosis failure [1,2].

To date, surgical management of patients suffering from severe tracheal lesions (mainly neoplastic), that are not eligible for TRA, still represents a significant challenge; endotracheal stents, tracheostomy tubes or Montgomery T-tubes are the only established treatment option in such clinical conditions, even though infection, stent migration, mucous plugging, or granulation tissue formation are common [1]. Within this scenario, intense efforts have been devoted towards the identification of an effective tracheal circumferential substitute. The requirements include lateral stiffness with longitudinal flexibility, adequate and airtight lumen, biocompatibility with low toxic/immunogenic effects, instructive behaviour for epithelial cell growth, and integration into adjacent tissues [3–6].

Graft characteristics directly affect the clinical outcome of the implant; hence, trying to address the "ideal substitute" needs, several synthetic prostheses (Dacron, polyurethane mesh, polytetrafluoroethylene, polypropylene mesh, silicone rubber, and even glass tubes [7]), autologous tissues composites (e.g., free periosteal, jejunal, muscular, oesophageal, bronchial and aortic grafts [8]), tracheal transplantation, allografts, and tissue engineering-based devices have been attempted for trachea reconstruction over the years. Unfortunately, none distinguished among the others for fully satisfactory outcomes in vivo [9–11]. Scar tissue formation with graft stenosis and obstruction, not adequate biomechanical characteristics, required stenting to avoid collapse, lifelong immunosuppressive therapies, and technical surgical challenges were included among the main critical issues [12]. Additionally, as supported by preclinical and early clinical evidence, incomplete or even absent re-epithelization of the graft was possibly encountered, responsible for impaired mucus clearance, recurrent infections, and consequent implant failure [13,14]. Despite the need for further investigation, two alternatives may be promising due to a specific anatomical origin and possibly reduced/absent immunogenicity, which also makes them suitable for cancer patients who cannot tolerate immunosuppressive therapies [15]. These include the cryopreserved tracheal allografts and the decellularized tracheal substitutes.

Cryopreservation is one of the most common procedures for allografts storage. After freezing by a thermally controlled procedure in the presence of a cryoprotectant, the tissue is preserved in vapor phase liquid nitrogen for a determined period (according to validations or directives), prior to being thawed under controlled warming conditions before use [7]. Several cryopreserved tissues are currently available in clinical practice including, for instance, amniotic membrane [16], bone [17], menisci [18], vascular tissues [19,20], and heart valves [21,22]. Cryopreserved tracheas show a native-like tubular structure, maintaining histological characteristics and mechanical properties and possibly reducing immunogenicity. This event occurs as a consequence of class II leukocyte antigen expression depletion, due to tracheal epithelium exfoliation during the freezing and thawing [23–25]. There is consensus in identifying the respiratory epithelium and lamina propria as the main targets for rejection; thus, cryopreservation, altering their integrity, may be a strategy of interest triggering a decline in allograft antigenicity. However, the overall procedure-related effects are still disputed due to conflicting evidence ascribable to preserved tracheal cartilage viability (chondrocytes are immunoprivileged) as well as epithelium and lamina propria partial maintenance [8,25–27]. According to our knowledge, despite sounding promising, the use of cryopreserved (−70 °C) (and irradiated) tracheal homograft in humans was only reported by Kunachak et al. [28] for cervical laryngotracheal reconstruction in four patients (follow-up: 18–20 months). No significant evidence of immunologic rejection was observed, even though a larger series and a longer follow-up time are required.

Decellularization is a common method for preparing tissue-engineered tracheal scaffolds that ideally retain mechanical properties, lumen patency, and support epithelial cell growth and angiogenesis, without triggering an immunogenic response thanks to the cellular components removal [25,29,30]. A wide variety of approaches are available based on physical, enzymatic, and chemical strategies. Briefly: physical treatments or ionic solutions induce breaking of the cell membrane; enzymatic treatments separate cellular components from the ECM; detergents solubilize the cytoplasmic components. Intensive washes with deionized water are also adopted to remove cellular debris [11]. Currently, a

great debate exists over the "decellularization grade": completely acellular supports and partially decellularized supports (removal of immunogenic cells and immunoprivileged chondrocytes preservation) are both under consideration [2,31–33]. A higher cells' removal is associated with a lower risk in immune/inflammatory responses; however, maintenance of the structural/ultrastructural features and density of the target tissue are also key elements of an efficient decellularization protocol [34]. To date, clinical transplantation of a decellularized and bioengineered tracheal allograft is a procedure still considered as compassionate [35,36].

Despite both being appealing, consensus over the optimal strategy is still lacking [37]. Several knowledge gaps exist about the effects of cryopreservation and thawing on tracheal tissue cell viability, immunogenicity, and extracellular matrix features [38]; furthermore, recurring to decellularization methods gives rise to several questions mainly related to ECM features and ultrastructural modification descending from the impact of potential "aggressive" protocols towards ultrastructure integrity. Hence, the aim of this study was to develop and describe pig-derived tracheal grafts obtained by cryopreservation and decellularization for a close comparison over tissue structural and ultrastructural features, ECM characteristics, eventual cytotoxicity descending from the preparation protocols, and biocompatibility in vivo. The results can be predictive for device outcomes after orthotopic implantation.

2. Materials and Methods

2.1. Tracheal Isolation

Donor tracheae were harvested from adult pigs (*n* = 10) weighing approximately 130 kg. The animals were sacrificed and the entire airway from the larynx to the lungs was extracted en bloc with the oesophagus. Then, two tracheal segments per animal, of approximatively 5 cm in length, were carefully isolated, cleaned from mucus, and put into antibiotic solution composed of BASE medium (Alchimia S.r.l., Ponte San Nicolò, Padova, Italy), gentamicin 200 µg/mL (Fisiopharma, Palomonte, Salerno, Italy), vancomycin 100 µg/mL (Fisiopharma) and meropenem 200 µg/mL (Venus Pharma, Werne, Germany) at +2 °C/+8 °C.

The two segments were intended for cryopreservation and decellularization, respectively; however, as for control, samples of 1 cm in length/animal were excised from tracts assigned to decellularization and properly fixed for subsequent comparative analyses.

2.2. Tracheal Cryopreservation

Cryopreservation of the tracheal segments (*n* = 10) was carried out by the tissue bank "Fondazione Banca dei Tessuti del Veneto ONLUS" (FBTV), in accordance with the requirements approved by the National Transplant Centre and following a method previously described [39]. Briefly, after the first overnight decontamination, the segments were again cleaned from mucus, valuated in their integrity, and further decontaminated with the same antibiotic cocktail composed of BASE medium (Alchimia S.r.l.), gentamicin (Fisiopharma), vancomycin (Fisiopharma), and meropenem (Venus Pharma) at +2 °C/+4 °C for at least 48 h [40,41]. At the end of the second decontamination step, tissues were immersed and washed in sterile saline solution for at least 5 min (min). Samples of the washing solutions were sent to Istituto Zooprofilattico Sperimentale delle Venezie to verify the absence of contaminants. Hence, before cryopreservation, the tracheas were placed within low temperature-resistant ethylene-vinyl acetate bags with a solution composed of BASE medium (Alchimia S.r.l.), 10% dimethylsulfoxide (DMSO) (Wak-Chemie Medical GmbH, Steinbach (Taunus), Germany), and 10% human serum albumin (Alburex 20%, CSL Behring GmbH, Milano, Italy). Cryopreservation was performed by means of a programmable cryogenic freezer (Planer KryoSave Integra, 750-30; Planer Limited, Middlesex, UK), which triggered a controlled cooling rate up to −140 °C. Tissues were stored at temperatures below −160 °C in liquid nitrogen vapor phase and thawed before use [42,43].

All procedures were carried out under a laminar flow hood; sterile disposable materials and solutions were used to avoid tissue contamination.

2.3. Tracheal Decellularization

The tracheal segments were decellularized according to a partially modified Tergitol™-based method, previously described by Barbon et al. [44,45]. Briefly, the samples (*n* = 10) were preliminarily decontaminated through 3 washes of 30 min each in a 2% P/S solution in sterile dH$_2$O (+4 °C, under stirring). Hence, they underwent a physical + enzymatic + chemical treatment protocol providing for: (i) tissues freezing (−20 °C/12 h) and lyophilization (12 h) (FreeZone 2.5 Liter Benchtop Freeze Dryer, Labconco™, Kansas City, MO, USA); (ii) enzymatic treatment with Deoxyribonuclease I (10,000 Kunitz units of DNase-I from bovine pancreas-5VL, Sigma Aldrich, St. Louis, MI, USA) in 1M sodium chloride (NaCl) solution (room temperature (RT)/6 h); washing with dH$_2$O and treatment with 0.05% trypsin + 0.02% EDTA enzymatic solution in dH$_2$O (37 °C/1 h), followed by extensive rinsing in dH$_2$O; (iii) washing with 2% Tergitol™ detergent solution + 0.8% ammonium hydroxide (NH$_4$OH) in dH$_2$O (+4 °C/3 days, under stirring); (iv) washing with dH$_2$O (+4 °C/2 days, under stirring) (1 cycle included the phases i–iv).

After phase (iv), the samples were frozen at −20 °C prior to being lyophilized as in (i). To obtain acellular tracheal segments, the decellularization was repeated for 12 cycles. At the end of the decellularization, the lyophilized segments were stored at −20 °C until their use.

Each phase involving tissue manipulation was performed under a second level biological hood; sterile filtered/autoclaved solutions and sterile disposable material were used with the aim of preventing any contamination.

2.4. 4′,6-Diamidino-2-Phenylindole Nuclear Staining

Cryopreserved and decellularized tracheal tissues were compared to native trachea by a fluorescence analysis based on 4′,6-Diamidino-2-Phenylindole (DAPI) aiming to assess nuclei presence/distribution. The epithelial layer, the mucosa, and submucosa layers and the cartilaginous compartments were all considered, for a full-thickness description of the tissue. Briefly, small tissue samples were excised, Optimal Cutting Temperature (OCT) medium embedded and frozen prior to being cut into 5 μm thick sections using a cryomicrotome (Leica CM 1850 UV; Leica Microsystems, Wetzlar, Germany); hence, the sections were fixed with acetone, mounted with Vectashield mounting medium for fluorescence with DAPI (Vector Laboratories, Burlingame, CA, USA) and photomicrographs were acquired with a Leica LMD6 (Leica Microsystems) connected to a Leica DFC320 high-resolution digital camera (Leica Microsystems) and a computer equipped with software for image acquisition (LasX, Leica Microsystems).

2.5. DNA Extraction and Quantification

Together with DAPI, DNA quantification was also performed to verify in which extent the immunogenic material was detectable in cryopreserved and decellularized tracheas, versus native tissue; to this purpose, the DNeasy Blood and Tissue Kit (Qiagen, Düsseldorf, Germany) was used. Briefly, following the manufacturer's protocol, a certain weighted amount of tissue (10 mg) was Proteinase K (Merck Life Science, Darmstadt, Germany)-lysed at 56 °C, overnight. Hence, the lysates were loaded onto the DNeasy Mini spin columns, allowing for a total DNA selective purification, and the eluted DNA was finally quantified according to a fluorometric method using a Qubit 4 fluorometer and kit (ThermoFisher Scientific, Waltham, MA, USA). Three replicates/group were considered.

2.6. Alpha-Gal Epitope Detection

Superficial epitopes, such as Alpha-Gal, may trigger hyperacute and acute vascular rejection phenomena after xenograft positioning [46]. Hence, immunohistochemistry was adopted to verify if tissue treatments were able to mask or inactivate the epitope Alpha-Gal.

Tracheal samples were fixed in 10% formalin solution, paraffin-embedded and then cut into 3 μm thick sections. After dewaxing with a series of ethanol (Arco Scientifica S.r.l., Padova, Italy) solutions (99%, 95%, and 70%) and rehydrating in distilled water, immunohistochemical reaction was performed by Dako Autostainer/Autostainer Plus (Dako, Milan, Italy) with the anti-Alpha-Gal epitope primary antibody (monoclonal mouse anti-rabbit, LS-C63415, LSBio, Seattle, WA, USA). The binding between primary antibody and specific antigen was then revealed using a labeled polymer (EnVision™ FLEX-HRP; Dako) and 3,3'-diaminobenzidine (EnVision™ FLEX Substrate buffer + DAB + Chromogen; Dako). In the meanwhile, negative controls were developed without incubation with primary antibodies.

2.7. Histological Analyses

Formalin-fixed and paraffin-embedded sections (5 μm thickness) were dewaxed and rehydrated with a series of ethanol (Vetrotecnica, Padova, Italy) solutions (99%, 95%, 70%) before being stained according to laboratory routine protocols.

Haematoxylin and eosin (H&E) staining was adopted to verify cells nuclei presence/distribution (hematoxylin, deep blue-purple color) and ECM integrity (eosin, pink staining). Dewaxed and rehydrated tissue slices were immersed in hematoxylin for 1 min (Sigma-Aldrich, St. Louis, MO, USA), tap water for 5 min, and eosin (Sigma-Aldrich) for 1 min. The sections were then dehydrated in a series of ethanol (95% for 45 s (s) and 100% for 3 min (×2)), and finally immersed in xylene. Each section was then mounted with Eukitt (Merck LifeScience, Bayswater VIC, Australia).

Masson's Trichrome and Sirius Red staining allowed to evaluate the connective tissue, typically collagen fibers. Briefly, Masson's Trichrome staining was performed using the Masson trichrome staining kit (Bio-Optica, Milano, Italy), according to the manufacturer's instructions. The rehydrated sections were exposed to Weigert's iron haematoxylin (A solution) + Weigert's iron haematoxylin (B solution) (for 10 min); without washing, the slides were drained, and picric acid alcoholic stable solution (C solution) was poured on the sections and allowed to act (for 4 min). Thus, after a quick wash in distilled water (3–4 s), Ponceau acid fuchsin according to Masson (D solution) was added to the section (for 4 min). Following a wash in distilled water, phosphomolybdic acid solution was added to the section (E solution) (for 10 min). Without washing, the slides were drained and a light green solution according to Goldner (reagent F) was left to act (for 5 min). Finally, the sections were washed in distilled water, dehydrated, and cleared in xylene as previously described and mounted with Eukitt (Merck LifeScience). Regarding Sirius Red, rehydrated sections were immersed in Picrosirius Red solution (Sigma-Aldrich) for 30 min, washed in deionized acidified water (HCl, 0.1%), washed in deionized water and then dehydrated and cleared in xylene (like above) before mounting with Eukitt (Merck LifeScience).

Alcian-blue staining was conducted to assess the acidic mucins and the GAGs retained in the submucosa and in the cartilage/adventitia, respectively. According to the staining protocol, rehydrated sections were exposed to Alcian-blue solution (Sigma-Aldrich) for 30 min. Hence, the slices were washed with tap water for 2 min, counterstained with hematoxylin (Sigma-Aldrich) for cells nuclei detection, washed with tap water for 5 min, dehydrated and cleared in xylene prior to be mounted with Eukitt (Merck LifeScience).

Weigert Van Gieson staining aimed at demonstrating the preservation of elastic fibres; to this purpose, the Weigert Staining Kit for Elastic Fibers-Rapid Method (Bio-Optica) was used. Following the manufacturer's instructions, the rehydrated slices were exposed to periodic acid solution (A solution) for 5 min; after rinsing the samples in distilled water, an incubation box was prepared in which the alcoholic reagent for incubation (B solution) and the slides were dropped, covered with Weigert's resorcin fuchsin (C solution), were incubated into for 30 min; thereafter, the sections were rinsed in distilled water and exposed to the acid differentiation buffer (D solution) for 2 min. Once washed in tap water (5 min) and rinsed in distilled water, carmalum according to Mayer (E solution) was put on the

sections for 5 min before rinsing in distilled water. Dehydration, clearing in xylene and mounting with Eukitt (Merck LifeScience) occurred as previously described.

2.7.1. Morphometric Analyses

Semi-quantitative analysis of ECM elements in native, cryopreserved, and decellularized tracheas was performed by previously standardized protocols [45,47]. Photomicrographs were acquired under a Leica DM4500B microscope (Leica Microsystems) connected to a Leica DFC320 high-resolution digital camera (Leica Microsystems). An ImageJ software was used for quantifications as described below.

Semi-automatic immunoreactivity quantification (Alpha-Gal Epitopes) was calculated on an average of three ×20 magnification photomicrographs/section as previously established [48,49].

Collagen and elastic fibers were quantified as percentage areas stained in green (collagen) and purplish (elastin) with Masson's Trichrome and Weigert Van Gieson, respectively. Images of stained sections were acquired in bright field at a ×5 and ×10 magnification. Green and purplish areas were identified by displaying histograms of the distribution of hue, saturation and brightness and setting adequate thresholds for each of these parameters, which were maintained for all the morphometric analyses. Specific hue, saturation and brightness ranges were, respectively, 50–138, 0–255, and 0–185 for green colour (collagen) and 127–211, 0–255, and 0–185 for purplish colour (elastic fibers). The coloured area corresponding to collagen/elastic fibres were selected and automatically measured and results were finally presented as percentage areas stained in green/purplish out of the total area of the acquisition field.

At the same time, type I and III collagen content was quantified on Sirius red-stained sections. After acquiring images by polarized microscopy at ×5 magnification and saving them as TIFF files, red-orange and green-yellow areas were identified by setting adequate thresholds of the hue component. In particular, hue, saturation and brightness ranges were, respectively, 0–39, 189–255, and 60–203 for red-orange, 210–255, 78–255, and 60–150 for red and 39–120, 78–255, and 135–255 for green-yellow. Mean percentage red-orange and green-yellow areas out of the total area of the image were finally calculated to define collagen content in native, cryopreserved and decellularized tracheas.

2.8. Biochemical Assay for Glycosaminoglycans Quantification

The sulphated glycosaminoglycans (GAGs) were quantified through the Chondrex Inc. Glycosaminoglycans Assay Kit (DBA Italia S.r.l., Milan, Italy), following the Manufacturer instructions. Briefly, a weighted amount of tissue samples (10 mg) was preliminarily digested in Papain solution at 56 °C, overnight to induce GASs solubilization; hence, the solubilized GAGs were labeled by the cationic dye 1,9 dimethylmethylene blue (DMB) and the colorimetric reaction was read at 530 nm using a Microplate auto reader VICTOR3™ (PerkinElmer, Waltham, MA, USA).

Together with cryopreserved and decellularized trachea samples, chondroitin sulphate standard was also analysed to allow for GAGs quantification into the specimens.

2.9. Scanning Electron Microscopy

Tracheal tissues were analysed for their ultrastructure considering both the external and the luminal sides. The samples were fixed with 2.5% glutaraldehyde in 0.2 M phosphate buffer solution (PBS) (pH 7.4) for 24 h, washed 5 times in PBS to remove chemical residues and then dehydrated with a graded ethanol series. After critical point drying and gold sputtering, micrograph acquisition was performed by using the tungsten thermionic emission SEM system JSM-6490 (Jeol USA, Peabody, MA, USA).

2.10. Two Photon Microscopy

Second Harmonic Generation (SHG) imaging was performed through a custom developed multiphoton microscope [50]. Briefly, an incident wavelength of 800 nm (~40 mW

average laser power, under the microscope objective) was adopted to detect the collagen's SHG signal at 400 nm. The images were acquired at a fixed magnification through the Olympus 25× water immersion objective with 1.05 numerical aperture (1024 × 1024 pixels), averaged over 100 consecutive frames, with a pixel dwell time of 0.14 μs and a pixel width of 0.8 μm. Coherency (C) was determined to assess the local dominant orientation of collagen fibers; to achieve that, it was used the ImageJ plugin OrientationJ, [51]. The estimated parameter is bounded between 0 and 1, indicating, respectively, the absence (isotropy) and the presence (anisotropy) of the dominant orientation. A graphic representation of the coherency, showing organization and distribution of the fibres, is achieved by Fast Fourier Transform (FFT) analysis. The transform-based texture analysis techniques convert the image into a new form using the spatial frequency properties of the pixel intensity variations allowing the extraction of textural characteristics from the image. Highly oriented fibre in a single direction shows an elliptic shape; whether a circular shape represents fibre spread in all directions [44,45,47,50,52,53]. Five samples/group were considered in this analysis; for each sample, 5 different areas were analyzed.

2.11. Compressive Mechanical Tests

Segments of trachea from three donors (respectively, NativeT, DecellT and CryoT) were cut transversally into ring-like samples including three cartilaginous structures. At least three samples were obtained for each trachea. The shape and size of each sample were evaluated by measuring the medio-lateral and proximal-distal diameters (d_1 and d_2, respectively), the tracheal wall thickness t and the length of the segment L (Figure 1A), by means of the image analysis software Fiji [51]. Specifically, the mean thickness of each sample was obtained by measuring in the transversal view the shortest distance between the user-drawn inner lumen and outer outline in 30 randomly selected points (Figure 1B). These data were used to calculate the average wall thickness.
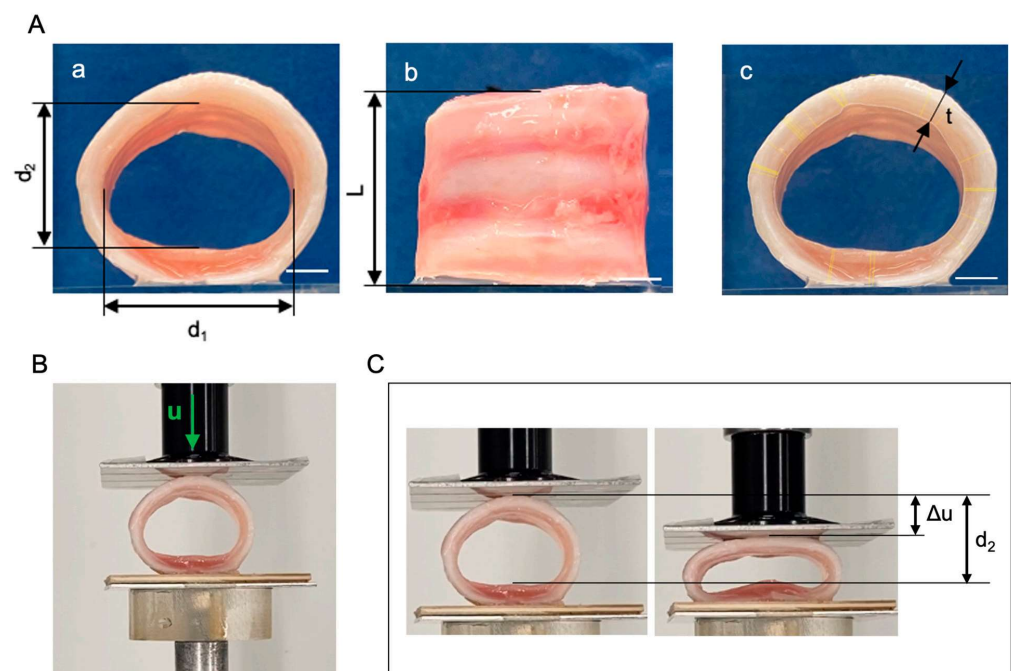

Figure 1. (**A**) Ring-like sample of trachea for mechanical testing, with measurements of the medio-lateral (d_1) and proximal-distal (d_2) diameters (**a**), the length of the segment L (**b**) and the tracheal wall thickness t (**c**). Yellow segments refer to the shortest distance between the inner and outer outline of the sample section in 30 random points. Scale bars = 5 mm. (**B**) Experimental set-up for compression tests with trachea sample between two flat plates. The displacement Δu of the upper plate is applied along the distal-proximal direction. (**C**) Undeformed and deformed trachea samples with reference to the plate displacement Δu and the initial diameter d_2.

Compression tests were carried out with Bose ElectroForce® Planar Biaxial Test Bench instrument (TA Instruments, New Castle, DE, USA) under displacement control, with a load cell of 22 N. Two flat plates were positioned parallel to each other (Figure 1C): samples were placed on the lower plate, leaning on the posterior tracheal wall, while the upper plate was gradually approached at a constant rate of 0.2 mm s^{-1}. Samples were compressed up to reducing of 50% the initial proximal-distal diameter. Tracheal compressive deformation s in the proximal–distal direction was measured as the ratio of the plate displacement Δu and the initial diameter d_2 (Figure 1D). To compare tracheal samples of different sizes, the force per unit of length of the sample f (in N mm^{-1}) was calculated as the ratio between the force value F measured by the load cell and the sample length L. The stiffness of the sample was estimated by considering the secant compressive modulus k, calculated as the slope of the straight line drawn from the experimental data at 20% and 50% compressive deformation. The values of the secant compressive modulus k were analyzed through Kruskal–Wallis nonparametric one-way Analysis of Variance (ANOVA) and post hoc comparison, considering as significant a *p*-value lower than 0.05.

2.12. Tissue Cytotoxicity and Biocompatibility

Tracheal tissue cytotoxicity and biocompatibility were assessed in vitro and in vivo, respectively.

Differently from the cryopreserved samples, acellular tissues were sterilized before the assays to exclude eventual contamination occurring during the decellularization process, as it implied extensive manipulation of the tissues. Briefly, the samples underwent three washes of 30 min each, in a 2% P/S solution in sterile dH$_2$O (+4 °C, under stirring), followed by exposure to UV light for 30 min/side.

2.12.1. In Vitro Cytotoxicity

3(4,5-dimethylthiazole-2-yl)-2,5-diphenyltetrazolium-bromide (MTT) (Merck Life Science) assay was performed to exclude cytotoxicity of cryopreserved and decellularized matrices, ascribable to chemical remnants adsorption and release. Considering the potential of mesenchymal stem cells (MSCs) for trachea regenerative purposes [54], human bone marrow-derived stromal cells (HM1-SV40, immortalized cell line) were used within this study.

Preliminarily, to obtain the tissue extracts, a weighted amount (400 mg) of decontaminated cryopreserved and decellularized tracheal samples were incubated in the HM1-SV40 cell proliferation medium (1 mL of medium/100 mg of tissue) consisting in Alpha-Modified Eagle Medium (α-MEM) (ThermoFisher Scientific), 16.5% of fetal bovine serum (FBS) (ThermoFisher Scientific), 1% glutamine (Merck Lifescience) and 1% penicillin/streptomycin solution (100 mg/mL) (Merck Lifescience). Incubation lasted 72 h at 37 °C (5% CO$_2$ and 95% humidity).

In parallel, 20,000 HM1-SV40 cells/well were seeded on 24-well culture plates (Corning). After 24 h, the cell culture medium was removed and replaced with the extract medium. As positive (cytotoxic) control, culture medium added with 50% dimethyl sulfoxide (DMSO; Sigma-Aldrich) was used, whereas the negative control was represented by untreated cultures. Both treated and controlled cultures were maintained for 24 h at 37 °C, 95% relative humidity and 5% CO$_2$. The effect of extract medium on cell survival was then evaluated by the MTT assay.

At the scheduled end-point, the cells were at first observed at the optical microscope and the culture medium was replaced with 0.5 mg/mL MTT in α-MEM for 4 h; hence, the formazan precipitates were dissolved by 2-propanol acid (0.04 M HCl in 2-propanol) and optical density of the solutions was measured at 570 nm with the Microplate Auto Reader VICTOR3™ (PerkinElmer). Results of the cytotoxicity test were expressed as percentages of viable and metabolically active cells in treated groups versus the untreated control, which was set as 100% cell viability. It was possible to infer the number of cells through an MTT standard curve, obtained as previously described [45].

2.12.2. Cell–Scaffold Interaction

Cytocompatibility of tracheal scaffolds was assessed also by investigating their ability to sustain the adhesion and proliferation of the immortalized human bone marrow cell line HM1-SV40. Cells were first expanded in culture by using proliferation medium (Section 2.12.1) until a sufficient number of cells was obtained for seeding experiments.

To prepare scaffolds for cell seeding, cryopreserved and decellularized tracheal patches (0.5×0.5 cm^2) were sterilized by immersion in 2% antibiotic/antimycotic solution (Merck Lifescience) for 4 days under mild agitation, followed by extensive washes in PBS for 2 days under mild agitation and final incubation under UV light for 1 h. After maintaining tracheal scaffolds in cell proliferation medium overnight at 37 °C, 100,000 HM1-SV40 cells/support were seeded on the luminal side and cultured for 3 and 7 days before assessing cell growth on samples.

At the defined endpoints, SEM analysis was performed as described in Paragraph 2.9 to verify cell adhesion and proliferation on scaffold surface.

2.12.3. In Vivo Biocompatibility

In vivo biocompatibility assay was performed implanting pig CryoT and DecellT samples in a subcutaneous pouch of Balb/C mice (International Organization for Standardization (ISO) 996-3) [55]. Animal surgery and husbandry were performed in accordance with the Italian guidelines on the use of experimental animals (DL n. 16/92 art. 5) and approved by the Ethical Committee of the University of Padova and by the Italian Department of Health (Authorisation n. 1076/2020-PR, 10 November 2020).

- Surgery

For in vivo biocompatibility study, disk-like tracheal samples were prepared from cryopreserved and decellularized tracheal matrices using a biopsy punch with 8 mm diameter. Hence, six twelve-week-old female mice were anesthetized using a binary gas mixture of isoflurane/oxygen and randomly assigned to the two experimental groups. After shaving and disinfecting the dorsal cutis with Betadine® (Bayer, Leverkusen, Germany) a No. 10 surgical blade (Becton-Dickinson, Franklin Lakes, NJ, USA) was used to create a dorsal subcutaneous pouch of about 10 mm. Thereafter, the scaffolds were anchored to the *latissimus* dorsi muscle by using Tycron 4/0 sutures; the respiratory-epithelium side was put in direct contact with the muscular side. Finally, absorbable Novosyn 4/0 sutures were used to stich the skin. An adequate antibiotic/anti-inflammatory therapy was administered for 5 days after surgery. Euthanasia was performed after 14 days; hence, the scaffolds were excised with the surrounding tissues and properly fixed for subsequent histological and immunohistochemical analyses and SEM ultrastructural characterization, as previously described.

- Explants characterization

Histological analyses including H&E, Masson's Trichrome, Sirius Red, Alcian-blue and Weigert Van Gieson staining were accomplished as previously reported to verify eventual ECM remodeling after in vivo implant. In addition, von Kossa staining was also included to establish a possible contribution of cryopreservation and decellularization to calcification of the specimens after implant. Briefly, re-hydrated sections were flooded with 5% of aqueous silver nitrate; hence they were exposed to sunlight for 20 min prior to be washed well in distilled water. The samples were than treated with 2% sodium thiosulphate for 2 min, washed in running tap water, rinsed in distilled water and counterstained with 1% Neutral red for 2 min. After a rapid dehydration, the slides were cleared in xylene prior to be mounted with Eukitt.

In parallel, immunological characterization for lymphomonocytic-fraction detection was performed with the following antibodies diluted in PBS: anti-CD3 (polyclonal rabbit anti-human CD3, A 0452; Dako, Milan, Italy) diluted 1:500 and anti-F4/80 (polyclonal rabbit anti-mouse anti-F4/80, sc-26643-R; Santa Cruz Biotechnology, CA, USA) diluted 1:800, to label lymphocytes and monocytes/macrophages, respectively. Antigen unmasking

was performed with 10 mM sodium citrate buffer, pH 6.0, at 90 °C for 10 min. The sections were then incubated for 30 min in blocking serum [0.04% bovine serum albumin (BSA; A2153, Sigma-Aldrich) and 0.5% normal goat serum (X0907, Dako)] to eliminate unspecific binding, and then incubated for 1 h at RT with the above primary antibodies. Primary antibody binding was revealed by incubation with anti-rabbit/mouse serum diluted 1:100 in blocking serum for 30 min at RT (Dako® EnVision™ + peroxidase, rabbit/mouse; Dako, Glostrup, Denmark) and developed in 3,3′-diaminobenzidine for 3 min at RT. Lastly, the sections were counterstained with haematoxylin. As a negative control, sections were incubated without primary antibodies. Immunopositive elements were quantified as described in Section 2.7.1.

SEM analyses, conducted as described above, supported histological/immunohistochemical characterization for description of explants surfaces ultrastructure.

2.13. Statistical Analysis

Data are presented as mean $\pm$ standard deviation (SD) of at least three replicates. The one-way analysis of variance (ANOVA) followed by the Tukey post hoc test for multiple comparisons were used to determine any significant differences among the experimental groups. Unpaired *t*-test was used when comparing two groups. Differences were considered significant with $p \leq 0.05$.

3. Results

3.1. Gross Appearance, Nuclear Staining, and DNA Content

Cryopreservation led to samples that after thawing (13 months of freezing) were characterized by an external whitish appearance and an internal pinkish lumen. The CryoT also maintained the tubular shape preserving lumen rigidity without evident differences versus NativeT.

Decellularization was accomplished in 12 weeks (12 decellularization cycles). Each cycle was introduced by a lyophilization treatment that imparted a wrinkled appearance to the graft but was not associated with evident tissue fractures/alterations. In addition, it guaranteed an optimal DNase-I solution penetration that is essential for protocol efficiency. Once rehydrated, the lyophilized samples returned to show a typical native tissue-like appearance. The decellularization protocol provided for segments with a white colour (both externally and internally), keeping a patent lumen without signs of collapse (Figure 2A).

DAPI staining allowed to detect presence/distribution of cellular nuclei and/or remnants within the CryoT and DecellT versus the native tissue, thus highlighting the protocol's effectiveness in reducing the immunogenic potential of the samples. Typically, the native tissue displayed a broad and homogeneous distribution of the cells (nuclei, blue dots) in the whole tissue thickness (mucosa and submucosa, cartilage); in the CryoT group, the fluorescent elements were still identifiable, but they were reduced in number. DAPI staining results showed that only the DecellT group was mainly cell-nuclei free; however, despite blue dots being nearly absent, fluorescent remnants were detected, mainly located at the lacunae edges. A certain autofluorescence of the ECM was identified in all the experimental groups (Figure 2B).

The DAPI staining results were supported and confirmed by the DNA quantification assay. As shown in Figure 2C, both cryopreservation and decellularization guaranteed a reduction in DNA content versus the NativeT group. Attributing to the NativeT group a DNA amount of 100% (522.30 ± 157.70 ng/mg), CryoT and DecellT samples showed a reduction of 60.4% (206.21 ± 71.26 ng/mg) ($p < 0.0001$) and 91% (55.84 ± 7.06 ng/mg) ($p < 0.0001$), respectively. Despite both cryopreservation and decellularization allowing a significant DNA amount decrease, decellularization was more effective. In fact, a significant difference in total DNA was detected comparing the CryoT and the DecellT groups (**: $p < 0.01$).
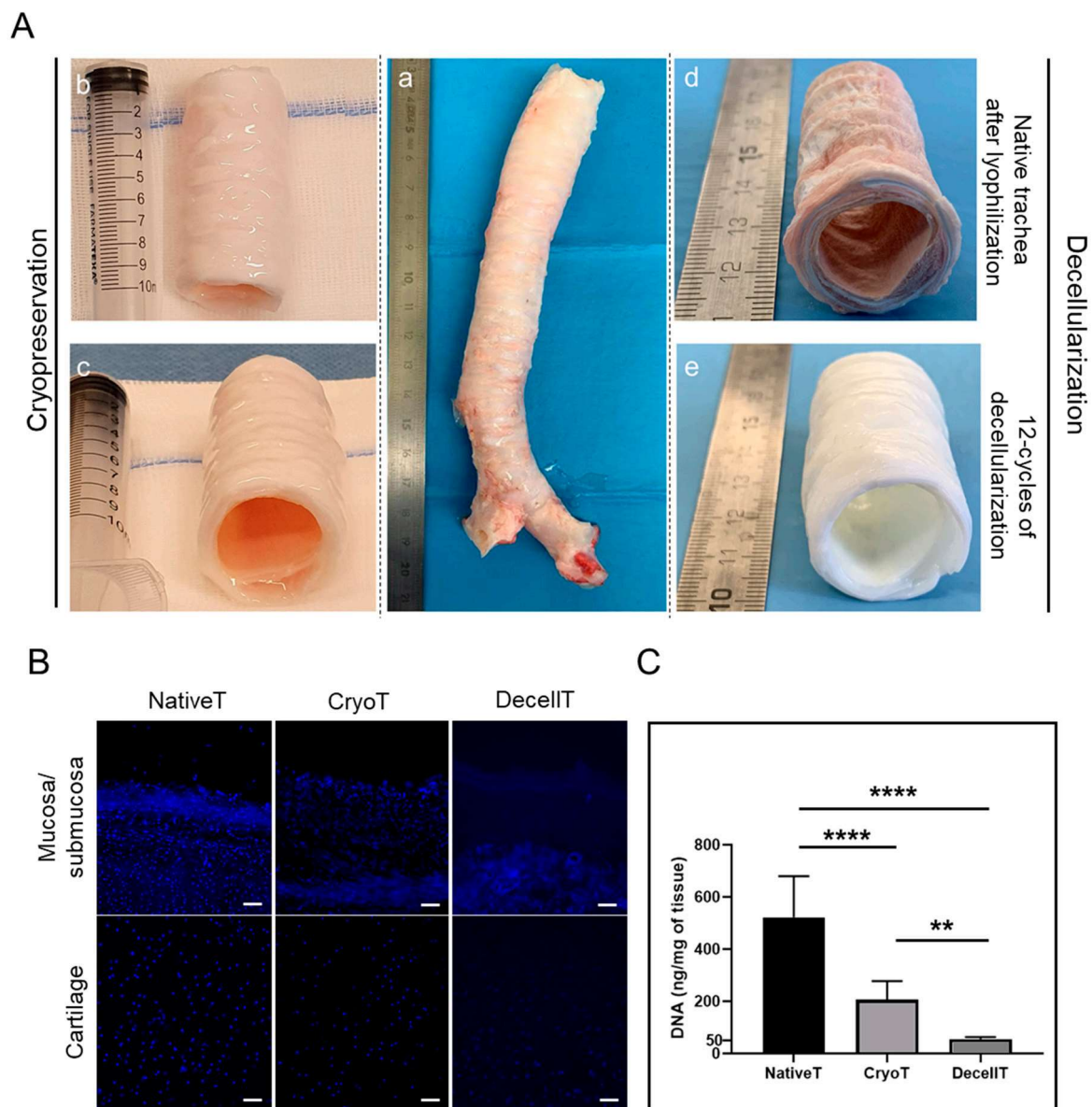
Figure 2. (**A**) Cryopreserved and decellularized pig trachea gross appearance. Soon after isolation (**a**) pig tracheas were divided into segments which underwent cryopreservation (**b**,**c**) and decellularization (**d**,**e**). Gross appearance of cryopreserved trachea segment (**b**,**c**); gross appearance of native tracheal segment after lyophilization (**d**); gross appearance of pig trachea after 12 decellularization cycles (**e**). (**B**) DAPI staining representative image of native (NativeT), cryopreserved (CryoT) and decellularized (DecellT) pig trachea. Blue dots (not detected in DecellT) correspond to cell nuclei. The presence of a diffused blue staining in the DecellT refers to extracellular matrix autofluorescence; autofluorescence was also detected in the Native T and CryoT samples. Scale bars = 100 μm. (**C**) Quantification of residual DNA into CryoT and DecellT samples versus the NativeT group (**: $p < 0.01$; ****: $p < 0.0001$).

3.2. Immunolocalization of Alpha-Gal Epitopes

To assess if cryopreservation and decellularization can modulate the distribution pattern of xeno-antigens, immunohistochemistry was adopted to describe Alpha-Gal epitope presence. This evaluation is fundamental when considering pig-derived CryoT or DecellT for an implant in humans. As shown in Figure 3A, Alpha-Gal positive elements were broadly detectable in NativeT at the level of mucosa and submucosa, mainly in correspondence of the glands; some positive lining cells were also identified at the inter-

face cartilage/submucosa and cartilage/adventitia. Conversely, Alpha-Gal was nearly not recognizable within cartilage. CryoT, despite reduction, still maintained a certain immunopositivity for the antigen, especially in correspondence with the mucosa and submucosa. No positive reaction was highlighted in the whole DecellT thickness.
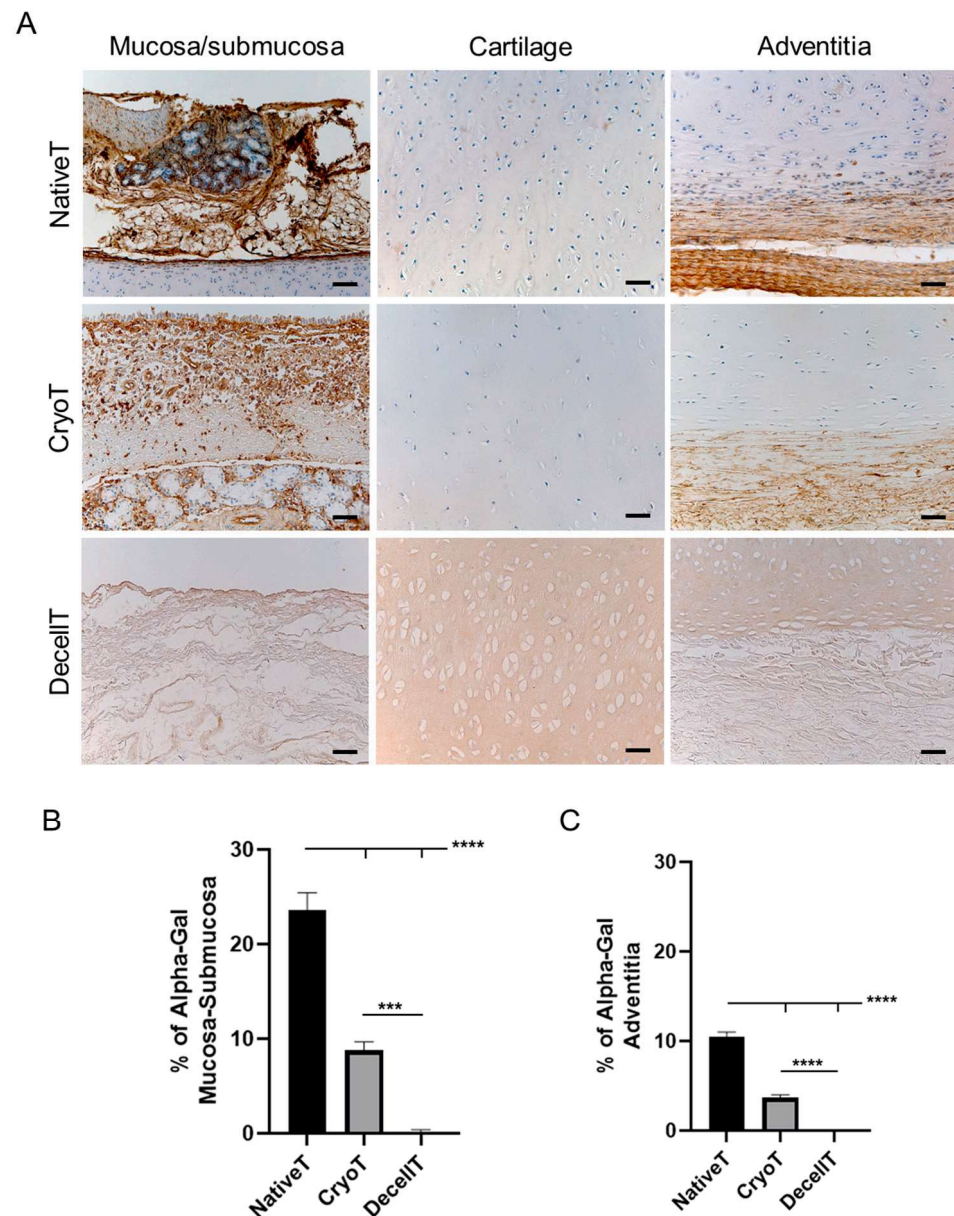

Figure 3. (**A**) Immunolocalization of Alpha-Gal epitopes in cryopreserved (CryoT) and decellularized (DecellT) samples versus native trachea (NativeT) (control). The mucosa/submucosa, cartilage and adventitia were considered separately. Positive elements are stained in brown. Scale bars: 50 μm. (**B**,**C**) Quantification of Alpha-Gal positive elements within the mucosa–submucosa and adventitia. (***: $p < 0.001$; ****: $p < 0.0001$).

Alpha-Gal immunoreactivity was quantified with a focus on mucosa/submucosa (Figure 3B) and adventitia (Figure 3C). CryoT showed an immunoreactivity percentage of $8.76 \pm 0.93\%$ and $3.68 \pm 0.33\%$ at the mucosa/submucosa and adventitia side, respectively; these values were higher than that quantified for the DecellT group (mucosa/submucosa: $0.20 \pm 0.18\%$ ($p < 0.001$); adventitia: $0.02 \pm 0.031\%$ ($p < 0.0001$)) but lower when compared to the NativeT (mucosa/submucosa: $23.56 \pm 1.87\%$ ($p < 0.0001$); adventitia: $10.46 \pm 0.54\%$ ($p < 0.0001$)). As expected, NativeT distinguished within the

cohort for Alpha-Gal immunoreactivity highest values at both the analyzed aspects of the tracheal tissue ($p < 0.0001$).

3.3. Histological and Biochemical Analyses

The CryoT maintained the typical microscopic structure of the NativeT with partial modifications likely descending from freezing and thawing. In the respiratory epithelium, only a few sparse cilia were detectable; the mucosa and submucosa tissues appeared looser than in the NativeT but the mixed glands were still recognizable and structurally intact. Focusing on cartilage, the tissue maintained its compact matrix organization. Despite the chondrocytes still being present, there were also void lacunae. The territorial matrix was still dark stained, similarly to NativeT; whereas the adventitia, even though identifiable, appeared looser and less organized than in NativeT.

The decellularization protocol partly modified the histological appearance of the tracheal segments by removing the cellular elements from the whole tissue thickness. After 12 treatment cycles, the respiratory epithelium disappeared. The mucosal and submucosal layers with the glands were not recognizable; only disorganized connective tissue remnants were identifiable. Considering the cartilaginous compartment, no cells were detectable within the lacunae which appeared wider than in the NativeT and CyoT, probably as consequence of the mechanical stress descending from lyophilization. Despite being lighter, staining of the territorial matrix was preserved. Decellularization also altered the adventitia, appearing as less organized than in the NativeT and CryoT groups.

Together with a description of tissue organization, H&E staining further supported qualitative/quantitative data from DAPI staining and DNA content analysis allowing for cell nuclei detection. As previously showed, a reduction in immunogenic elements (cells) was evident in CryoT; whereas, no cells were detected in DecellT (Figure 4).
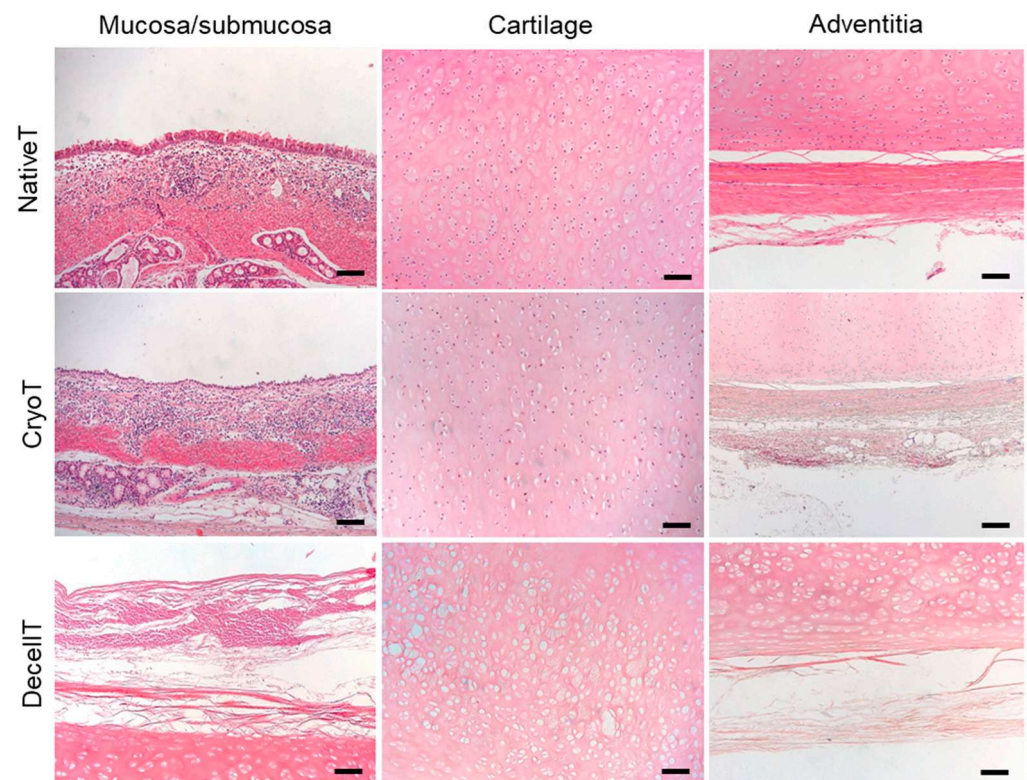

Figure 4. Histological appearance of pig tracheas obtained by cryopreservation (CryoT) and decellularization (DecellT) compared with native trachea (NativeT) showed by haematoxylin and eosin (H&E) staining. The whole tissue thickness was considered, highlighting the microscopic organization of the mucosa/submucosa, cartilage and adventitia. Scale bars = 100 µm.

Within each group, the glands secretory cells and the ECM were characterized by Alcian Blue staining showing cytoplasmic granules and GAGs presence, respectively. NativeT and CryoT samples displayed a similar blue staining. Conversely, a less intense blue colour was detected in the DecellT samples, suggesting glands' modification and a certain GAGs depletion in cartilage ECM (Figure 5A). Typically, in the cartilaginous compartment, GAGs are mainly located in the territorial matrix: this was evident observing NativeT and CryoT samples. In accordance with preliminary H&E, DecellT territorial matrix was only faintly blue colored compared with the other experimental groups.
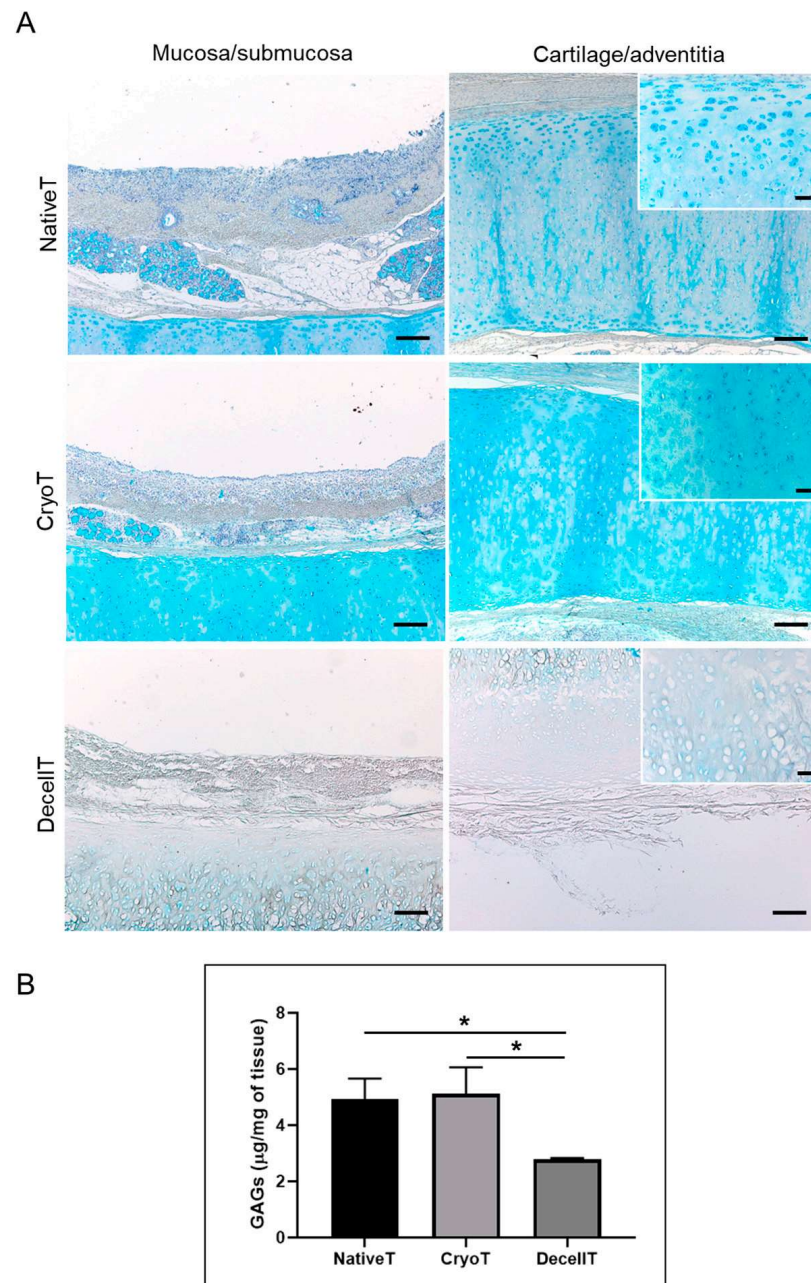

Figure 5. (**A**) Histological appearance of pig tracheas obtained by cryopreservation (CryoT) and decellularization (DecellT) compared with native trachea (NativeT) showed by Alcian Blue staining. The whole tissue thickness was considered. Scale bars: 100 μm (mucosa/submucosa); 50 μm (cartilage/adventitia); 200 μm (cartilage/adventitia, insert). (**B**) Sulphated glycosaminoglycans (GAGs) quantification, showing a reduction in GAGs content after decellularization (DecellT) compared with cryopreserved tracheas (CryoT) and native tracheas (NativeT) (*: $p < 0.05$).

The biochemical assay corroborated the microscopic evidences. CryoT showed a mean GAGs content similar to that displayed by the NativeT (5.21 ± 0.90 μg/mg versus 4.93 ± 0.60 μg/mg). Conversely, decellularization was responsible for a significant ($p < 0.05$) loss of GAGs content (2.79 ± 0.04 μg/mg) versus the NativeT and the CryoT groups; despite that, the 56.4% of the initial GAGs amount was maintained (Figure 5B).

Collagen content was evaluated through different histological characterization studies. After Masson's trichrome staining (Figure 6A), the mucosa/submucosa, the cartilage compartment and the adventitia were focused and quantification analysis was performed (Figure 6B–D). The green staining colour was uniformly represented, suggesting the presence of a broadly distributed collagen component in the hyaline cartilage. This evidence was also confirmed by green intensity quantification: the calculated mean values were 90.71 ± 1.79% for NativeT; 83.27 ± 14.30% for CryoT and 84.41 ± 7.95% for DecellT. No statistically significant differences were detected (Figure 6C). Differently, statistically higher values in total collagen were calculated for the mucosa/submucosa compartment and the adventitia in the DecellT group versus the other two groups (mucosa/submucosa: DecellT: 37.48 ± 2.99%; NativeT: 14.44 ± 2.59%; CryoT: 13.12 ± 6.61% ($p < 0.0001$). Adventitia: DecellT: 39.83 ± 3.73%; CryoT: 38.37 ± 4.18%; NativeT: 25.07 ± 5.23% ($p < 0.05$)) (Figure 6B,D).
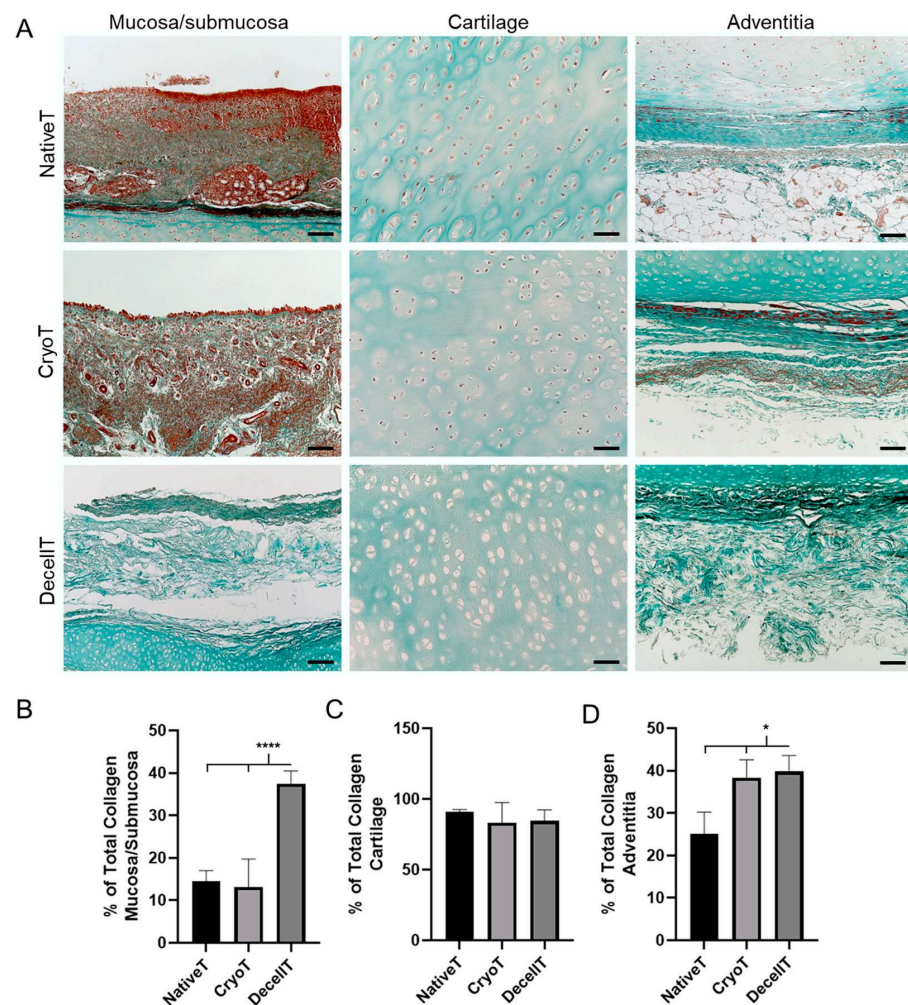

Figure 6. (**A**) Histological appearance of trachea cartilage tissue. Native trachea (NativeT), cryopreserved trachea (CryoT) and decellularized trachea (DecellT) were compared after Goldner Masson's Trichrome staining for collagen fibers. was here focused. Scale bars = 100 μm (upper row); 200 μm (lower row). (**B–D**) Collagen content quantification within the mucosa/submucosa, cartilagineous compartment and adventitia. (*: $p < 0.05$; ****: $p < 0.0001$).

Contextually, Picrosirius Red staining allowed to specifically detect collagen type I (orange-red) and type III (green) fibers under polarized light. Specifically, bifringence allowed to recognize a broad collagen type I presence (larger fibers) in both the mucosa/submucosa and perichondrium for the NativeT and CryoT groups; conversely, the DecellT samples displayed collagen type I fibers at the perichondrium but also within the cartilagineous compartment, at the level of the territorial matrix. Collagen type III (thinner fibers) was nearly not identifiable here (Figure 7A).

Similarly, also the adventitia distinguished for preferential localization of collagen type I fibers than collagen type III; however, this latter one was slightly more represented here than in the mucosa/submucosa (Figure 7B). Dark areas corresponded to portions revealing less density in collagen fibers.

Prevalence of collagen type I and III was determined at both the mucosa/submucosa/cartilage and adventitia side. Focusing on the mucosa/submucosa/cartilage compartment, CryoT samples showed a higher content in collagen type I than the DecellT group ($8.41 \pm 2.05\%$ and $3.85 \pm 1.04\%$, respectively; $p < 0.05$). A statistically significant difference ($p < 0.0001$) was also calculated between NativeT ($12.21 \pm 1.54\%$) and DecellT. As regards collagen type III, NativeT and CryoT showed a comparable amount in this protein ($3.81 \pm 1.34\%$ and $4.15 \pm 1.01\%$, respectively); a significant difference was only identified between CryoT and DecellT ($1.20 \pm 0.68\%$) (Figure 7C,D). Regarding the adventitia, an opposite collagens preponderance was recognized here versus the mucosa/submucosa/cartilage side. In fact, the DecellT group showed the highest calculated values in collagen type I and type III than the other groups. While the difference was not statistically significant for collagen type I (NativeT: $11.08 \pm 3.14\%$; CryoT $13.89 \pm 4.06\%$; DecellT $17.46 \pm 2.48\%$), a $p < 0.01$ aroused comparing DecellT ($21.22 \pm 2.26\%$) with CryoT ($10.48 \pm 3.08\%$) and NativeT ($8.32 \pm 2.82\%$), respectively (Figure 7E,F).
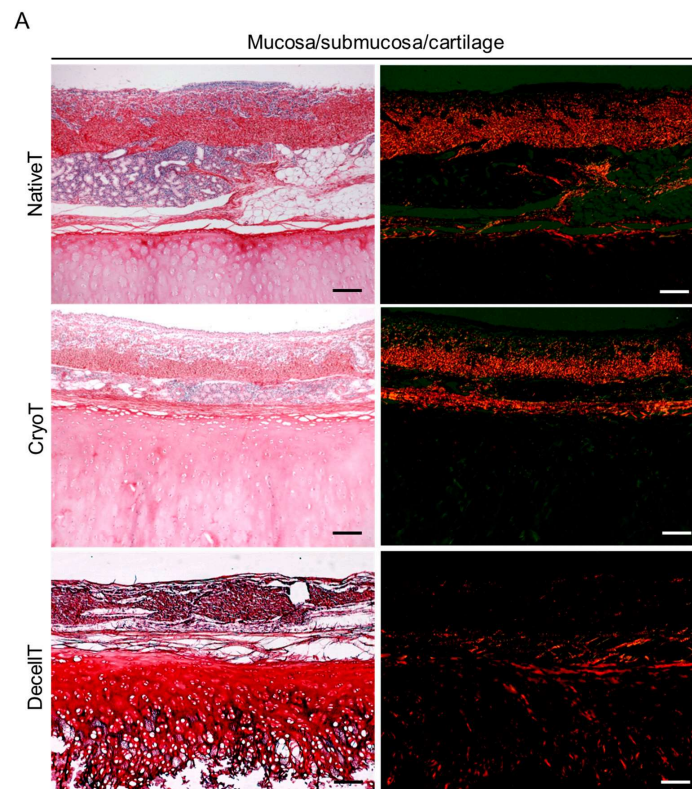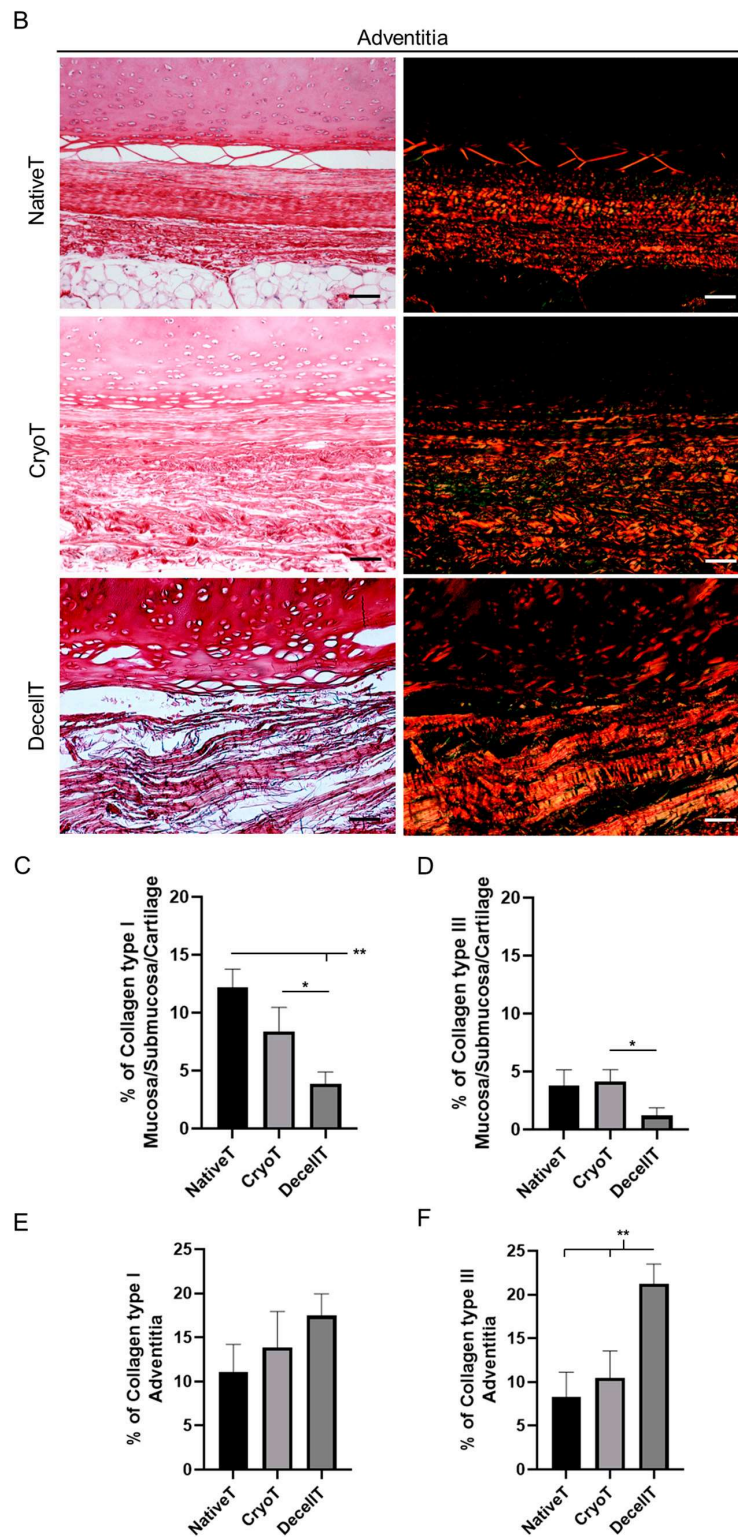

Figure 7. *Cont.*

Figure 7. Histological appearance of pig tracheas obtained by cryopreservation (CryoT) and decellularization (DecellT) compared with native tracheas (NativeT) showed by Picrosirius Red staining and visualized under optical microscope (left column) and optical microscope in polarized light (right column). Taking advantage from bifringence, type I or type III collagen fibers were detected appearing as red-orange or green-yellow, respectively. The whole tissue thickness was analyzed: (**A**) mucosa/submucosa and cartilage; scale bars: 50 μm; (**B**) adventitia; scale bars = 100 μm. Quantification of collagen type I and type III within (**C,D**) the mucosa/submucosa/cartilage and (**E,F**) the adventitia (*: $p < 0.05$; **: $p < 0.01$).

Considering the elastic fibers, their presence and distribution was compared among the experimental groups to verify eventual modifications ascribable to cryopreservation or decellularization. Typically, as showed in NativeT, the elastic fibers form the lamina elastica (separating the mucosal from the submucosal layers) where they are densely packed as longitudinally running elements. Besides the lamina elastica, they can also be detected in subepithelial position, as a sheath; at the surface of glands, organized in a net; in close contact to the inner surface of the cartilaginous ring, condensed at the deep border and outside the cartilage, within the adventitia. While the CryoT samples showed to maintain the elastic fibers pattern, a different appearance was displayed by DecellT tissues. Decellularization affected the elastic fibers content whose remnants were partly identifiable as slightly stained elements at the lamina elastica and at the deep and outer layers of the cartilaginous ring (Figure 8A).
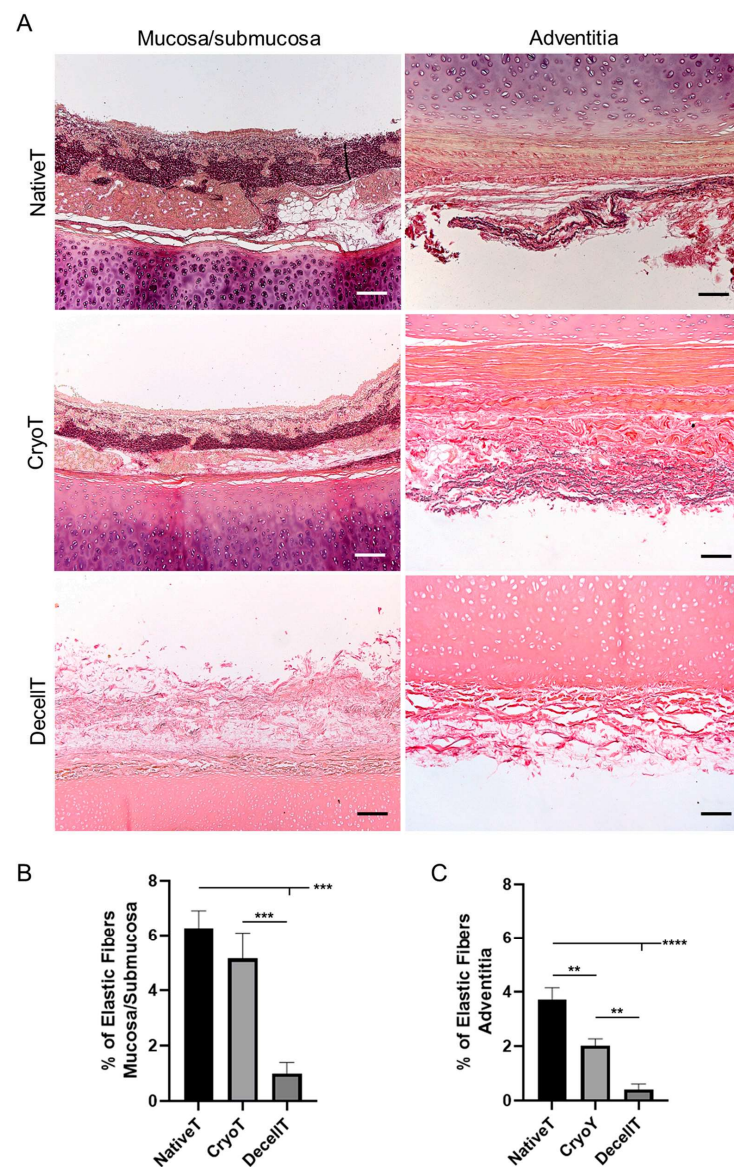

Figure 8. (**A**) Histological appearance of pig tracheas obtained by cryopreservation (CryoT) and decellularization (DecellT) compared with native tracheas (NativeT) showed by Weigert Van Gieson staining highlighting presence and distribution of elastic fibers (purplish elements). The mucosa/submucosa and adventitia were focused. Scale bars: 50 μm (mucosa/submucosa); 100 μm (adventitia). (**B**) Elastic fibers content within the mucosa/submucosa and (**C**) adventitia. (**: $p < 0.01$; ***: $p < 0.001$; ****: $p < 0.0001$).

The elastic fibers content within the mucosa/submucosa (Figure 8B) and adventitia (Figure 8C) was determined for a comparison in terms of prevalence among the three groups. CryoT showed at both sides (mucosa/submucosa: $5.15 \pm 0.94\%$; adventitia: $2.02 \pm 0.25\%$) lower values than NativeT (mucosa/submucosa: $6.67 \pm 0.64\%$; adventitia: $3.72 \pm 0.43\%$ ($p < 0.01$)) but a higher content in elastic fibers than the DecellT group (mucosa/submucosa: $0.99 \pm 0.41\%$ ($p < 0.001$); adventitia: $0.42 \pm 0.19\%$ ($p < 0.01$)). As expected, NativeT distinguished over DecellT at both sides (mucosa/submucosa: $p < 0.001$; adventitia: $p < 0.0001$).

3.4. Ultrastructure and Collagen Fibers Organization

The ultrastructure of both the respiratory epithelium and adventitia was investigated by SEM (Figure 9). The NativeT luminal surface showed the typical appearance of the intact respiratory epithelium characterized by cilia and microvilli. Conversely, a different ultrastructure was associated with CryoT and DecellT samples; in fact, despite in a different manner, cryopreservation and decellularization showed to impact the respiratory epithelium integrity. A certain de-epthelization was identified in the CryoT group, respiratory cells lost cilia or cilia completeness and only few remnants were recognizable; in some portions, it was possible to identify basal lamina fibrillae. Regarding the DecellT specimens, the protocol adopted led to respiratory epithelium cells removal, suggesting they were peeled-off by physical+enzymatic+chemical approach. Although DecellT showed a complete removal of the epithelium, basal membrane with a smooth and convoluted appearance was still detectable. No significant differences were recognized between the NativeT and the CryoT in the adventitia; both displayed finely organized collagen fibers, clearly identifiable even after cryopreservation. Differently, the collagen fibers were still identifiable in the DecellT samples (at higher magnification) but they appeared as partially fused, likely as consequence of the treatment they were exposed to.
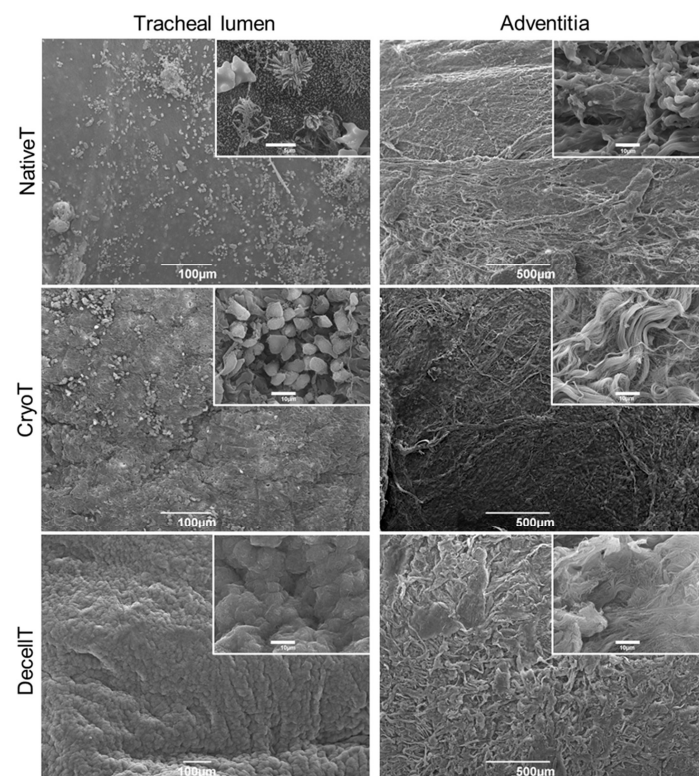

Figure 9. Representative photomicrographs showing ultrastructural appearance of both tracheal lumen and adventitia for native trachea (NativeT), cryopreserved trachea (CryoT) and decellularized trachea (DecellT). Scale bars: 100 μm (tracheal lumen); 500 μm (adventitia); 5 μm (NativeT tracheal lumen, insert); 10 μm (all other inserts).

In parallel, tissue fibers spatial organization was described by SHG microscopy. Like NativeT, the CryoT and DecellT groups showed collagen fibers mainly oriented in one direction (ellipsoidal shape for FFT) (see the three red elliptic profiles in Figure 10A) in both the compartments (cartilage and adventitia), suggesting an anisotropic behaviour. No significant difference was detected among groups regarding both cartilage and adventitia (Figure 10B,C).
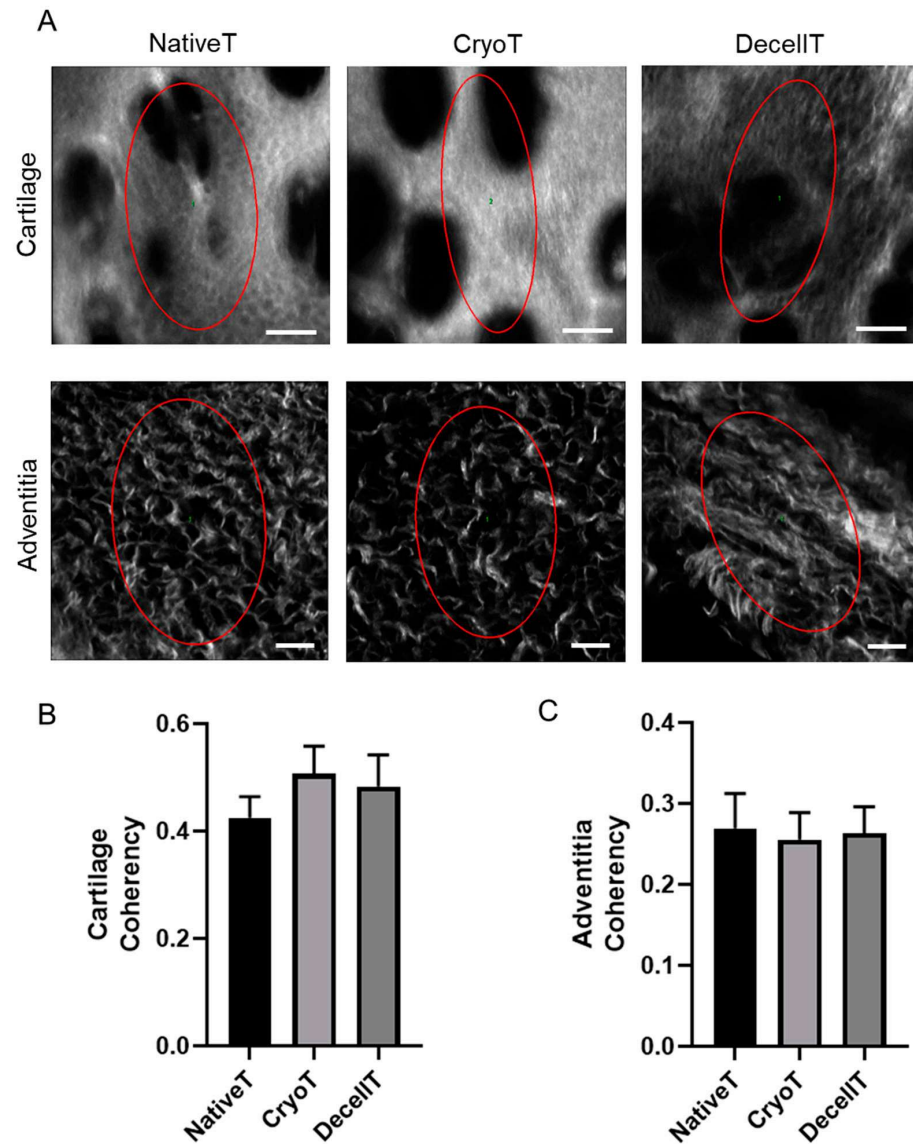

Figure 10. Evaluation of collagen fibers distribution into the cartilaginous compartment and adventitia side of cryopreserved and decellularized tracheas (CryoT and DecellT, respectively) versus native trachea (NativeT) used as reference. (**A**) Second Harmonic Generation (SHG) signal is showed in gray; in accordance with the Fast Fourier Transforms (FFTs), the ellipsoidal fibre orientation, suggesting anisotropy, is described by the red ellipse profile inside each photomicrograph. (**B,C**) Average values of collagen Coherency, which estimates the local orientation of the fibres in the cartilage (0.42 ± 0.04; 0.51 ± 0.05; 0.48 ± 0.06 for NativeT, CryoT and DecellT respectively) and adventitia (0.27 ± 0.04; 0.25 ± 0.03; 0.26 ± 0.03 for NativeT, CryoT and DecellT respectively); coherency was calculated using the ImageJ plugin OrientationJ. No significant difference was identified among groups. Scale bar: 20 μm.

3.5. Compressive Mechanical Behavior

In order to compare the compressive mechanical behaviour of different trachea samples, their size and shape were first analyzed. The obtained measurements are reported

in Table 1. These data show that all the samples had homogenous sizes in DecellT, CryoT and NativeT segments, with only few differences in the medio-lateral diameter of DecellT samples, which was slightly higher than the other groups.

Table 1. Size of DecellT, CryoT and NativeT samples.

	d_1 [mm]	d_2 [mm]	t [mm]	L [mm]	d_1 [mm]
NativeT	19.6	14.9	2.4	15.9	19.6
	19.8	14.5	2.6	17.3	19.8
	19.7	15.7	2.7	18.5	19.7
	21.6	16.9	2.7	14.7	21.6
CryoT	20.0	15.4	1.9	12.6	20
	21.4	16.3	2.7	15.3	21.4
	20.7	16.3	2.3	16.5	20.7
	20.8	15.2	2.1	14.7	20.8
DecellT	27.9	13.7	2.4	17.7	27.9
	26.6	11.8	2.8	13.2	26.6
	27.9	13.9	2.8	15.7	27.9

The results of the compression tests, carried out on DecellT, CryoT and NativeT, are summarized in Figure 11. The typical trend (Figure 11A), reported in terms of force per unit of length of a sample *f* vs. tracheal compressive deformation *s* in the proximal-distal direction, showed an initial region, below 10% of deformation, with lower stiffness, followed by a quasi-linear region with increased stiffness up to the highest reached compression. This change of the slope in the compression curve was due to a variation of contact area during the test. Indeed, since the sample diameter was not constant all over its length, just one of the cartilaginous rings was in contact with the upper plate at the beginning of the test. While the upper plate was approaching the samples, the other cartilaginous rings came in contact with it. This typically occurred in the range between 5% and 20% of deformation. The contact has then become homogenous on the overall sample length and the compressive behaviour was almost linear. The compressive stiffness of the trachea samples was therefore evaluated in this region, considering the secant modulus between 20% and 50% of compressive deformation. The experimental data in Figure 11B show that the compressive behaviour of NativeT and CryoT was very similar, while the DecellT could be occluded up to 50% of compressive deformation with a much lower force per unit of length. The comparison among compressive stiffness values (Figure 11C) highlighted a significant difference between DecellT and Native T samples.
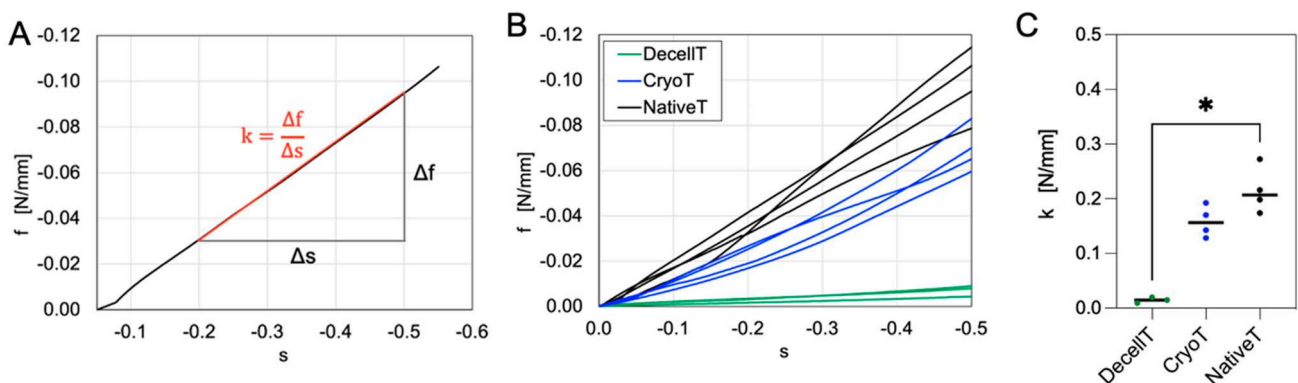

Figure 11. Results of compression tests: (**A**) Typical compression curve in terms of force per unit of length of the sample f vs. tracheal compressive deformation s in the proximal-distal direction. The compressive modulus k is the slope of the secant line between 20% and 50% of compressive deformation. (**B**) Compression curves of all the testes samples of DecellT, CryoT and NativeT. (**C**) Comparison of stiffness among all the testes samples of DecellT, CryoT and NativeT (*: $p < 0.05$).

3.6. Cytocompatibility Assessment In Vitro

The in vitro cytocompatibility study, developed as schematically reported in Figure 12A, allowed to predict biocompatibility in vivo, excluding possible undesired reactions amenable to chemicals retains. After 24 h of culture with proliferative medium previously conditioned with CryoT and DecellT, the HM1-SV40 cells showed to preserve typical morphology, viability and proliferative behaviour, reaching about 50–60% confluence on the growth surface. The MTT analysis also supported optical microscopy data.
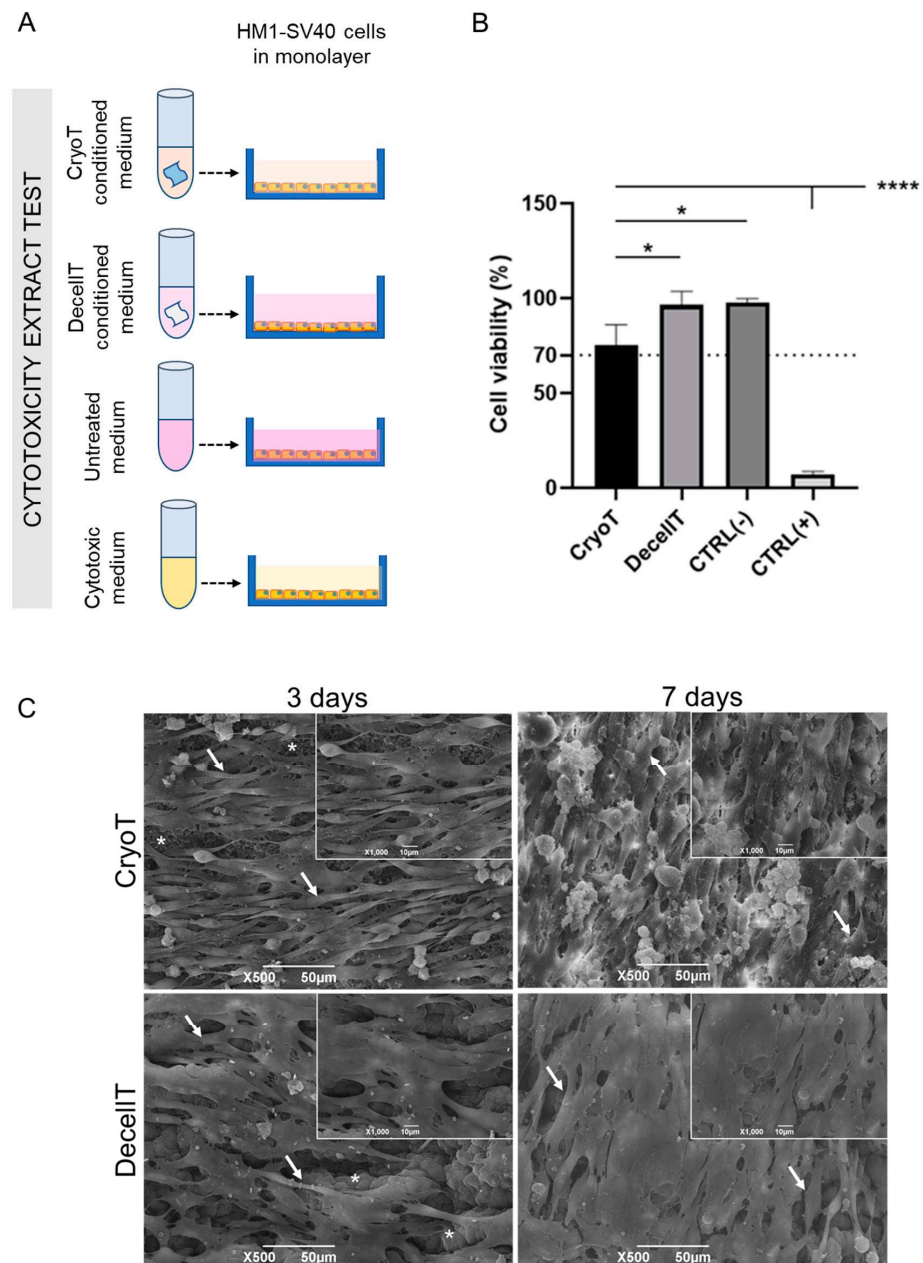

Figure 12. Cytocompatibility evaluation through the indirect and the direct methods. (**A**) Schematic figure showing the methodological approach to perform the cytotoxicity extract test. (**B**) test results on HM1-SV40 cell line. The cells were incubated for 24 h with culture media previously conditioned with cryopreserved and decellularized trachea (CryoT and DecellT, respectively). For each group, cell viability percentage was determined by comparison with that of untreated cell cultures, set at 100% of viability (*: $p < 0.05$; ****: $p < 0.0001$). (**C**) SEM analysis of cell-scaffold interactions in terms of cell attachment, morphology and proliferation on tracheal matrices. Scale bar: 50 μm; 10 μm (top right insert).

Compared to untreated cultures (CTRL-) (viability set at 100%), cells growth in CryoT and DecellT conditioned medium was 77.3% and 98.9%, respectively ($p < 0.05$). Both values remained above the reference threshold value (70% cell viability) which is required to consider a sample as non-cytotoxic. As expected, significant differences ($p < 0.0001$) were detected between the cytotoxic control and other groups. Interestingly, higher viability was observed for cells treated with the DecellT conditioned medium than the CryoT ones ($p < 0.05$) (Figure 12B).

Scaffold cytocompatibility was further demonstrated by HM1-SV40 cell seeding on cryopreserved and decellularized tracheas. SEM micrographs reported in Figure 12C show that both samples were colonized by seeded cells since day 3 from seeding, with HM1-SV40 populations exhibiting the typical fibroblastoid morphology on scaffolds. At day 7 cells seemed to be more numerous on both samples, suggesting adequate proliferation over time. On CryoT supports, cells appeared to grow more rapidly, reaching over confluence, and starting to detach from the seeding surface.

3.7. Biocompatibility Assessment In Vivo and Explants Characterization

At surgery the two groups' samples displayed a similar gross appearance; when anchoring the specimens, no rupture or layers decoupling occurred. The mucosal layer was easily identifiable in both CryoT and DecellT samples, thus allowing for adequate positioning in vivo (tracheal mucosa in contact with the *latissimus dorsi*). No decoupling occurred between the two aspects during sampling and/or surgery manipulation (Figure 13A).
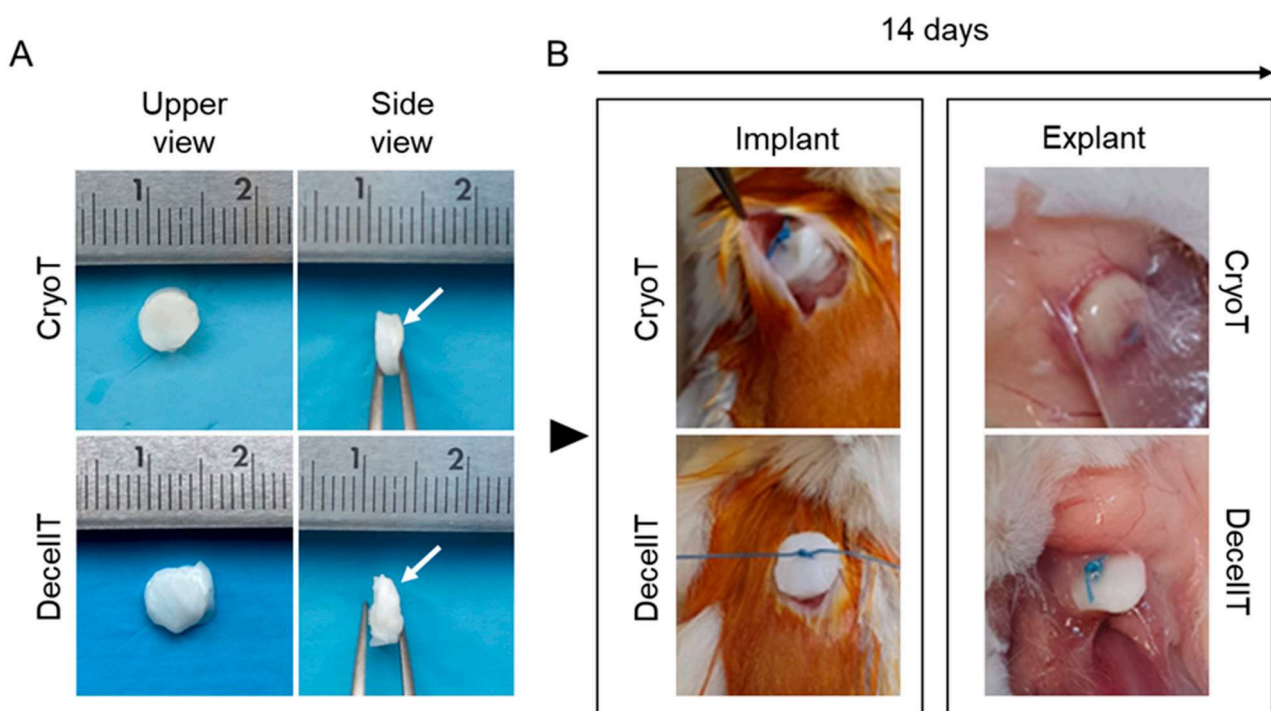

Figure 13. Gross appearance of cryopreserved (CryoT) and decellularized (DecellT) trachea samples before implant (the white arrows show the mucosa side) (**A**), after in vivo positioning in Balb/C mice (subcutaneous dorsal pouch) and at retrieval (14 days from surgery) (**B**). The mucosa side was placed in contact with the *latissimus dorsi*.

At 14 days from implant, all the specimens were clearly identifiable at retrieval, without giving rise to dislocations or severe inflammatory reactions; only a thin fibro-connective capsule was detectable surrounding the CryoT scaffolds (Figure 13B).

The histological analyses supported the macroscopic evidence at dissection (Figure 14A,B). No alteration occurred within the CryoT and the DecellT samples, at the level of the cartilagineous compartment, which remained intact and well recognizable

in all the sections (H&E and Alcian Blue stainings). Considering the external borders of the implants, a slight host reaction was evident in both groups, compatible with the type of surgery performed. In particular, the connective sheath, also characterized by elastic fibers presence (Weigert Van Gieson), was similar in CryoT and DecellT at the sub-cutis/cartilage interface but thicker in CryoT than in DecellT at the mucosa/*latissimus dorsi* muscle contact area.
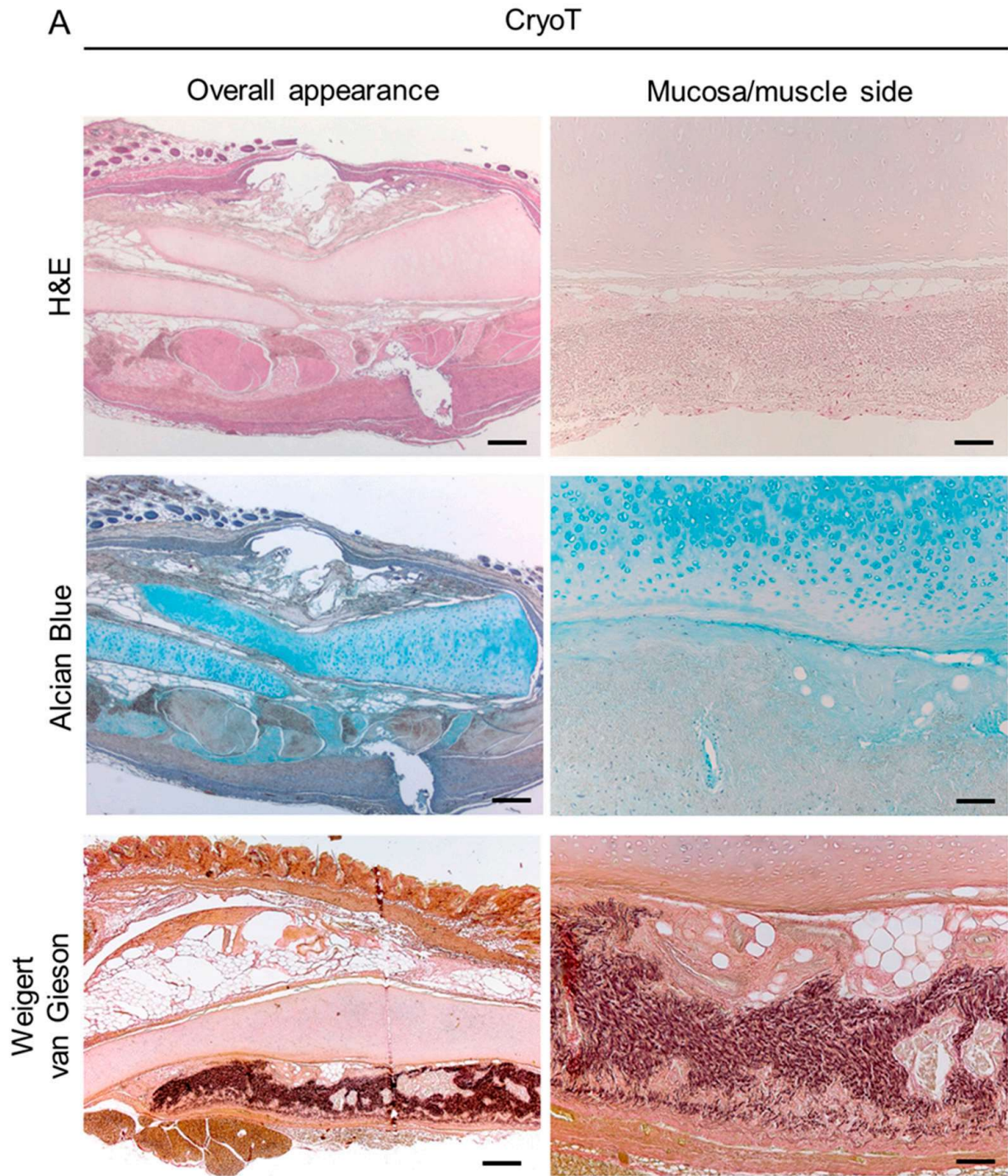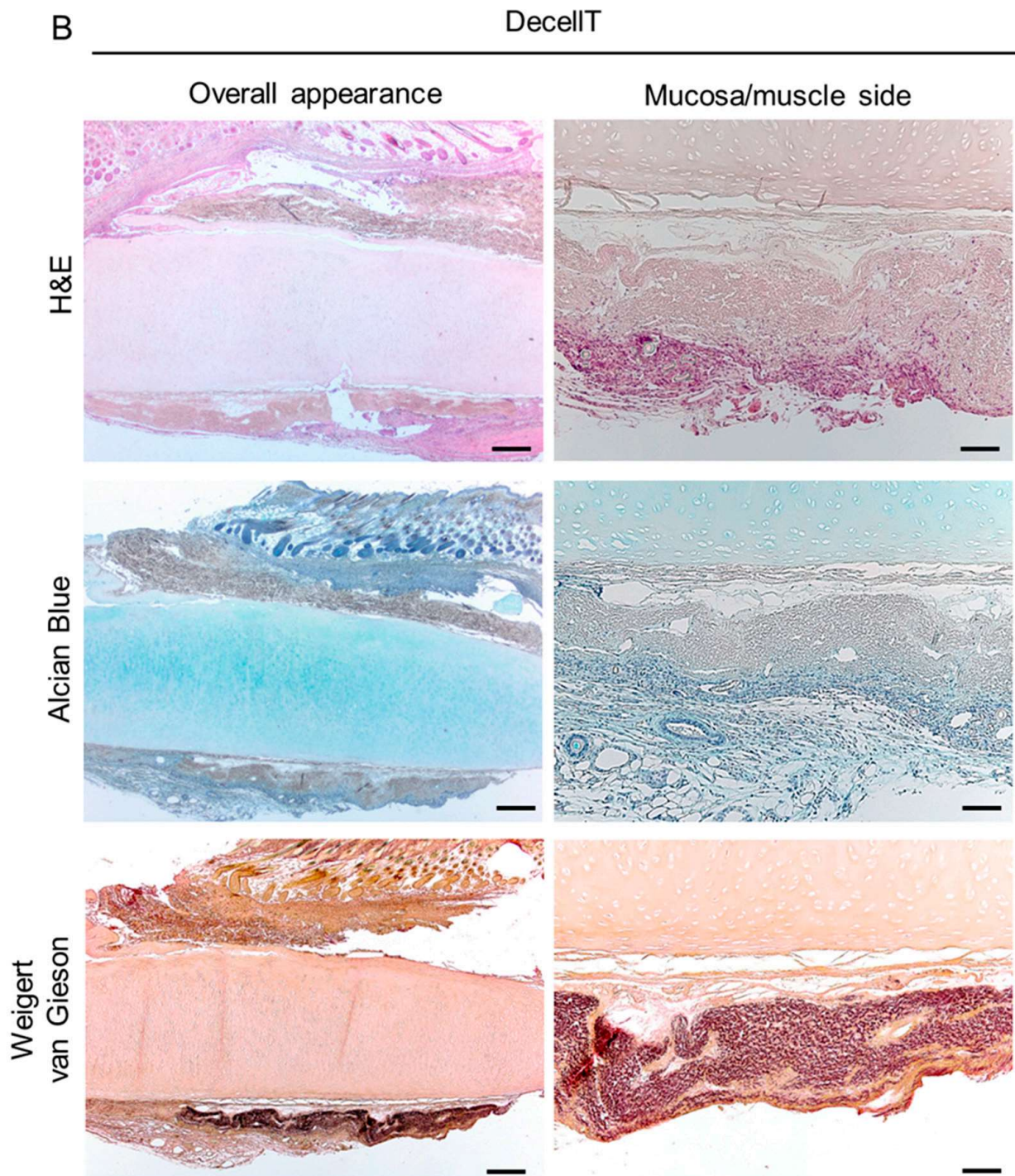

Figure 14. *Cont.*

Figure 14. Histological characterization of the explants by haematoxylin end eosin (H&E), Alcian Blue and Weigert van Gieson stainings. Both the overall appearance of the explants with the surrounding tissues and the mucosa/submucosa side were highlighted for the cryopreserved (**A**) and decellularized (**B**) tracheas (CryoT and DecellT, respectively). Scale bars: 400 μm (overall appearance); 100 μm (mucosa/muscle side).

No detection of positive reaction after von Kossa staining (black deposits) highlighted that neither cryopreservation nor de-cellularization affected calcification of the samples after in vivo implant (Figure 15). Both the subcutis/cartilage interface and the mucosa/*latissimus dorsi* muscle contact area were analyzed.
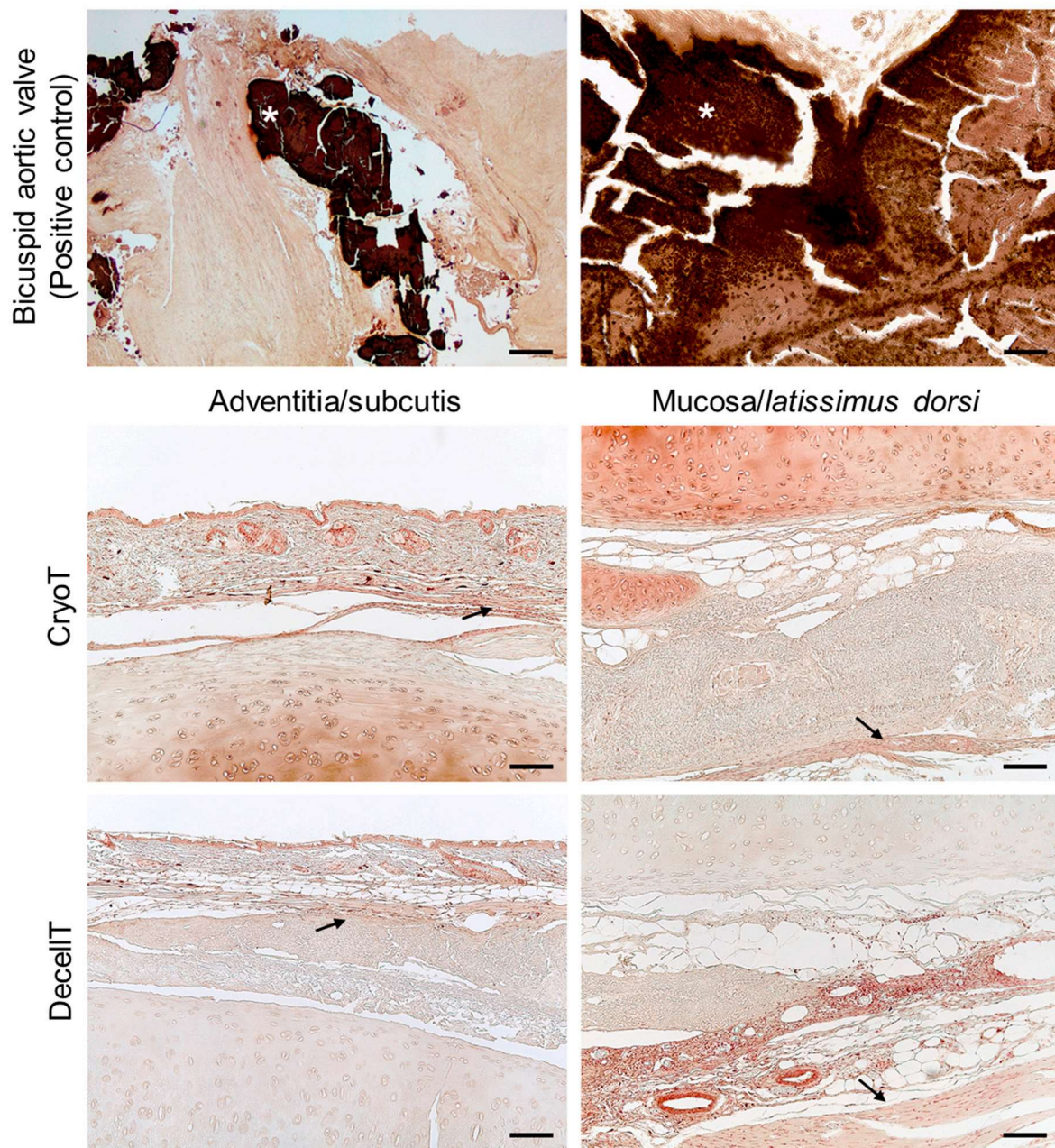
Figure 15. Histological characterization of the CryoT and DecellT explants by von Kossa staining. Both the mucosa/submucosa side and adventitia, in contact with the subcutis and the latissimus dorsi, respectively, were focused (the back arrow shows the interface) (scale bars: 100 µm) A positive control (calcification of bicuspid aortic valve, white asterisk (*)) was included in the first row (scale bars from the left to the right: 100 µm; 50 µm).

Immunohistochemistry further confirmed histological characterization study data, proving the presence of T lymphocytes (CD3 positive elements) and monocytes/macrophages (F4/80 positive elements) in correspondence of the connective tissue surrounding the implants, mainly at the muscle side (Figure 16A). Immune reaction severity was mild; in addition, the infiltrate was more evident in correspondence of the stiches, suggesting a certain physiological response to suture. Quantification of CD3 and F4/80 positive elements showed no significant difference between the CryoT (CD3: 2.43 ± 0.42%; F4/80: 2.26 ± 0.85%) and the DecellT (CD3: 3.11 ± 1.50%; F4/80: 2.58 ± 0.61%) groups (Figure 16B).
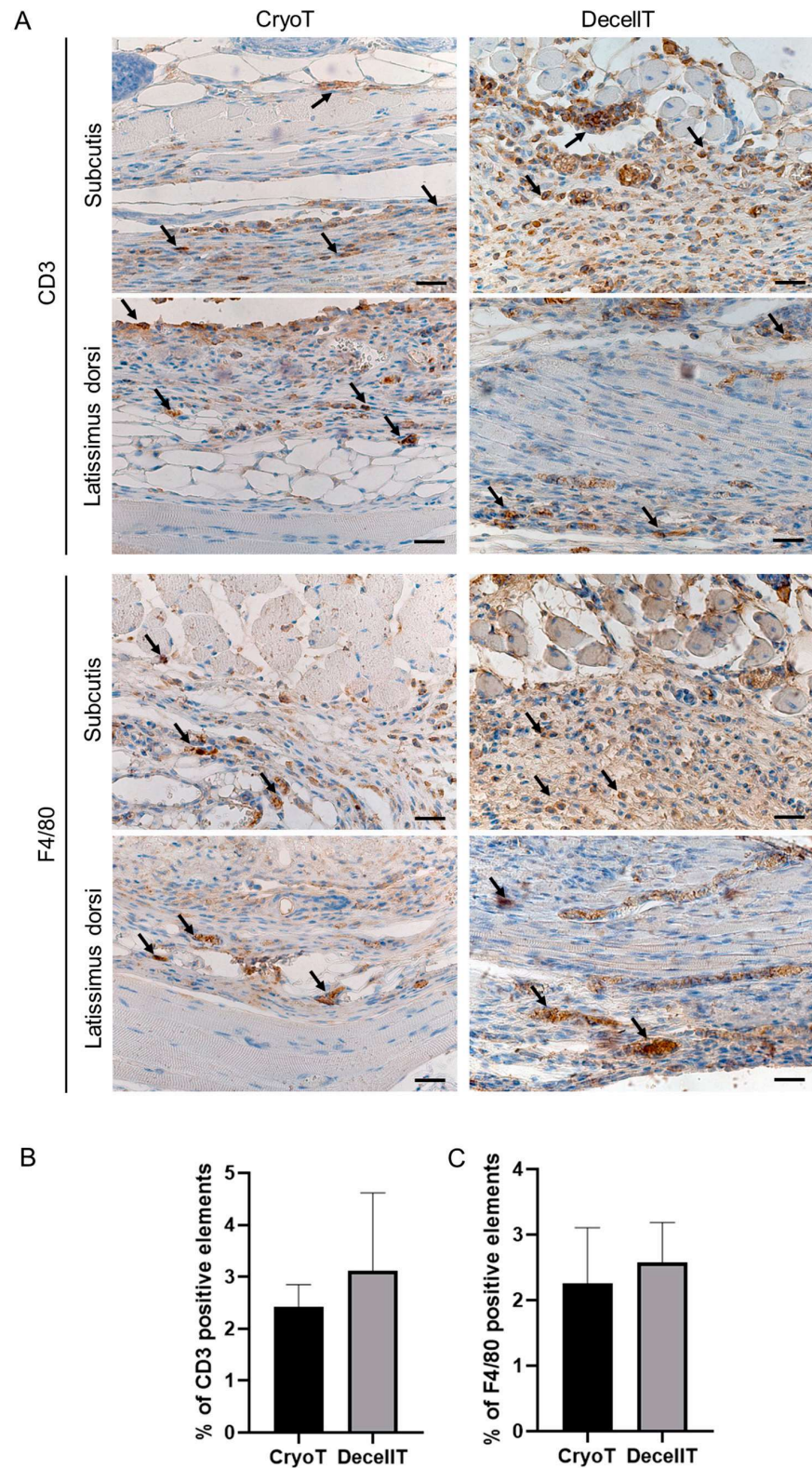
Figure 16. (**A**) Immunohistochemical characterization of cryopreserved (CryoT) and decellularized (DecellT) samples after heterotopic positioning in Balb/C mice subcutaneous pouch and retrieval at day 14 from surgery. The immunolocalization of CD3+ and F4/80+ cells (dotted brown-stained elements, black arrows) at the boundaries between the tracheal specimens and the host tissues showed the presence of a mild lympho-monocytic infiltration triggered by the scaffolds. Scale bars: 25 μm. Quantification of CD3 and F4/80 positive elements (**B,C**) within the CryoT and DecellT samples, after retrieval. No significant difference was detected.

To broadly characterize the explants, an ultrastructural analysis was also performed. The CryoT samples showed the presence of numerous cellular elements at the respiratory epithelium side. These were fused in a monolayer or roundish. Conversely, few host cells were evident at the adventitia side, adhering to collagen fibers. In a different manner than CryoT, the DecellT samples were broadly colonized by the host cells in the two sides; cells monolayers were clearly distinguishable, and no scaffold ultrastructure was evident (Figure 17).
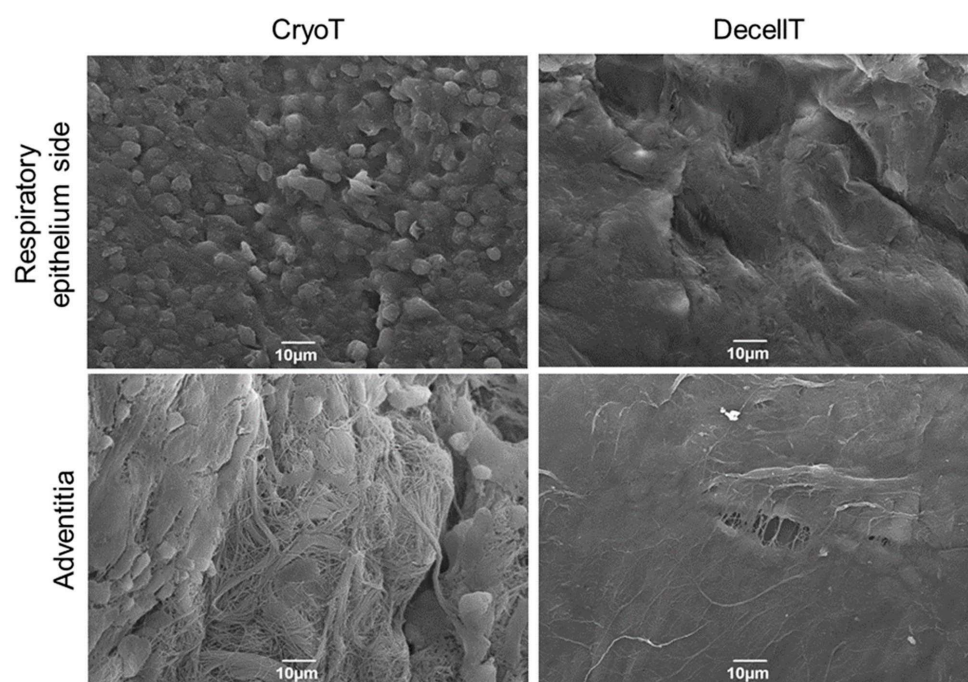

Figure 17. Ultrastructural characterization of retrieved cryopreserved (CryoT) and decellularized (DecellT) samples after heterotopic implant in Balb/C mice (end-point: 14 days). The respiratory epithelium side and the adventitia were both considered. Scale bars: 10 μm.

4. Discussion

In case TRA is not feasible, identification of effective transplantation options, free from need of immunosuppressant therapies to preserve grafted tissue structural/functional integrity, are an ambitious goal to pursue. Together with eliminating immunosuppressant therapy side effects and the related costs, they would guarantee for significant improvements of patients' life quality, especially (but not limited) to the oncologic category [11,56–58].

To date, several studies regarding fabrication of tubular substitutes to restore trachea continuity have been encouraged by the apparent simplicity of the "windpipe" [11] but a resolutive reconstructive option is still lacking, as suggested by the intense research still ongoing in this field [10]. Patent grafts development and integration after positioning, with also respiratory epithelium recovery, is fundamental to guarantee for a native-like tissue regeneration (instead of reparation) whose functions by far exceed the simple conduction and conditioning of air [59]. It descends that trachea allograft (or even xenograft) are possibly the most compliant option to resort to, as suggested by derivative' adequate macroscopic and microscopic anatomy, ECM proteins type/content and ultrastructural organization [60–62].

Given the shortage of human donor material for allotransplantation, animal-derived tissues enlarge the options for treatment, being used directly as a transplant (xenotransplant, xenograft) after processing like cryopreservation, or being prepared as a decellularized ECM. These products intended for biomedical applications are regulated either as medicinal products or as medical devices. Specifically, in Europe, the Directive 2001/83/EC13 and

Regulation (EC) No. 726/200414 regulate the use of xenogenic materials as medicinal products. In addition, the Regulation (EC) No. 1394/2007/EC15 has been approved as a *lex specialis* regarding advanced therapy medicinal products (ATMP). On the other hand, animal-derived materials for transplantation are regulated also as medical devices according to the Regulation No. 2017/745/EU. For xenogeneic products, further guidance information for general safety and risk assessment are provided by the *CHMP Guideline on xenogeneic cell-based medicinal products*, whereas the WHO Changsha Communique and follow-up documents have been approved to guarantee regulation and guidance on animals, donor source, processing, risk management, and safety evaluation (reviewed by Godehardt and Tönjes, 2020 [63]).

4.1. Trachea Substitutes Development

In this work, pig-derived CryoT and DecellT substitutes were developed and compared in a broad study aiming to provide a useful structural description of these two alternatives for trachea reconstruction. Several cryopreservation and decellularization protocols were attempted over the years, since the first efforts [64–66]; however, due to the contradictory results reported, their translation to medicine is still limited [8,67], except for compassionate use [28,35,36].

Cryopreservation approaches depend on temperature freezing rate, cryoprotective agents, and duration of cryopreservation [7]. The first preclinical study (pig) reporting about cryopreserved tracheal graft implantation in orthotopic position was described by Lenot et al. [68]. Despite surgery failure due to inadequate blood supply, the histologic structures and the mechanical properties were well preserved, stimulating intense research on this substitute type [15,24,26,28,38,60,61,67,69–97]. Hence, focusing on freezing temperature and liquid nitrogen storage, cryopreserved tracheal graft protocols can be distinguished into two groups: (a) freezing at −60° to −140 °C and storage in liquid nitrogen until use; (b) freezing at −80°/−85 °C, without recurring to liquid nitrogen storage [24]. The first strategy was here followed (freezing at −140 °C; storage in vapor phase liquid nitrogen), since long time adopted by the FBTV for successful cryopreservation of different other tissues used in clinical practice. These include, for instance, fascia lata allograft for surgical facial reanimation [39]; amniotic membrane for the treatment of gingival recessions [43] and cryptoglandular anal fistulas [98]; aortic homograft for aortic valve or aortic root replacements [22]. Interestingly, also decellularized human aortic valves underwent to this cryopreservation within an in vitro study [42].

Regarding tracheal decellularization, both physical + chemical methods [31,33,99–103] and physical + enzymatic + chemical methods [6,104–114] were approached and verified by several Authors considering orthotopic positioning. However, to date, no gold-standard strategy exists among decellularization protocols; the method can vary or be tuned along with tissue/sample characteristics mainly affected by the species of origin. Several factors, such as native tissue cells density, matrix thickness, lipid content, and species of origin (small or large animals) may influence decellularization efficiency [115]. To this purpose, evaluations on porcine trachea were performed, as it shows biomechanical properties similar to those of humans [116], providing for valuable data in perspective of implant on large animals as relevant translational model [117].

According to pre-clinical studies, miscellaneous protocols, combining chemical and enzymatic treatments to physical strategies, seem to be the preferred choice for effective trachea decellularization [6,104–114], including pig trachea [104,108,114]. Hence, this procedure was here followed adopting DNase, trypsin and Tergitol™ detergent solution. DNAse helped in nucleic acid sequences cleavage and, therefore, in nucleotides removal. Its use was documented by several Authors that recurred to physical+enzymatic+chemical methods for trachea decellularization [6,104,105,109–112], eventually mixed with the Rnase [106,107,113]. The serine protease trypsin supported the complete elimination of cell nuclei from the dense tracheal ECM. However, the exposure was limited to 1 h (concentration: 0.05% *w/v*) being disruptive to elastin and collagen (despite showing better

preservation of GAGs than sodium dodecyl sulphate (SDS)) in a time-dependent manner [34,118]. Focusing on detergents, Tergitol^{TM} was chosen. According to our knowledge, this is the first time that Tergitol^{TM} is adopted within a protocol for tracheal tissue decellularization. Others reported the use of sodium deoxycholate (SDC) [102,103,107–110,112], eventually combined with Triton X-100 [106,107,113]. SDC is an ionic surfactant leading to complete cell and nucleic membranes solubilization, with possible proteins' denaturation. Triton X-100 is a non-ionic surfactant; recently, it was included by the European Chemicals Agency (ECHA) in the list of substances of very high concern of the Registration, Evaluation, Authorisation and Restriction of Chemicals (REACH) Regulation, due to its potential toxicity to the endocrine human system. Hence, the need for its replacement is urgent, driving towards the identification of a valid substitute.

Chemicals may impair the ECM characteristics; hence, a combination with physical techniques can ameliorate the interaction solution/tissue, while reducing the exposure time. Moreover, tracheal cartilage density, despite essential for a functional graft, is likely an obstacle to detergents/enzymes penetration [119]. In the past, cartilage tissue ultrastructure was sacrificed to finally develop an acellular suspension to combine with synthetic polymers in a functional composite scaffold [120,121]. Considering the importance of tissue structure preservation for trachea, lyophilization was here introduced before each cycle (typically, prior to soak the tissue in Dnase solution) to boost decellularization solutions' penetration. As previously discussed for larynx by Hung et al. [122], improving tissue tendency to absorb fluids (as during rehydration after the freeze-drying) may enhance the method effectiveness. According to our knowledge, trachea lyophilization was firstly suggested in 1951, as a long-term preserving method prior to proceed with segment implant [123]. Later, it was introduced as an important decellularization step before trachea sonication in sodium dodecyl sulfate (SDS) solution [100] or within other complex decellularization protocols [124]. Osmotic shock through several washes in dH$_2$O was also included; the aim was to trigger cell membranes lysis but also support enzymatic/chemical solutions removal avoiding retains within the ECM net.

4.2. Cryopreservation and Decellularization Decrease Immunogenicity

Cryopreservation of the tissues was protracted for 13 months, prior to proceed with the subsequent characterization analyses; decellularization took 12 weeks (12 cycles) to be completed, as corroborated by DAPI staining (later also confirmed by histology) and DNA quantification assay, revealing a—91% in DNA total content. This is a crucial fact because residual DNA fragments in decellularized ECM may lead to cytocompatibility issues in vitro and adverse immunological response upon implantation [125,126]. Likewise, also cryopreservation was associated with an important reduction in genetic material (−60.4%). These are intriguing data, considering the limited tissue manipulation required by the method. Cells were still recognizable in each of the tissue three-layers; however, cryopreservation showed its potential in the tissues' antigenicity modification, suggesting that freezing periods modulation might further decrease the immunogenic potential of the tissue [8,25,74,88,97]. Intermittent immunosuppression was reported in preclinical studies [86], even though tracheas implant without recurring to immunosuppression, was also successfully assessed [72,74,80,89,96]. Freezing and thawing may induce a depletion and loss of class II antigen expression amenable to respiratory epithelium [24,76,79,91,96,127]. Together with these promising data, contrasting evidence also arose suggesting that no effect was exerted by prolonged periods of cryopreservation on the chondrocytes' viability and thus tracheal allogenicity [83,85,92]. It is very important to confirm the immunomodulatory effect of cryopreservation on tracheal allografts to allow potential clinical application of tracheal transplantation in the future [8]. Intense research efforts focusing on freezing time, cooling speed, cryoprotectant type/mixture may guarantee for the development of effective, cost-saving and safe allografts [23], not eliciting adverse immune reaction but also growing without calcifications and remaining patent [89,90,97]. Within this scenario, xenografts may represent a valuable resource to bridge the gap between the supply

and demand of organs/tissues; however, immunological barriers must be considered as xenotransplants are prone to rejection [128]. In particular, in case of wild-type pig organ transplantation into a human, a hyperacute rejection with graft destruction may occur and the major xenoantigen responsible of that is Alpha-Gal epitope [128,129]. In consideration of this, the effects mediated by cryopreservation and decellularization over Alpha-Gal epitope expression were analyzed. Compared to NativeT, CryoT still showed positive elements at the mucosa/submucosa layer and few remnants at the adventitia side, lining the cartilage. Conversely, the DecellT was Alpha-Gal epitope-free; morphometric analysis corroborated this evidence also highlighting a Alpha-Gal reduction after cryopreservation of about 37,18% and 35,18% in mucosa/submucosa and adventitia, respectively. The results provided by this study, despite only qualitative, are consistent with the literature. Cryopreservation may reduce the risk of immune rejection but cannot completely eradicate all the immune rejection inducing Alpha-Gal antigens [130]. Decellularization can be effective in removal of donor cells but also xenoantigens, including Alpha-Gal epitopes [131,132].

Regarding the immunogenicity of cryopreserved grafts after transplantation, clinical examination of patient immune response during the early postoperative course and long-term follow-up have scarcely been reported so far. Some trials investigated the immunogenicity of cryopreserved valved and nonvalved allografts used in the surgical repair of congenital heart defects, describing relevant HLA antibody response induced by transplanted materials [133–135]. Similar results were reported also for cryopreserved arterial homografts used to treat patients suffering from aortoiliac or aortobifemoral prosthetic infections [136]. However, the association between graft failure and immunologic injury is still debated. In light of this, pre-clinical studies aimed at validating the quality of cryopreserved grafts before clinical translation appear to be fundamental for controlling and standardizing the preparation methods of these materials in order to increase their biocompatibility.

Together with cryopreservation effect on immunogenicity also the "most adequate decellularization grade" is under controversy. As stated above, to obtain a completely decellularized trachea while preserving tissue ultrastructure/organization and ECM proteins content represents a difficult challenge to face. Because of this, many Authors started to eventually consider the development of partially acellular tracheas [31,33,100–102,113,114]. Cells removal from the mucosa/submucosa (respiratory epithelium and glands) decreases trachea antigenicity [137]; whereas cartilage could be identified as an "immune privileged" component [100] due to vessels absence and isolated/masked chondrocytes within a dense collagen-proteoglycans ECM [112]. Despite this encouraging assumption, presence of residual donor cells in the tissue to implant may affect graft safety, as eventual host reactions cannot be excluded. Furtherly, immunosuppressive therapy would be required after surgery, excluding malignancies-suffering patients from this kind of approach.

4.3. ECM and Structural Proteins Content Modification

Genetic material removal/reduced immunogenicity while retaining scaffold function is an ambitious goal to pursue [138]. Hence, preservation of the native ECM ultrastructure and composition during cryopreservation and decellularization is highly desirable. CryoT and DecellT grafts were preliminarily compared by H&E for an overall overview on tissue organization and/or evidence of eventual modification/disruptions. Cryopreservation only caused a partial exfoliation of the respiratory epithelium, in accordance with many other studies reported in the literature [24,60,83,97]. In accordance with Nakanishi et al. [83] it is possible that partial maintenance of epithelial cells in tracheal allografts, eventually capable of survival, may be ascribed to cryoprotection itself. Mucosa and submucosa were still identifiable, no damage occurred within the cartilaginous compartment showing well preserved lacunae; however, less DAPI/haematoxylin-stained elements were showed. Nakanishi et al. [8] sustained that cryoprotectants may not penetrate deeply into cartilage leading to chondrocytes degeneration with decreased antigenicity. As regards the adventitia, cellular presence was still detectable, but they were dispersed in a less compact tissue.

Despite some expected modifications, overall, CryoT appearance resembled that of NativeT, in accordance with other authors facing tracheal cryopreservation [38,87,93]. Possibly, the adequate freezing rate together with DMSO and albumin presence provided a synergic role in the maintenance of the tissue characteristics, depressing the freezing temperature of water and inhibiting ice formation [139]. Regarding decellularization, the main effects were reported at the respiratory epithelium, appearing as completely denuded. Only the basal membrane was identifiable; this is an intriguing feature, considering that the preservation of this structural element is supposed to facilitate cells' attachment, viability, and proliferation during repopulation, providing for functional epithelialization following orthotopic transplantation [31,32,140]. Focusing on the cartilaginous compartment, a certain dilation of the lacune was observed as possible consequence of the lyophilization. Lyophilization induces intracellular ice crystal formation, osmotic dehydration, and mechanical forces during rapid freezing with consequent cell membranes disruption, fragmentation of genetic material up to cell lysis. This physical strategy may be associated with ECM modification as well; however, as discussed above, fluids absorption optimization may minimize the amounts of chemical agents required for effective decellularization and their toxic effect [124]. DecellT adventitia, similarly to that of CryoT, appeared less dense but still identifiable. In parallel, H&E data were supported by SEM analysis; the respiratory epithelium modifications, exfoliation in CryoT and denuded in DecellT, were clearly recognizable versus NativeT.

Together with full-thickness tissue organization, the protocol's impact over ECM proteins was also verified. A fundamental consideration for organ decellularization is minimizing the undesirable alteration and loss of ECM components [126]. Typically, tissues matrix distinguishes fibrous elements (e.g., collagen and elastic fibers) and macromolecules (e.g., proteoglycans) organized in a network [141]. As regards the trachea, its viscoelastic properties convey from its ECM composition of glycosaminoglycans (15–30%), collagen (50–75%), and water (70–80%) [142,143]. Although ionic detergents in tracheal decellularization are very successful, they may affect the natural tissue structure disrupting ECM structure, eliminating growth factors and/or denaturing essential proteins [124,144]; thus, the non-ionic detergent Tergitol^{TM} was preferred. Here, GAGs, collagen (also focusing on collagen type I and type III), elastic fibers were also analysed through the integration of different approaches for a broad description.

Considering GAGs, Sutherland et al. [119], in a comparative study focused on physically devitalized cartilage (freezing at −20 °C, lyophilization, processing in a freezer-mill and frozen at −20 °C) versus decellularized cartilage (physical + enzymatic + chemical method), showed no significant effect after devitalization; conversely, decellularization led to 55% reduction in GAGs content. The same was also highlighted within our study, despite the total GAGs were slightly higher (reduction of 43.6%). GAGs' role is fundamental in preserving an adequate mechanical behaviour of the tissue, influencing collagen fibrils formation [142]; moreover, they support chondro-induction. However, partial reduction in GAGs content might be beneficial to create a less dense matrix that allows for cell infiltration and migration [119,145]. Masson's Trichrome staining confirmed collagen maintenance in DecellT and CryoT at the cartilagineous compartment, with a histological appearance resembling that of NativeT. This is essential to assure cartilage integrity [143]. This evidence was also supported by quantification analysis, showing no differences among groups at this level. Differently, a higher content in collagen for DecellT than CryoT and NativeT was calculated at the mucosa/submucosa and adventitia sides. Likely, this descends from removal of cells-associated red-coloured elements that masked the green-intensity within the mucosa/submucosa. Focusing on adventitia, this layer appeared more expanded after decellularization thus resulting in a more consistent area to measure in the photomicrographs. Furtherly, also Sirius Red staining was done, allowing for a specific focus over the mucosa/submucosa/cartilage side and adventitia. Under polarized light, a reduction in collagen type I signal (red-orange colour) was identified for the DecellT group within the mucosa/submucosa compartment versus CryoT and NativeT (these showing the same ap-

pearance); here, collagen type III was scantly represented in the whole cohort. An opposite trend was observed within the adventitia, where both collagens were mainly represented in DecellT than in the other groups. Possibly, this may depend on structural modifications following decellularization.

Intriguingly, thanks to advanced optical imaging techniques including multi-photon microscopy, it is possible to describe fibers' architecture in tissues through SHG, without recurring to any staining/fixation thus integrating the previous analyses [44,45,47,146–148]. Typically, collagen type I, II, III and V can produce SHG signals, differently from collagen type IV. Revising the literature, trachea SHG imaging is often limited to cartilage [147]. Ayyalasomayajula and Skallerud [147] provided data on the microstructure of the different tracheal components (mucosa/submucosa, cartilage, adventitia, and trachealis muscle layers), serving as a comparison. Here, together with cartilage, adventitia was also evaluated. Type II collagen was confirmed as the dominant protein of the hyaline cartilage; without any identifiable spatial organization (meshwork-like), it surrounded the lacunae. Hence, in accordance with the description by Ayyalasomayajula and Skallerud [147] on the bovine trachea, collagen in the adventitia was observed to be organized in thick type I collagen bundles emitting an extremely strong and robust SHG signal. These data are in accordance with polarized-light images after Sirius-Red staining.

Together with GAGs and collagen, elastic fibers' retain after cryopreservation and decellularization was analyzed. Little research on the elastic network in the major airways exists, even though their importance is outstanding providing for trachea ability to increase in length, diameter, being also involved in its elastic recoil [149]. Additionally, as well as collagen, the elastic fibers system has a fundamental role in tissue regeneration and recipient cells in-growth. In the human trachea, elastic fibers are abundantly represented in the submucosa with bundles displaying a longitudinal organization. Circular fibers are also detectable in close contact to the cartilage [149]. This organization resembles that of the pig NativeT and is also identifiable in the CryoT counterpart. Focusing on the DecellT, even if the elastic fibers elements were scant at the mucosa/submucosa layer (which appeared swelled), they were maintained at the interface with cartilage. Differently from CryoT, only elastic fibers remnants were maintained at the adventitia side. Histological evidence was well supported by morphometric analysis data. At the mucosa/submucosa side, NativeT and CryoT were comparable; differently, adventitia was more affected by treatments as highlighted by quantification study.

4.4. Compressive Mechanical Properties

Suitable mechanical properties are fundamental in the development of tracheal substitutes, in order to avoid post-surgical occlusion and collapse. Indeed, insufficient stiffness of substitutes and the occurrence of intratracheal stenosis are closely related, being the major reason of failure in tracheal reconstruction. In this framework, the characterization of the compressive mechanical behaviour of the native trachea and potential substitutes is crucial for developing successful surgical solutions [150]. The compressive mechanical properties of NativeT, DecellT, and CryoT were compared following a literature test protocol [151]. Ring-like samples had homogenous sizes, to avoid size- and shape-dependent effects on the compressive behavior. The compressive behaviour of NativeT was consistent with literature data on porcine trachea [116,151]. CryoT did not show any significant difference in stiffness with respect to NativeT, while DecellT had a strong stiffness reduction. This means that DecellT could be occluded up to 50% of compressive deformation with a force per unit of length which is one order of magnitude lower with respect to NativeT. This decrease in the compressive modulus is consistent with the reduction in GAGs content highlighted by histological analysis.

4.5. Confirmation of Tracheal Substitutes Cytocompatibility and Biocompatibility

Cryoprotectants exert a fundamental role in guiding, reducing, or preventing ice crystal formation, in turn protecting the biological structures during preservation and

guaranteeing ECM integrity after thawing; however, they bear the risk of possible undesired effects over the biological system [152]. Similarly, detergent type has significant effects on the biochemical composition of the decellularized ECM but also on cytocompatibility [141]. To this purpose, a cytotoxicity extract test was conducted prior to verifying biocompatibility through a heterotopic implant. As reported by Sugishita et al. [153], diffusion washing is necessary to significantly reduce the residual cryoprotectants. Similarly, Milian et al. [14] approaching porcine trachea decellularization by SDS, supported osmotic shock steps with distilled water to lessen undesirable effects of detergents. Following this method, nor CryoT neither DecellT showed toxic remnants adsorption/desorption, influencing in a negative manner human bone marrow-derived stromal cells (HM1-SV40) adhesion and proliferation. DecellT showed better outcomes than CryoT; possibly, the presence of a looser matrix (GAGs reduction), favored detergents removal. Moreover, cytocompatibility was assessed also by investigating CryoT and DecellT ability to sustain the adhesion and proliferation the HM1-SV40 cells. SEM analysis confirmed supports repopulation after 3 and 7 days from seeding, thus suggesting the scaffolds attitude to be colonized by cells prior to be implanted and/or in situ after surgical positioning.

To effectively evaluate the quality of a decellularized tissue, subcutaneous implantation constitutes an important step allowing to describe the efficiency of cell-associated proteins removal and local tissue response to eventually adsorbed chemical substances used during decellularization [62,154]. Regarding CryoT, preclinical evaluation allows to predict adverse reactions that may correlate not only with possible cyoprotectant residues but also with donor vital cells. Explants characterization by histology for general appearance (H&E) and ECM characteristics (GAGs, elastic fibers) showed a similar appearance between CryoT and DecellT, after 14 days from surgery; moreover, von Kossa staining excluded presence of any calcification. Hence, immunohistochemistry focused on lympho-monocytic infiltrate evaluation, distinguishing between the mucosa/submucosa-host latissimus dorsi interface and the adventitia-host subcutis interface, respectively. Matrix resorption takes place mainly through phagocytic cells such as mast cells, dendritic cells, and macrophages [155]. According with the analyses performed, a certain immunoreactivity (CD3, F4/80) was detected at both sides for the two experimental groups. It is possible that lymphocytes, exhibiting a certain cytokine secretory activity, triggered the recruitment of monocytes/macrophage, in turn implied in graft degradation and possible remodeling [44,45]. No substantial differences, nor in immune cells infiltration neither in fibrotic capsule formation, were highlighted comparing the CryoT and the DecellT sample groups. SEM explants analysis showed the presence of host cells covering the implant's surfaces.

Development of an efficient substitute for tracheal reconstruction remains a significant challenge. However, despite intense effort still being needed, the study results confirm that trachea allografts/xenografts may be a compliant option to resort to. Within this promising scenario, large animal studies are a fundamental stage to validate tissue engineered constructs due to sizes resembling that of human anatomy and allowing to face technical challenges, similar to those in clinical practice [117]. In consideration of this, orthotopic implants in an animal model of disease will represent the next step of this comparative work, allowing to analyze CryoT and DecellT ability in overcoming common issues in tracheal reconstruction. Re-epithelialization and vascularization of the grafts are fundamental to achieve functional graft survival.

5. Conclusions

Several studies focused on trachea cryopreservation or decellularization; however, according to our knowledge, this is the first investigation providing an in vitro and in vivo comparative analysis of the impact of both methods over tracheal tissue characteristics.

DecellT, developed here, appeared as a non-immunogenic substitute; lyophilization assured for adequate detergents/enzymes penetration, only partly depleting GAGs content; furthermore, Tergitol™ detergent showed favourable results in terms of collagen preservation. In parallel, CryoT maintained native tissue characteristics, while guaranteeing a

surprising reduction in genetic material content after freezing and thawing. However, as most cell nuclei were still detectable in whole tissue thickness, immunosuppression would be required in the perspective of an in vivo implant. According to the study evidence, both substitutes, despite being promising, showed strengths and weaknesses; hence, preclinical studies are unavoidable to guide clinicians. It is also possible that, in the future, these two treatments (i.e., decellularization and cryopreservation) will be combined. In fact, cryopreservation may allow for the safe storage of decellularized grafts prior to their use, or storage of native grafts prior to decellularization. Combining these two strategies may also aid in reducing the number of DNase-I-based treatments required for decellularization, and the associated costs of this procedure.

References

1. Grillo, H.C. Tracheal replacement: A critical review. *Ann. Thorac. Surg.* **2002**, *73*, 1995–2004. [CrossRef] [PubMed]
2. Wang, Z.; Sun, F.; Lu, Y.; Zhang, B.; Zhang, G.; Shi, H. Rapid Preparation Method for Preparing Tracheal Decellularized Scaffolds: Vacuum Assistance and Optimization of DNase I. *ACS Omega* **2021**, *6*, 10637–10644. [CrossRef]
3. Belsey, R. Resection and reconstruction of the intrathoracic trachea. *Br. J. Surg.* **1950**, *38*, 200–205. [CrossRef] [PubMed]
4. Zhao, L.; Sundaram, S.; Le, A.V.; Huang, A.H.; Zhang, J.; Hatachi, G.; Beloiartsev, A.; Caty, M.G.; Yi, T.; Leiby, K.; et al. Engineered Tissue–Stent Biocomposites as Tracheal Replacements. *Tissue Eng. Part A* **2016**, *22*, 1086–1097. [CrossRef] [PubMed]
5. Pan, S.; Lu, Y.; Li, J.; Shi, H. The biological properties of the decellularized tracheal scaffolds and 3D printing biomimetic materials: A comparative study. *J. Biomed. Mater. Res. Part A* **2022**, *110*, 1062–1076. [CrossRef] [PubMed]
6. Zhang, B.; Sun, F.; Lu, Y.; Wang, Z.; Shen, Z.; Yuan, L.; Wu, Q.; Wu, C.; Shi, H. A novel decellularized trachea preparation method for the rapid construction of a functional tissue engineered trachea to repair tracheal defects. *J. Mater. Chem. B* **2022**, *10*, 4810–4822. [CrossRef]
7. Sotres-Vega, A.; Villalba-Caloca, J.; Jasso-Victoria, R.; Olmos-Zúñiga, J.R.; Gaxiola-Gaxiola, M.; Baltazares-Lipp, M.; San-tibañez-Salgado, A.; Santillán-Doherty, P. Cryopreserved Tracheal Grafts: A Review of the Literature. *J. Investig. Tive Surg.* **2006**, *19*, 125–135. [CrossRef]
8. Nakanishi, R. Cryopreservation of the Tracheal Grafts: Review and Perspective. *Organogenesis* **2009**, *5*, 113–118. [CrossRef]
9. Virk, J.S.; Zhang, H.; Nouraei, S.A.R.; Sandhu, G. Prosthetic reconstruction of the trachea: A historical perspective. *World J. Clin. Cases* **2017**, *5*, 128–133. [CrossRef]
10. Etienne, H.; Fabre, D.; Gomez Caro, A.; Kolb, F.; Mussot, S.; Mercier, O.; Mitilian, D.; Stephan, F.; Fadel, E.; Dartevelle, P. Tracheal replacement. *Eur. Respir. J.* **2018**, *51*, 1702211. [CrossRef]
11. Damiano, G.; Palumbo, V.; Fazzotta, S.; Curione, F.; Monte, G.L.; Brucato, V.; Monte, A.L. Current Strategies for Tracheal Replacement: A Review. *Life* **2021**, *11*, 618. [CrossRef]
12. Xu, C.; Ma, Y.; Huang, H.; Ruan, Z.; Li, Y. A Review of Woven Tracheal Stents: Materials, Structures, and Application. *J. Funct. Biomater.* **2022**, *13*, 96. [CrossRef]

13. Gowers, K.H.; Hynds, R.E.; Thakrar, R.M.; Carroll, B.; Birchall, M.A.; Janes, S.M. Optimized isolation and expansion of human airway epithelial basal cells from endobronchial biopsy samples. *J. Tissue Eng. Regen. Med.* **2018**, *12*, e313–e317. [CrossRef]

14. Milian, L.; Sancho-Tello, M.; Roig-Soriano, J.; Foschini, G.; Martínez-Hernández, N.J.; Más-Estellés, J.; Ruiz-Sauri, A.; Zurriaga, J.; Carda, C.; Mata, M. Optimization of a decellularization protocol of porcine tracheas. Long-term effects of cryopreservation. A histological study. *Int. J. Artif. Organs* **2021**, *44*, 998–1012. [CrossRef]

15. De Wolf, J.; Brieu, M.; Zawadzki, C.; Ung, A.; Kipnis, E.; Jashari, R.; Hubert, T.; Fayoux, P.; Mariette, C.; Copin, M.-C.; et al. Successful immunosuppressant-free heterotopic transplantation of tracheal allografts in the pig. *Eur. J. Cardio-Thorac. Surg.* **2017**, *52*, 248–255. [CrossRef] [PubMed]

16. Paolin, A.; Trojan, D.; Leonardi, A.; Mellone, S.; Volpe, A.; Orlandi, A.; Cogliati, E. Cytokine expression and ultrastructural alterations in fresh-frozen, freeze-dried and γ-irradiated human amniotic membranes. *Cell Tissue Bank.* **2016**, *17*, 399–406. [CrossRef] [PubMed]

17. Viscioni, A.; Franco, M.; Paolin, A.; Cogliati, E.; Callegari, M.; Zollino, I.; Sollazzo, V.; Carinci, F. Effectiveness of fresh frozen and cryopreserved homologue iliac crest grafts used in sinus lifting: A comparative study. *Cell Tissue Bank.* **2011**, *12*, 263–271. [CrossRef]

18. Ahmad, S.; Singh, V.A.; Hussein, S.I. Cryopreservation versus Fresh Frozen Meniscal Allograft: A Biomechanical Comparative Analysis. *J. Orthop. Surg.* **2017**, *25*, 230949901772794. [CrossRef]

19. Teebken, O.; Pichlmaier, M.; Brand, S.; Haverich, A. Cryopreserved Arterial Allografts for In situ Reconstruction of Infected Arterial Vessels. *Eur. J. Vasc. Endovasc. Surg.* **2004**, *27*, 597–602. [CrossRef]

20. Müller-Schweinitzer, E. Cryopreservation of vascular tissues. *Organogenesis* **2009**, *5*, 97–104. [CrossRef] [PubMed]

21. Yousif, A.; Ali, K.; Anssar, M.; Harringer, W.; El-Essawi, A.; Brouwer, R. A 20-Year Experience with Cryopreserved Al-lografts as the Valve Replacement of Choice in Aortic Root Reconstruction for Destructive Endocarditis with Abscess Formation. *Interact. Cardio Vasc. Thorac. Surg.* **2022**, *35*, ivac188. [CrossRef]

22. Galeone, A.; Trojan, D.; Gardellini, J.; di Gaetano, R.; Faggian, G.; Luciani, G.B. Cryopreserved aortic homografts for complex aortic valve or root endocarditis: A 28-year experience. *Eur. J. Cardio-Thorac. Surg.* **2022**, *62*, ezac193. [CrossRef]

23. Bakhach, J. The Cryopreservation of Composite Tissues: Principles and Recent Advancement on Cryopreservation of Different Type of Tissues. *Organogenesis* **2009**, *5*, 119–126. [CrossRef]

24. Sotres-Vega, A.; Baltazares-Lipp, M.; Villalba-Caloca, J.; Gaxiola-Gaxiola, M.O.; Santibañez-Salgado, J.A.; Olmos-Zúñiga, J.R.; Jasso-Victoria, R. Tracheal Cryopreservation: Caspase-3 Immunoreactivity in Tracheal Epithelium and in Mixed Glands. *Braz. J. Med. Biol. Res.* **2009**, *42*, 1156–1162. [CrossRef]

25. Wang, J.; Zhang, H.; Feng, Y.; Sun, Y.; Ma, R.; Cui, P. Biomechanical changes of freezer-stored and decellularized pig tracheal scaffoldings. *J. Biomater. Appl.* **2021**, *35*, 1208–1217. [CrossRef]

26. Yokomise, H.; Inui, K.; Wada, H.; Ueda, M.; Hitomi, S. Long-term cryopreservation can prevent rejection of canine tracheal allografts with preservation of graft viability. *J. Thorac. Cardiovasc. Surg.* **1996**, *111*, 930–934. [CrossRef] [PubMed]

27. Cui, P.; Liu, P.; Li, S.; Ma, R. De-Epithelialized Heterotopic Tracheal Allografts without Immunosuppressants in Dogs: Long-Term Results for Cartilage Viability and Structural Integrity. *Ann. Otol. Rhinol. Laryngol.* **2021**, *130*, 441–449. [CrossRef] [PubMed]

28. Kunachak, S.; Kulapaditharom, B.; Vajaradul, Y.; Rochanawutanon, M. Cryopreserved, Irradiated Tracheal Homograft Transplantation for Laryngotracheal Reconstruction in Human Beings. *Otolaryngol. Neck Surg.* **2000**, *122*, 911–916. [CrossRef]

29. Porzionato, A.; Stocco, E.; Barbon, S.; Grandi, F.; Macchi, V.; de Caro, R. Tissue-Engineered Grafts from Human Decellu-larized Extracellular Matrices: A Systematic Review and Future Perspectives. *Int. J. Mol. Sci.* **2018**, *19*, 4117. [CrossRef]

30. Liu, L.; Dharmadhikari, S.; Spector, B.M.; Tan, Z.H.; E Van Curen, C.; Agarwal, R.; Nyirjesy, S.; Shontz, K.; A Sperber, S.; Breuer, C.K.; et al. Tissue-engineered composite tracheal grafts create mechanically stable and biocompatible airway replacements. *J. Tissue Eng.* **2022**, *13*, 2041731422110879. [CrossRef] [PubMed]

31. Kutten, J.C.; McGovern, D.; Hobson, C.M.; Luffy, S.A.; Nieponice, A.; Tobita, K.; Francis, R.; Reynolds, S.D.; Isenberg, J.S.; Gilbert, T.W. Decellularized Tracheal Extracellular Matrix Supports Epithelial Migration, Differentiation, and Function. *Tissue Eng. Part A* **2015**, *21*, 75–84. [CrossRef] [PubMed]

32. Aoki, F.G.; Varma, R.; Marin-Araujo, A.E.; Lee, H.; Soleas, J.P.; Li, A.H.; Soon, K.; Romero, D.; Moriya, H.T.; Haykal, S.; et al. De-epithelialization of porcine tracheal allografts as an approach for tracheal tissue engineering. *Sci. Rep.* **2019**, *9*, 1023. [CrossRef]

33. Liu, L.; Dharmadhikari, S.; Shontz, K.M.; Tan, Z.H.; Spector, B.M.; Stephens, B.; Bergman, M.; Manning, A.; Zhao, K.; Reynolds, S.D.; et al. Regeneration of partially decellularized tracheal scaffolds in a mouse model of orthotopic tracheal replacement. *J. Tissue Eng.* **2021**, *12*, 20417314211017417. [CrossRef] [PubMed]

34. Crapo, P.M.; Gilbert, T.W.; Badylak, S.F. An overview of tissue and whole organ decellularization processes. *Biomaterials* **2011**, *32*, 3233–3243. [CrossRef] [PubMed]

35. Elliott, M.J.; De Coppi, P.; Speggiorin, S.; Roebuck, D.; Butler, C.R.; Samuel, E.; Crowley, C.; McLaren, C.; Fierens, A.; Vondrys, D.; et al. Stem-cell-based, tissue engineered tracheal replacement in a child: A 2-year follow-up study. *Lancet* **2012**, *380*, 994–1000. [CrossRef]

36. Hamilton, N.J.; Kanani, M.; Roebuck, D.J.; Hewitt, R.J.; Cetto, R.; Culme-Seymour, E.J.; Toll, E.; Bates, A.J.; Comerford, A.P.; McLaren, C.A.; et al. Tissue-Engineered Tracheal Replacement in a Child: A 4-Year Follow-Up Study. *Am. J. Transplant.* **2015**, *15*, 2750–2757. [CrossRef] [PubMed]

37. Ahmed, A.; Ahmed, S.; Varghese, K.S.; Mathew, D.M.; Pandey, R.; Rogando, D.O.; Salazar, S.A.; Fusco, P.J.; Levy, K.H. Decellularized versus cryopreserved pulmonary allografts for right ventricular outflow tract reconstruction during the Ross procedure: A meta-analysis of short- and long-term outcomes. *Egypt. Heart J.* **2021**, *73*, 100. [CrossRef]

38. Lauk-Dubitskiy, S.E.; Pushkarev, A.V.; Korovin, I.A.; Shakurov, A.V.; Burkov, I.A.; Severgina, L.O.; Zherdev, A.A.; Tsiganov, D.I.; Novikov, I.A. Porcine heart valve, aorta and trachea cryopreservation and thawing using polydime-thylsiloxane. *Cryobiology* **2020**, *93*, 91–101. [CrossRef]

39. Silan, F.; Consiglio, F.; Dell'Antonia, F.; Montagner, G.; Trojan, D.; Berna, G. Cryopreserved fascia lata allograft use in surgical facial reanimation: A retrospective study of seven cases. *Maxillofac. Plast. Reconstr. Surg.* **2020**, *42*, 1–6. [CrossRef]

40. Paolin, A.; Spagnol, L.; Battistella, G.; Trojan, D. Evaluation of allograft decontamination with two different antibiotic cocktails at the Treviso Tissue Bank Foundation. *PLoS ONE* **2018**, *13*, e0201792. [CrossRef]

41. Montagner, G.; Trojan, D.; Cogliati, E.; Manea, F.; Vantini, A.; Paolin, A. Stability analysis of the antibiotic cocktail used by Treviso Tissue Bank Foundation for tissues decontamination. *Cell Tissue Bank.* **2018**, *19*, 721–726. [CrossRef] [PubMed]

42. Iop, L.; Paolin, A.; Aguiari, P.; Trojan, D.; Cogliati, E.; Gerosa, G. Decellularized Cryopreserved Allografts as Off-the-Shelf Allogeneic Alternative for Heart Valve Replacement: In Vitro Assessment Before Clinical Translation. *J. Cardiovasc. Transl. Res.* **2017**, *10*, 93–103. [CrossRef]

43. Martelloni, M.; Boccaletto, P.; Montagner, G.; Trojan, D.; Abate, R. Bilaminar Technique with Coronally Advanced Flap and Cryopreserved Human Amniotic Membrane in the Treatment of Gingival Recessions. *Case Rep. Dent.* **2020**, *2020*, 1–4. [CrossRef]

44. Barbon, S.; Biccari, A.; Stocco, E.; Capovilla, G.; D'Angelo, E.; Todesco, M.; Sandrin, D.; Bagno, A.; Romanato, F.; Macchi, V.; et al. Bio-Engineered Scaffolds Derived from Decellularized Human Esophagus for Functional Organ Reconstruction. *Cells* **2022**, *11*, 2945. [CrossRef]

45. Barbon, S.; Stocco, E.; Contran, M.; Facchin, F.; Boscolo-Berto, R.; Todros, S.; Sandrin, D.; Romanato, F.; Pavan, P.; Macchi, V.; et al. Preclinical Development of Bioengineered Allografts Derived from Decellularized Human Diaphragm. *Biomedicines* **2022**, *10*, 739. [CrossRef] [PubMed]

46. Naso, F.; Gandaglia, A.; Iop, L.; Spina, M.; Gerosa, G. Alpha-Gal detectors in xenotransplantation research: A word of caution. *Xenotransplantation* **2012**, *19*, 215–220. [CrossRef] [PubMed]

47. Stocco, E.; Belluzzi, E.; Contran, M.; Boscolo-Berto, R.; Picardi, E.; Guidolin, D.; Fontanella, C.G.; Olivotto, E.; Filardo, G.; Borile, G.; et al. Age-Dependent Remodeling in Infrapatellar Fat Pad Adipocytes and Extracellular Matrix: A Comparative Study. *Front. Med.* **2021**, *8*, 661403. [CrossRef]

48. Emmi, A.; Antonini, A.; Sandre, M.; Baldo, A.; Contran, M.; Macchi, V.; Guidolin, D.; Porzionato, A.; De Caro, R. To-pography and distribution of adenosine A2A and dopamine D2 receptors in the human Subthalamic Nucleus. *Front. Neurosci.* **2022**, *16*, 945574. [CrossRef]

49. Emmi, A.; Stocco, E.; Boscolo-Berto, R.; Contran, M.; Belluzzi, E.; Favero, M.; Ramonda, R.; Porzionato, A.; Ruggieri, P.; De Caro, R.; et al. Infrapatellar Fat Pad-Synovial Membrane Anatomo-Fuctional Unit: Microscopic Basis for Piezo1/2 Mechanosensors Involvement in Osteoarthritis Pain. *Front. Cell Dev. Biol.* **2022**, *10*, 886604. [CrossRef]

50. Filippi, A.; Sasso, E.D.; Iop, L.; Armani, A.; Gintoli, M.; Sandri, M.; Gerosa, G.; Romanato, F.; Borile, G. Multimodal label-free ex vivo imaging using a dual-wavelength microscope with axial chromatic aberration compensation. *J. Biomed. Opt.* **2018**, *23*, 091403. [CrossRef]

51. Schindelin, J.; Arganda-Carreras, I.; Frise, E.; Kaynig, V.; Longair, M.; Pietzsch, T.; Preibisch, S.; Rueden, C.; Saalfeld, S.; Schmid, B.; et al. Fiji: An open-source platform for biological-image analysis. *Nat. Methods* **2012**, *9*, 676–682. [CrossRef]

52. Wu, S.; Li, H.; Yang, H.; Zhang, X.; Li, Z.; Xu, S. Quantitative analysis on collagen morphology in aging skin based on multiphoton microscopy. *J. Biomed. Opt.* **2011**, *16*, 040502. [CrossRef] [PubMed]

53. Borile, G.; Sandrin, D.; Filippi, A.; Anderson, K.; Romanato, F. Label-Free Multiphoton Microscopy: Much More Than Fancy Images. *Int. J. Mol. Sci.* **2021**, *22*, 2657. [CrossRef] [PubMed]

54. Stocco, E.; Barbon, S.; Mammana, M.; Zambello, G.; Contran, M.; Parnigotto, P.P.; Macchi, V.; Conconi, M.T.; Rea, F.; De Caro, R.; et al. Preclinical and clinical orthotopic transplantation of decellularized/engineered tracheal scaffolds: A systematic literature review. *J. Tissue Eng.* **2023**, *14*, 20417314231151826. [CrossRef]

55. *ISO 10993-6 2009*; Biological Evaluation of Medical Devices—Part 6: Tests for Local Effects after Implantation. Organization for Standardization: Geneva, Switzerland, 2009.

56. Parshad, S.; Gogna, S.; Saroha, V.; Lohchab, S.S.; Karwasra, R.K. Tracheal Resection and Reconstruction for Malignant Tumor. *Indian J. Surg. Oncol.* **2020**, *11*, 199–203. [CrossRef]

57. He, J.; Yang, C.; Yang, H.; Chen, H.; He, J.; Li, S. Resection and reconstruction via median sternotomy incision for tracheal tumors. *Transl. Lung Cancer Res.* **2022**, *11*, 600–606. [CrossRef] [PubMed]

58. Wen, W.; Du, X.; Zhu, L.; Wang, S.; Xu, Z.; Lu, Z. Surgical management of long-segment congenital tracheal stenosis with tracheobronchial malacia. *Eur. J. Cardio-Thorac. Surg.* **2022**, *61*, 1001–1010. [CrossRef]

59. Brand-Saberi, B.E.M.; Schäfer, T. Trachea: Anatomy and Physiology. *Thorac. Surg. Clin.* **2014**, *24*, 1–5. [CrossRef] [PubMed]

60. Mabrut, J.; Adham, M.; Bourgeot, J.; Eljaafari, A.; DelaRoche, E.; Ducerf, C.; Baulieux, J.; Rigal, D. Mechanical and histological characteristics of human trachea before and after cryopreservation: An opportunity for tracheal tissue banking. *Transplant. Proc.* **2001**, *33*, 609–611. [CrossRef]

61. Candas, F.; Gorur, R.; Haholu, A.; Yildizhan, A.; Yucel, O.; Ay, H.; Memis, A.; Isitmangil, T. Is Tracheal Transplantation Possible with Cryopreserved Tracheal Allograft and Hyperbaric Oxygen Therapy? An Experimental Study. *Ann. Thorac. Surg.* **2016**, *101*, 1139–1144. [CrossRef]

62. Aamodt, J.M.; Grainger, D.W. Extracellular matrix-based biomaterial scaffolds and the host response. *Biomaterials* **2016**, *86*, 68–82. [CrossRef]

63. Godehardt, A.W.; Tönjes, R.R. Xenotransplantation of decellularized pig heart valves—Regulatory aspects in Europe. *Xenotransplantation* **2020**, *27*, e12609. [CrossRef]

64. Deschamps, C.; Trastek, V.F.; Ferguson, J.L.; Martin, W.J.; Colby, T.V.; Pairolero, P.C.; Payne, W. Cryopreservation of canine trachea: Functional and histological changes. *Ann. Thorac. Surg.* **1989**, *47*, 208–212. [CrossRef] [PubMed]

65. Liu, Y.; Nakamura, T.; Yamamoto, Y.; Matsumoto, K.; Sekine, T.; Ueda, H.; Shimizu, Y. A New Tracheal Bioartificial Organ: Evaluation of a Tracheal Allograft with Minimal Antigenicity after Treatment by Detergent. *ASAIO J.* **2000**, *46*, 536–539. [CrossRef] [PubMed]

66. Liu, Y.; Nakamura, T.; Sekine, T.; Matsumoto, K.; Ueda, H.; Yoshitani, M.; Toba, T.; Shimizu, Y. New Type of Tracheal Bioartificial Organ Treated with Detergent: Maintaining Cartilage Viability Is Necessary for Successful Immunosuppressant Free Allotransplantation. *ASAIO J.* **2002**, *48*, 21–25. [CrossRef]

67. Sotres-Vega, A.; Santibañez-Salgado, J.A.; Villalba-Caloca, J.; Gaxiola-Gaxiola, M.; Ramos-Abraham, C.; Rosales-Torres, A.M.; Jiménez-García, L.F. Canine Tracheal Cartilage Cryopreservation: Freezing Injury Is Not Related to Caspase-3 Ex-pression. *Biopreserv. Biobank.* **2013**, *11*, 45–50. [CrossRef] [PubMed]

68. Lenot, B.; Macchiarini, P.; Dulmet, E.; Weiss, M.; Dartevelle, P. Tracheal allograft replacement *1An unsuccessful method. *Eur. J. Cardio-Thorac. Surg.* **1993**, *7*, 648–652. [CrossRef]

69. Messineo, A.; Filler, R.M.; Bahoric, A.; Smith, C.R. Repair of long tracheal defects with cryopreserved cartilaginous allografts. *J. Pediatr. Surg.* **1992**, *27*, 1131–1135. [CrossRef]

70. Messineo, A.; Filler, R.M.; Joseph, T.; Bahoric, A.; Smith, C.R. Tracheoplasty without stent, using preshaped cryopreserved cartilage allografts in neonatal pigs. *J. Pediatr. Surg.* **1994**, *29*, 697–700. [CrossRef]

71. Yokomise, H.; Inui, K.; Wada, H.; Hasegawa, S.; Ohno, N.; Hitomi, S. Reliable cryopreservation of trachea for one month in a new trehalose solution. *J. Thorac. Cardiovasc. Surg.* **1995**, *110*, 382–385. [CrossRef]

72. Inutsuka, K.; Kawahara, K.; Takachi, T.; Okabayashi, K.; Shiraishi, T.; Shirakusa, T. Reconstruction of trachea and carina with immediate or cryopreserved allografts in dogs. *Ann. Thorac. Surg.* **1996**, *62*, 1480–1484. [CrossRef]

73. Tojo, T.; Niwaya, K.; Sawabata, N.; Nezu, K.; Kawachi, K.; Kitamura, S. Tracheal allogenic immunoresponse is reduced by cryopreservation: Canine experiment. *Transplant. Proc.* **1996**, *28*, 1814–1815. [PubMed]

74. Ueda, M.; Yokomise, H.; Wada, H.; Hitomi, S. Experimental tracheal transplantation for possible clinical application. *Transplant. Proc.* **1997**, *29*, 871–873. [CrossRef] [PubMed]

75. Zhao, H.; Hua, T.-C.; Zhou, Y.-Z.; Wang, Q.-F.; Yang, Y.; Bao, L.-L. Cryopreservation and Transplantation of Dog Tra-cheaa. *Ann. N. Y. Acad. Sci.* **1998**, *858*, 270–275. [CrossRef] [PubMed]

76. Mukaida, T.; Shimizu, N.; Aoe, M.; Andou, A.; Date, H.; Okabe, K.; Yamashita, M.; Ichiba, S. Experimental study of tracheal allotransplantation with cryopreserved grafts. *J. Thorac. Cardiovasc. Surg.* **1998**, *116*, 262–266. [CrossRef]

77. Tojo, T.; Kitamura, S.; Gojo, S.; Kushibe, K.; Nezu, K.; Taniguchi, S. Epithelial regeneration and preservation of tracheal cartilage after tracheal replacement with cryopreserved allograft in the rat. *J. Thorac. Cardiovasc. Surg.* **1998**, *116*, 624–627. [CrossRef]

78. Kawahara, K.; Inutsuka, K.; Hiratsuka, M.; Makihata, S.; Okabayashi, K.; Shiraishi, T.; Shirakusa, T. Tracheal Trans-plantation for Carinal Reconstruction in Dogs. *J. Thorac. Cardiovasc. Surg.* **1998**, *116*, 397–401. [CrossRef]

79. Mukaida, T.; Shimizu, N.; Aoe, M.; Andou, A.; Date, H. Tracheal Allotransplantation after Varying Terms of Cryopreservation. *Transpl. Proc.* **1998**, *30*, 3397–3400. [CrossRef]

80. Tojo, T.; Niwaya, K.; Sawabata, N.; Kushibe, K.; Nezu, K.; Taniguchi, S.; Kitamura, S. Tracheal Replacement with Cryo-preserved Tracheal Allograft: Experiment in Dogs. *Ann. Thorac. Surg.* **1998**, *66*, 209–213. [CrossRef]

81. Aoki, T.; Yamato, Y.; Tsuchida, M.; Souma, T.; Yoshiya, K.; Watanabe, T.; Hayashi, J.-I. Successful tracheal transplantation using cryopreserved allografts in a rat model. *Eur. J. Cardio-Thorac. Surg.* **1999**, *16*, 169–173. [CrossRef]

82. Moriyama, H.; Sasajima, T.; Hirata, S.; Yamazaki, K.; Yatsuyanagi, E.; Kubo, Y. Revascularization of canine cryopreserved tracheal allografts. *Ann. Thorac. Surg.* **2000**, *69*, 1701–1706. [CrossRef]

83. Nakanishi, R.; Hashimoto, M.; Muranaka, H.; Yasumoto, K. Effect of cryopreservation period on rat tracheal allografts. *J. Heart Lung Transplant.* **2001**, *20*, 1010–1015. [CrossRef] [PubMed]

84. Kushibe, K.; Nezu, K.; Nishizaki, K.; Takahama, M.; Taniguchi, S. Tracheal allotransplantation maintaining cartilage viability with long-term cryopreserved allografts. *Ann. Thorac. Surg.* **2001**, *71*, 1666–1669. [CrossRef] [PubMed]

85. Kawahara, K.; Hiratsuka, M.; Mikami, K.; Makihata, S.; Yoneda, S.; Shiraishi, T.; Okabayashi, K.; Shirakusa, T. Obliterative airway disease and graft stenting in pig-to-dog tracheal xenotransplantation. *Jpn. J. Thorac. Cardiovasc. Surg.* **2001**, *49*, 53–57. [CrossRef]

86. Hashimoto, M.; Nakanishi, R.; Umesue, M.; Muranaka, H.; Hachida, M.; Yasumoto, K. Feasibility of Cryopreserved Tra-cheal Xenotransplants with the Use of Short-Course Immunosuppression. *J. Thorac. Cardiovasc. Surg.* **2001**, *121*, 241–248. [CrossRef]

87. Nakanishi, R.; Onitsuka, T.; Shigematsu, Y.; Hashimoto, M.; Muranaka, H.; Yasumoto, K. The immunomodulatory effect of cryopreservation in rat tracheal allotransplantation. *J. Heart Lung Transplant.* **2002**, *21*, 890–898. [CrossRef]

88. Murakawa, T.; Nakajima, J.; Motomura, N.; Murakami, A.; Takamoto, S. Successful allotransplantation of cryopreserved tracheal grafts with preservation of the pars membranacea in nonhuman primates. *J. Thorac. Cardiovasc. Surg.* **2002**, *123*, 153–160. [CrossRef]

89. Tanaka, H.; Maeda, K.; Okita, Y. Transplantation of the cryopreserved tracheal allograft in growing rabbits. *J. Pediatr. Surg.* **2003**, *38*, 1707–1711. [CrossRef]

90. Hisamatsu, C.; Maeda, K.; Tanaka, H.; Okita, Y. Transplantation of the cryopreserved tracheal allograft in growing rabbits: Effect of immunosuppressant. *Pediatr. Surg. Int.* **2006**, *22*, 881–885. [CrossRef] [PubMed]

91. Liu, Y.; Zheng, R.; Ding, J.; Qiao, Y.; Wang, Q. Histological Examination of Cryopreserved Rat Tracheal Grafts. *ASAIO J.* **2007**, *53*, 492–496. [CrossRef] [PubMed]

92. Liu, Y.; Yang, Y.; Ding, J.; Wang, H.; Zheng, R.; Wang, Q. Ultrastructural Changes in Cryopreserved Tracheal Grafts of Sprague-Dawley Rats. *ASAIO J.* **2009**, *55*, 509–513. [CrossRef] [PubMed]

93. Iyikesici, T.; Tuncozgur, B.; Sanli, M.; Isik, A.F.; Meteroglu, F.; Elbeyli, L. Two-Piece Cryopreserved Tracheal Allotrans-plantation: An Experimental Study. *Eur. J. Cardio-Thorac. Surg.* **2009**, *36*, 722–726. [CrossRef]

94. Han, Y.; Lan, N.; Pang, C.; Tong, X. Bone Marrow-Derived Mesenchymal Stem Cells Enhance Cryopreserved Trachea Allograft Epithelium Regeneration and Vascular Endothelial Growth Factor Expression. *Transplantation* **2011**, *92*, 620–626. [CrossRef]

95. Hysi, I.; Wurtz, A.; Zawadzki, C.; Kipnis, E.; Jashari, R.; Hubert, T.; Ung, A.; Copin, M.-C.; Jude, B. Immune tolerance of epithelium-denuded-cryopreserved tracheal allograft. *Eur. J. Cardio-Thorac. Surg.* **2014**, *45*, e180–e186. [CrossRef] [PubMed]

96. Hysi, I.; Kipnis, E.; Fayoux, P.; Copin, M.-C.; Zawadzki, C.; Jashari, R.; Hubert, T.; Ung, A.; Ramon, P.; Jude, B.; et al. Successful orthotopic transplantation of short tracheal segments without immunosuppressive therapy. *Eur. J. Cardio-Thorac. Surg.* **2015**, *47*, e54–e61. [CrossRef]

97. Lu, T.; Huang, Y.; Liu, Y.; Shen, Y.; Qiao, Y.; Zhang, Y. Effects of cryopreservation on tracheal allograft antigenicity in dogs. *J. Thorac. Dis.* **2017**, *9*, 2038–2047. [CrossRef]

98. Ratto, C.; Parolini, O.; Marra, A.A.; Orticelli, V.; Parello, A.; Campennì, P.; de Simone, V.; Trojan, D.; Litta, F. Human Amniotic Membrane for the Treatment of Cryptoglandular Anal. *Fistulas. J. Clin. Med.* **2022**, *11*, 1350. [CrossRef]

99. Wood, M.W.; Murphy, S.V.; Feng, X.; Wright, J.S.C. Tracheal Reconstruction in a Canine Model. *Otolaryngol. Neck Surg.* **2014**, *150*, 428–433. [CrossRef] [PubMed]

100. Hung, S.-H.; Su, C.-H.; Lin, S.-E.; Tseng, H. Preliminary experiences in trachea scaffold tissue engineering with segmental organ decellularization. *Laryngoscope* **2016**, *126*, 2520–2527. [CrossRef] [PubMed]

101. Dang, L.H.; Hung, S.-H.; Tseng, Y.; Quang, L.X.; Le, N.T.N.; Fang, C.-L.; Tseng, H. Partial Decellularized Scaffold Com-bined with Autologous Nasal Epithelial Cell Sheet for Tracheal Tissue Engineering. *Int. J. Mol. Sci.* **2021**, *22*, 10322. [CrossRef]

102. Dang, L.; Tseng, Y.; Tseng, H.; Hung, S.-H. Partial Decellularization for Segmental Tracheal Scaffold Tissue Engineering: A Preliminary Study in Rabbits. *Biomolecules* **2021**, *11*, 866. [CrossRef]

103. Tan, Z.H.; Dharmadhikari, S.; Liu, L.; Wolter, G.; Shontz, K.M.; Reynolds, S.D.; Johnson, J.; Breuer, C.K.; Chiang, T. Tra-cheal Macrophages During Regeneration and Repair of Long-Segment Airway Defects. *Laryngoscope* **2022**, *132*, 737–746. [CrossRef] [PubMed]

104. Go, T.; Jungebluth, P.; Baiguero, S.; Asnaghi, A.; Martorell, J.; Ostertag, H.; Mantero, S.; Birchall, M.; Bader, A.; Macchiarini, P. Both epithelial cells and mesenchymal stem cell–derived chondrocytes contribute to the survival of tissue-engineered airway transplants in pigs. *J. Thorac. Cardiovasc. Surg.* **2010**, *139*, 437–443. [CrossRef] [PubMed]

105. Gray, F.L.; Turner, C.G.; Ahmed, A.; Calvert, C.E.; Zurakowski, D.; Fauza, D.O. Prenatal tracheal reconstruction with a hybrid amniotic mesenchymal stem cells–engineered construct derived from decellularized airway. *J. Pediatr. Surg.* **2012**, *47*, 1072–1079. [CrossRef]

106. Batioglu-Karaaltin, A.; Karaaltin, M.V.; Ovali, E.; Yigit, O.; Kongur, M.; Inan, O.; Bozkurt, E.; Cansiz, H. In Vivo Tis-sue-Engineered Allogenic Trachea Transplantation in Rabbits: A Preliminary Report. *Stem. Cell Rev. Rep.* **2015**, *11*, 347–356. [CrossRef] [PubMed]

107. Maughan, E.F.; Butler, C.R.; Crowley, C.; Teoh, G.Z.; den Hondt, M.; Hamilton, N.J.; Hynds, R.E.; Lange, P.; Ansari, T.; Urbani, L.; et al. A comparison of tracheal scaffold strategies for pediatric transplantation in a rabbit model. *Laryngoscope* **2017**, *127*, E449–E457. [CrossRef] [PubMed]

108. Ohno, M.; Fuchimoto, Y.; Hsu, H.-C.; Higuchi, M.; Komura, M.; Yamaoka, T.; Umezawa, A.; Enosawa, S.; Kuroda, T. Airway reconstruction using decellularized tracheal allografts in a porcine model. *Pediatr. Surg. Int.* **2017**, *33*, 1065–1071. [CrossRef]

109. Ershadi, R.; Rahim, M.; Jahany, S.; Rakei, S. Transplantation of the decellularized tracheal allograft in animal model (rabbit). *Asian J. Surg.* **2018**, *41*, 328–332. [CrossRef]

110. Jang, S.J.; Park, M.-H.; Lee, T.-K.; Choi, S.H. Healing Effect of Platelet-Rich Plasma on Decellularized Tracheal Allotrans-plantation in Rabbits. *Vivo* **2018**, *32*, 1443–1447. [CrossRef]

111. Zhou, Q.; Ye, X.; Ran, Q.; Kitahara, A.; Matsumoto, Y.; Moriyama, M.; Ajioka, Y.; Saijo, Y. Trachea Engineering Using a Centrifugation Method and Mouse-Induced Pluripotent Stem Cells. *Tissue Eng. Part C Methods* **2018**, *24*, 524–533. [CrossRef]

112. Zhong, Y.; Yang, W.; Pan, Z.Y.; Pan, S.; Zhang, S.Q.; Wang, Z.H.; Gu, S.; Shi, H. In Vivo transplantation of stem cells with a genipin linked scaffold for tracheal construction. *J. Biomater. Appl.* **2019**, *34*, 47–60. [CrossRef] [PubMed]

113. Sun, F.; Lu, Y.; Wang, Z.; Zhang, B.; Shen, Z.; Yuan, L.; Wu, C.; Wu, Q.; Yang, W.; Zhang, G.; et al. Directly construct microvascularization of tissue engineering trachea in orthotopic transplantation. *Mater. Sci. Eng. C* **2021**, *128*, 112201. [CrossRef] [PubMed]

114. Villalba-Caloca, J.; Sotres-Vega, A.; Giraldo-Gómez, D.M.; O Gaxiola-Gaxiola, M.; Piña-Barba, M.C.; A García-Montes, J.; Martínez-Fonseca, S.; Alonso-Gómez, M.; Santibáñez-Salgado, J.A. In Vivo performance of decellularized tracheal grafts in the reconstruction of long length tracheal defects: Experimental study. *Int. J. Artif. Organs* **2021**, *44*, 718–726. [CrossRef]

115. Nakamura, N.; Kimura, T.; Kishida, A. Overview of the Development, Applications, and Future Perspectives of Decellularized Tissues and Organs. *ACS Biomater. Sci. Eng.* **2017**, *3*, 1236–1244. [CrossRef]

116. Han, M.-N.; Kim, J.-H.; Choi, S.H. Evaluation of Biomechanical Properties and Morphometric Structures of the Trachea in Pigs and Rabbits. *Vivo* **2022**, *36*, 1718–1725. [CrossRef] [PubMed]

117. Weber, J.F.; Rehmani, S.S.; Baig, M.Z.; Jadoon, Y.; Bhora, F.Y. Successes and Failures in Tracheal Bioengineering: Lessons Learned. *Ann. Thorac. Surg.* **2021**, *112*, 1089–1094. [CrossRef] [PubMed]

118. Yang, M.; Chen, C.-Z.; Wang, X.-N.; Zhu, Y.-B.; Gu, Y.J. Favorable effects of the detergent and enzyme extraction method for preparing decellularized bovine pericardium scaffold for tissue engineered heart valves. *J. Biomed. Mater. Res. Part B Appl. Biomater.* **2009**, *91B*, 354–361. [CrossRef] [PubMed]

119. Sutherland, A.J.; Beck, E.C.; Dennis, S.C.; Converse, G.L.; Hopkins, R.A.; Berkland, C.J.; Detamore, M.S. Decellularized Cartilage May Be a Chondroinductive Material for Osteochondral Tissue Engineering. *PLoS ONE* **2015**, *10*, e0121966. [CrossRef]

120. Stocco, E.; Barbon, S.; Dalzoppo, D.; Lora, S.; Sartore, L.; Folin, M.; Parnigotto, P.P.; Grandi, C. Tailored PVA/ECM Scaffolds for Cartilage Regeneration. *BioMed Res. Int.* **2014**, *2014*, 1–12. [CrossRef]

121. Stocco, E.; Barbon, S.; Radossi, P.; Rajendran, S.; Dalzoppo, D.; Bortolami, M.; Bagno, A.; Grandi, F.; Gamba, P.G.; Parnigotto, P.P.; et al. Autologous chondrocytes as a novel source for neo-chondrogenesis in haemophiliacs. *Cell Tissue Res.* **2016**, *366*, 51–61. [CrossRef]

122. Hung, S.-H.; Su, C.-H.; Lee, F.-P.; Tseng, H. Larynx Decellularization: Combining Freeze-Drying and Sonication as an Effective Method. *J. Voice* **2013**, *27*, 289–294. [CrossRef]

123. Marrangoni, A.G. Homotransplantation of tracheal segments preserved by lyophilization; an experimental study. *J. Thorac. Surg.* **1951**, *21*, 398–401. [CrossRef]

124. Batioglu-Karaaltin, A.; Ovali, E.; Karaaltin, M.V.; Yener, M.; Yılmaz, M.; Eyüpoğlu, F.; Yılmaz, Y.Z.; Bozkurt, E.R.; Demir, N.; Konuk, E.; et al. Decellularization of Trachea With Combined Techniques for Tissue-Engineered Trachea Transplantation. *Clin. Exp. Otorhinolaryngol.* **2019**, *12*, 86–94. [CrossRef]

125. Keane, T.J.; Londono, R.; Turner, N.J.; Badylak, S.F. Consequences of ineffective decellularization of biologic scaffolds on the host response. *Biomaterials* **2012**, *33*, 1771–1781. [CrossRef]

126. Giraldo-Gomez, D.M.; Garcia-Lopez, J.; Tamay-De-Dios, L.; Sánchez-Sánchez, R.; Villalba-Caloca, J.; Sotres-Vega, A.; Del Prado-Audelo, M.L.; Gómez-Lizárraga, K.K.; Garciadiego-Cázares, D.; Piña-Barba, M.C. Fast cyclical-decellularized trachea as a natural 3D scaffold for organ engineering. *Mater. Sci. Eng. C* **2019**, *105*, 110142. [CrossRef]

127. Bujia, J.; Wilmes, E.; Hammer, C.; Kastenbauer, E. Tracheal Transplantation: Demonstration of HLA Class II Subregion Gene Products on Human Trachea. *Acta Oto-Laryngol.* **1990**, *110*, 149–154. [CrossRef] [PubMed]

128. Lu, T.; Yang, B.; Wang, R.; Qin, C. Xenotransplantation: Current Status in Preclinical Research. *Front. Immunol.* **2020**, *10*, 3060. [CrossRef]

129. Yu, Y.; Zhang, W.; Liu, X.; Wang, H.; Shen, J.; Xiao, H.; Mei, J.; Chai, Y.; Wen, G. Extracellular matrix scaffold-immune microenvironment modulates tissue regeneration. *Compos. Part B Eng.* **2022**, *230*, 109524. [CrossRef]

130. Feng, W.; Li, D.; Zang, J.; Fu, L. Biomechanical comparison of xenogeneic bone material treated with different methods. *Xenotransplantation* **2017**, *24*, e12343. [CrossRef] [PubMed]

131. Lu, Y.; Shao, A.; Shan, Y.; Zhao, H.; Leiguo, M.; Zhang, Y.; Tang, Y.; zhang, W.; Jin, Y.; Xu, L. A Standardized Quantitative Method for Detecting Remnant Alpha-Gal Antigen in Animal Tissues or Animal Tissue-Derived Biomaterials and Its Ap-plication. *Sci. Rep.* **2018**, *8*, 15424. [CrossRef] [PubMed]

132. Hashimoto, Y.; Tsuchiya, T.; Doi, R.; Matsumoto, K.; Higami, Y.; Kobayashi, E.; Nagayasu, T. Alteration of the extracellular matrix and alpha-gal antigens in the rat lung scaffold reseeded using human vascular and adipogenic stromal cells. *J. Tissue Eng. Regen. Med.* **2019**, *13*, 2067–2076. [CrossRef] [PubMed]

133. Shaddy, R.E.; Hunter, D.D.; Osborn, K.A.; Lambert, L.M.; Minich, L.L.; Hawkins, J.A.; McGough, E.C.; Fuller, T.C. Prospective Analysis of HLA Immunogenicity of Cryopreserved Valved Allografts Used in Pediatric Heart Surgery. *Circulation* **1996**, *94*, 1063–1067. [CrossRef] [PubMed]

134. Breinholt, J.P., 3rd; Hawkins, J.A.; Lambert, L.M.; Fuller, T.C.; Profaizer, T.; Shaddy, R.E. A prospective analysis of the immuno-genicity of cryopreserved nonvalved allografts used in pediatric heart surgery. *Circulation* **2000**, *102*, III179–III182. [CrossRef]

135. Hooper, D.K.; Hawkins, J.A.; Fuller, T.C.; Profaizer, T.; Shaddy, R.E. Panel-Reactive Antibodies Late After Allograft Implantation in Children. *Ann. Thorac. Surg.* **2005**, *79*, 641–644. [CrossRef] [PubMed]

136. Mirelli, M.; Buzzi, M.; Pasquinelli, G.; Tazzari, P.; Testi, G.; Ricchi, E.; Conte, R.; Stella, A. Fresh and Cryopreserved Arterial Homografts: Immunological and Clinical Results. *Transplant. Proc.* **2005**, *37*, 2688–2691. [CrossRef] [PubMed]

137. Sharma, D.; Iyer, S.; Subramaniam, S.; Ramu, J.; Sharma, M.; Nambiar, A.; Unni, A.; Sivanarayanan, S. Evaluation of Antigenicity of Components of Tracheal Allotransplant and Effect of Immunosuppressant Regime in a Rodent Model. *Indian J. Plast. Surg.* **2020**, *53*, 357–362. [CrossRef]

138. García-Gareta, E.; Abduldaiem, Y.; Sawadkar, P.; Kyriakidis, C.; Lali, F.; Greco, K.V. Decellularised scaffolds: Just a framework? Current knowledge and future directions. *J. Tissue Eng.* **2020**, *11*, 2041731420942903. [CrossRef]

139. Jena, S.; Aksan, A. Effect of high DMSO concentration on albumin during freezing and vitrification. *RSC Adv.* **2017**, *7*, 43611–43620. [CrossRef]

140. Butler, C.R.; Hynds, R.E.; Crowley, C.; Gowers, K.H.; Partington, L.; Hamilton, N.J.; Carvalho, C.; Platé, M.; Samuel, E.R.; Burns, A.J.; et al. Vacuum-assisted decellularization: An accelerated protocol to generate tissue-engineered human tracheal scaffolds. *Biomaterials* **2017**, *124*, 95–105. [CrossRef]

141. Jeong, W.; Kim, M.K.; Kang, H.-W. Effect of detergent type on the performance of liver decellularized extracellular matrix-based bio-inks. *J. Tissue Eng.* **2021**, *12*, 2041731421997091. [CrossRef]

142. Huey, D.J.; Hu, J.C.; Athanasiou, K.A. Unlike Bone, Cartilage Regeneration Remains Elusive. *Science* **2012**, *338*, 917–921. [CrossRef]

143. Frejo, L.; Goldstein, T.; Swami, P.; Patel, N.A.; Grande, D.A.; Zeltsman, D.; Smith, L.P. A two-stage in vivo approach for implanting a 3D printed tissue-engineered tracheal replacement graft: A proof of concept. *Int. J. Pediatr. Otorhinolaryngol.* **2022**, *155*, 111066. [CrossRef]

144. Faulk, D.; Carruthers, C.; Warner, H.; Kramer, C.; Reing, J.; Zhang, L.; D'Amore, A.; Badylak, S. The effect of detergents on the basement membrane complex of a biologic scaffold material. *Acta Biomater.* **2014**, *10*, 183–193. [CrossRef]

145. Burdick, J.A.; Mauck, R.L.; Gorman, J.H.; Gorman, R.C. Acellular Biomaterials: An Evolving Alternative to Cell-Based Therapies. *Sci. Transl. Med.* **2013**, *5*, 176ps4. [CrossRef]

146. Stocco, E.; Barbon, S.; Macchi, V.; Tiengo, C.; Petrelli, L.; Rambaldo, A.; Borean, A.; Capelli, S.; Filippi, A.; Romanato, F.; et al. New bioresorbable wraps based on oxidized polyvinyl alcohol and leukocyte-fibrin-platelet membrane to support peripheral nerve neurorrhaphy: Preclinical comparison versus NeuraWrap. *Sci. Rep.* **2019**, *9*, 17193. [CrossRef] [PubMed]

147. Ayyalasomayajula, V.; Skallerud, B. Microstructure and mechanics of the bovine trachea: Layer specific investigations through SHG imaging and biaxial testing. *J. Mech. Behav. Biomed. Mater.* **2022**, *134*, 105371. [CrossRef]

148. Stocco, E.; Porzionato, A.; de Rose, E.; Barbon, S.; de Caro, R.; Macchi, V. Meniscus Regeneration by 3D Printing Tech-nologies: Current Advances and Future Perspectives. *J. Tissue Eng.* **2022**, *13*, 204173142110658. [CrossRef] [PubMed]

149. Kamel, K.S.; Beckert, L.E.; Stringer, M.D. Novel insights into the elastic and muscular components of the human trachea. *Clin. Anat.* **2009**, *22*, 689–697. [CrossRef] [PubMed]

150. Lee, J.S.-J.; Park, J.; Shin, D.-A.; Ryu, Y.-J.; Kim, H.C.; Lee, J.C.; Kwon, S.K. Characterization of the biomechanical properties of canine trachea using a customized 3D-printed apparatus. *Auris Nasus Larynx* **2019**, *46*, 407–416. [CrossRef] [PubMed]

151. Martínez-Hernández, N.J.; Mas-Estellés, J.; Milián-Medina, L.; Martínez-Ramos, C.; Cerón-Navarro, J.; Galbis-Caravajal, J.; Roig-Bataller, A.; Mata-Roig, M. A Standardised Approach to the Biomechanical Evaluation of Tracheal Grafts. *Biomolecules* **2021**, *11*, 1461. [CrossRef] [PubMed]

152. Marzi, J.; Biermann, A.C.; Brauchle, E.M.; Brockbank, K.G.M.; Stock, U.A.; Schenke-Layland, K. Marker-Independent In Situ Quantitative Assessment of Residual Cryoprotectants in Cardiac Tissues. *Anal. Chem.* **2019**, *91*, 2266–2272. [CrossRef] [PubMed]

153. Sugishita, Y.; Meng, L.; Suzuki-Takahashi, Y.; Nishimura, S.; Furuyama, S.; Uekawa, A.; Tozawa-Ono, A.; Migitaka-Igarashi, J.; Koizumi, T.; Seino, H.; et al. Quantification of residual cryoprotectants and cytotoxicity in thawed bovine ovarian tissues after slow freezing or vitrification. *Hum. Reprod.* **2022**, *37*, 522–533. [CrossRef] [PubMed]

154. Sotnichenko, A.S.; Nakokhov, R.Z.; Gubareva, E.A.; Kuevda, E.V.; Gumenyuk, I.S. Morphological Evaluation of the Tissue Reaction to Subcutaneous Implantation of Decellularized Matrices. *Bull. Exp. Biol. Med.* **2018**, *166*, 287–292. [CrossRef] [PubMed]

155. Methe, M.K.N.; Nayakawde, N.B.; Banerjee, D.; Sihlbom, C.; Agbajogu, C.; Travnikova, M.G.; Olausson, M. Differential Activation of Immune Cells for Genetically Different Decellularized Cardiac Tissues. *Tissue Eng. Part A* **2020**, *26*, 1180–1198. [CrossRef]